

5-8-2020

Investigating the Transcriptional Regulation of Secondary Cell Wall Synthesis and Thigmomorphogenesis in the Model Grass *Brachypodium distachyon*

Joshua Coomey

Follow this and additional works at: https://scholarworks.umass.edu/dissertations_2



Part of the [Molecular Genetics Commons](#), and the [Plant Biology Commons](#)

Recommended Citation

Coomey, Joshua, "Investigating the Transcriptional Regulation of Secondary Cell Wall Synthesis and Thigmomorphogenesis in the Model Grass *Brachypodium distachyon*" (2020). *Doctoral Dissertations*. 1941.

<https://doi.org/10.7275/kgzs-j573> https://scholarworks.umass.edu/dissertations_2/1941

This Open Access Dissertation is brought to you for free and open access by the Dissertations and Theses at ScholarWorks@UMass Amherst. It has been accepted for inclusion in Doctoral Dissertations by an authorized administrator of ScholarWorks@UMass Amherst. For more information, please contact scholarworks@library.umass.edu.

Investigating the transcriptional regulation of secondary cell wall synthesis and thigmomorphogenesis in the model grass *Brachypodium distachyon*

A Dissertation Presented

by

JOSHUA H. COOMEY

Submitted to the Graduate School of the
University of Massachusetts Amherst in partial fulfillment
of the requirements for the degree of

DOCTOR OF PHILOSOPHY

May 2020

Plant Biology

© Copyright by Joshua H. Coomey 2020

All Rights Reserved

Investigating the transcriptional regulation of secondary cell wall synthesis and thigmomorphogenesis in the model grass *Brachypodium distachyon*

A Dissertation Presented

by

JOSHUA H. COOMEY

Approved as to style and content by:

Samuel P. Hazen, Chair

Elizabeth Vierling, Member

Madelaine E. Bartlett, Member

Joshua Gendron, Member

Samuel P. Hazen, Director

Plant Biology Graduate Program

ACKNOWLEDGMENTS

I would like to first give thanks to my family for all their love and support. To my father, the first scientist in my life, who instilled me with a ‘can do’ attitude and who taught me that any task can be accomplished with the right tools. To my mother, whose enthusiasm for education and clear communication shaped so much of my approach to academics and mentoring. To my sister, who’s drive, determination, and commiseration has always been a source of inspiration and support.

I would like to thank my mentor, Samuel Hazen, who has been a tremendous source of scientific and personal support throughout my graduate career. Without his understanding and guidance I would not be pursuing a career in science. I would also like to thank all the past and present members of the Hazen Lab for being such stellar labmates. A special thanks to all the UMass, RIT, and NTID undergraduates who have worked on my projects, their help has been invaluable.

I would also like to thank the faculty and graduate students of the Plant Biology Graduate Program for cultivating such an excellent learning environment, and particularly my committee members, Elizabeth, Madelaine, and Josh for their support and guidance.

Finally, I want to thank my fantastic girlfriend Kristin for her unending patience, support, and encouragement.

ABSTRACT

INVESTIGATING THE TRANSCRIPTIONAL REGULATION OF SECONDARY
CELL WALL SYNTHESIS AND THIGMOMORPHOGENESIS IN THE MODEL
GRASS *BRACHYPODIUM DISTACHYON*

MAY 2020

JOSHUA H. COOMEY, B.S. UNIVERSITY OF MASSACHUSETTS AMHERST

Ph.D. UNIVERSITY OF MASSACHUSETTS AMHERST

Directed by: Professor Samuel P. Hazen

A key aspect of plant growth is the synthesis and deposition of cell walls. In specific tissues and cell types including xylem and fiber, a thick secondary wall composed of cellulose, hemicellulose, and lignin is deposited. Secondary cell walls provide a physical barrier that protects plants from pathogens, promotes tolerance to abiotic stresses, and fortifies cells to withstand the forces associated with water transport and the physical weight of plant structures. Grasses have numerous cell wall features that are distinct from eudicots and other plants. Study of the model species *Brachypodium distachyon* has helped us begin to understand the internal and external cues that regulate the synthesis of grass secondary cell walls. In this dissertation, I investigate the function of two transcription factors in regulating cell wall biosynthesis, *SWIZ* and *KNOB7*. *SWIZ* controls wall synthesis and plant growth in response to external mechanical force. In response to touch, *SWIZ* protein moves into the nucleus, a translocation that is modulated by the level of bioactive gibberellic acid in the cell. Positive and negative perturbation of *SWIZ* results in shorter plants with thicker fiber cell walls, phenotypes that are enhanced

in plants treated with regular mechanical stimulus during growth. *KNOB7* is orthologous to the characterized cell wall regulator *AtKNAT7* in *Arabidopsis thaliana*. *KNOB7* negatively regulates fiber wall thickness and lignification, as is observed in *AtKNAT7*, but *KNOB7* shows unique control of lignin composition, hydroxycinnamic acid content, and cell wall polysaccharide content. These observations may reflect control of grass specific cell wall characteristics not present in eudicots, such as high levels of wall bound hydroxycinnamic acids and the prevalence of heteroxylan polysaccharides. Together, these insights from *SWIZ* and *KNOB7* function further our understanding of how grasses regulate their growth and secondary cell wall synthesis.

TABLE OF CONTENTS

	Page
ACKNOWLEDGMENTS.....	iv
ABSTRACT.....	v
LIST OF TABLES.....	xi
LIST OF FIGURES.....	xii
CHAPTER	
1. TANSLEY REVIEWS: GRASS SECONDARY CELL WALLS, BRACHYPODIUM DISTACHYON AS A MODEL FOR DISCOVERY.....	1
1.1 Introduction to the secondary cell wall.....	1
1.2 Brachypodium distachyon, a model grass system.....	3
1.3 Cellulose.....	5
1.4 Mixed-linkage glucans.....	7
1.5 Grass heteroxylans.....	12
1.6 Xylan acetylation.....	15
1.7 Lignins.....	17
1.8 Hydroxycinnamic acids.....	21
1.9 Tricin.....	24
1.10 Silicon.....	27
1.11 Transcriptional regulation of secondary cell wall thickening.....	28
1.12 Conclusions.....	38
2. SECONDARY WALL INTERACTING BZIP (SWIZ) IS A TOUCH-SENSITIVE REGULATOR OF PLANT HEIGHT AND CELL WALL THICKENING.....	39
2.1 Introduction.....	39
2.1.1 Mechanosensing and thigmomorphogenesis.....	39
2.1.2 bZIPS.....	42
2.1.3 Summary.....	45

2.2 Methods.....	45
2.2.1. Plasmid construction.....	45
2.2.2. Plant transformation.....	46
2.2.3. Plant growth.....	47
2.2.4. Transverse stem sections, histology.....	47
2.2.5 Measuring cell wall thickness.....	47
2.2.6. Translocation assay.....	48
2.2.6.1. Plant growth.....	48
2.2.6.2. Pharmacology treatments.....	48
2.2.6.3. Confocal microscopy.....	48
2.2.6.4. Touch treatment.....	49
2.2.6.5. Analysis.....	49
2.2.7. Cell wall material insoluble in alcohol (MIA).....	50
2.2.8. ABSL quantification.....	50
2.2.9. Thigmomatic construction and operation.....	51
2.2.10. DAP-seq.....	52
2.2.11. HOMER identification of motifs.....	53
2.2.12. GO analysis.....	53
2.2.13. Yeast one-hybrid assay for protein DNA interaction.....	53
2.2.14. Genomic DNA Extraction.....	55
2.2.15 RNA extraction and RT-qPCR.....	55
2.3 Results.....	56
2.3.1 SWIZ is a Group I bZIP transcription factor and candidate cell wall regulator.....	56
2.3.2 SWIZ binds a conserved motif.....	59
2.3.3 SWIZ genetic reagents.....	60
2.3.4 SWIZ effects cell wall thickness, lignification, and plant morphology.....	62

2.3.5 SWIZ translocates into the nucleus in response to mechanical stimulus and cellular GA levels.....	64
2.3.6 Thigmomorphogenesis in <i>B. distachyon</i>	72
2.3.7 Thigmomorphogenesis in SWIZ genetic reagents.....	75
2.4 Discussion.....	81
2.4.1 SWIZ is a likely cell wall regulator.....	81
2.4.2 SWIZ translocation dynamics are consistent with reported bZIP dynamics in response to mechanical stimulus and GA.....	82
2.4.3 Thigmomorphogenesis in <i>B. distachyon</i>	83
2.4.4 SWIZ touch responsive phenotypes.....	83
2.4.5 Bioactive GA status may act in SWIZ mechanosignaling and explain touch responsive height phenotypes.....	85
2.4.6 SWIZ touch responsive cell wall phenotypes may depend on interacting partners.....	86
2.4.7 SWIZ in vitro binding targets relate to hormone cross talk and mechanoperception pathways.....	87
2.5 Conclusions.....	88
3. KNOTTED OF BRACHYPODIUM 7 (KNOB7) IS A CLASS II KNOX GENE AND NEGATIVE REGULATOR OF INTERFASCICULAR FIBER SECONDARY CELL WALLS.....	90
3.1 Introduction.....	90
3.2 Methods.....	93
3.2.1. Plasmid construction.....	93
3.2.2 Identification of mutants.....	93
3.2.2. Plant transformation.....	94
3.2.3. Plant growth.....	95
3.2.4. Transverse stem sections, histology.....	95
3.2.5 Measuring cell wall thickness.....	95
3.2.6. Cell wall material insoluble in alcohol (MIA).....	95
3.2.7. ABSL quantification.....	96

3.2.8. Mild alkaline hydrolysis.....	97
3.2.9 Thioacidolysis.....	97
3.2.10. Neutral sugar analysis.....	98
3.2.11. Yeast one-hybrid assay for protein DNA interaction.....	98
3.2.12. Genomic DNA Extraction.....	99
3.2.13. RNA extraction and RT-qPCR.....	100
3.3 Results.....	101
3.3.1 KNOB7 is a candidate wall regulator and a Class II KNOX gene.....	105
3.3.2 KNOB7 genetic reagents.....	106
3.3.3 KNOB7 localizes to the nucleus.....	109
3.3.4 KNOB7 is a negative regulator of interfascicular fiber wall thickening and lignification.....	110
3.3.5 KNOB7 alters lignin composition and levels of wall bound hydroxycinnamic acids.....	113
3.3.6 KNOB7 alters cell wall polysaccharide content.....	115
3.4 Discussion.....	117
4. CONCLUSIONS.....	121
APPENDIX	
1. SUPPLEMENTAL DATA.....	123
BIBLIOGRAPHY.....	136

LIST OF TABLES

Table	Page
Table 1. SWIZ binding motifs identified by DNA affinity purified sequencing.....	60
Table A1. GO terms from BdSWIZ DAP-seq, all peaks.....	125
Table A2. GO terms from BdSWIZ DAP-seq, filtered for those containing the conserved bZIPS binding motif.....	130
Table A3. SWIZ protein-DNA interactions from yeast one hybrid assay.....	132
Table A4. Primers used in these studies.....	138

LIST OF FIGURES

Figure	Page
Figure 1.1. General schematic of grass secondary cell wall matrix.....	3
Figure 1.2. Transverse section of <i>B. distachyon</i> and <i>A. thaliana</i> stems.....	5
Figure 1.3. Mixed-linkage glucan structure.....	11
Figure 1.4. Grass heteroxylan structure.....	16
Figure 1.5. Alternative routes to lignin biosynthesis.....	26
Figure 1.6. Transcriptional regulation of secondary cell wall deposition.....	37
Figure 2.1. Thigmomatic.....	52
Figure 2.2. <i>SWIZ</i> is highly expressed in maturing stem and root.....	56
Figure 2.3. <i>SWIZ</i> phylogeny.....	57
Figure 2.4. <i>SWIZ</i> protein interacts with cell wall gene regulatory regions.....	58
Figure 2.5. Diagram of <i>SWIZ</i> transgenic reagents.....	61
Figure 2.6. <i>SWIZ</i> reagent phenotypes.....	63
Figure 2.7. <i>SWIZ</i> translocates to the nucleus in response to mechanical stress.....	65
Figure 2.8. <i>SWIZ</i> translocation dynamics are similar in amplitude and timing following repeated stimuli.....	66
Figure 2.9. <i>SWIZ</i> translocation is localized to the region of tissue that experiences mechanical stimulus.....	68
Figure 2.10. <i>SWIZ</i> translocation to the nucleus is dampened by the addition of exogenous GA4.....	70
Figure 2.11. <i>SWIZ</i> translocation to the nucleus is enhanced by the addition of paclobutrazol (PBZ), a GA synthesis inhibitor.....	71
Figure 2.12. <i>B. distachyon</i> displays classic thigmomorphogenic phenotypes.....	73
Figure 2.13. <i>B. distachyon</i> stem biology under mechanical stress conditions.....	74
Figure 2.14. Stem parenchyma pockets contain starch granules.....	75
Figure 2.15. Thigmomorphogenic whole plant phenotypes are enhanced in <i>SWIZ</i> reagents under mechanical stress.....	76
Figure 2.16. Stem biology of <i>SWIZ</i> transgenic reagents under touched conditions.....	78
Figure 2.17. Quantification of interfascicular fiber wall thickness under touch and control conditions in <i>SWIZ</i> genetic reagents.....	79

Figure 2.18. Cell wall gene expression in SWIZ transgenic plants following mechanical stimulus.....	80
Figure 3.1 <i>Bradi1g76970</i> is highly expressed in maturing stem and root.....	102
Figure 3.2 KNOX protein phylogeny.....	103
Figure 3.3 KNOB7 protein interacts with cell wall gene regulatory regions.....	105
Figure 3.4 Diagram of <i>KNOB7</i> genetic reagents.....	107
Figure 3.5 Expression of <i>KNOB7</i> in mutant and overexpression lines.....	108
Figure 3.6 <i>KNOB7</i> localizes to the nucleus.....	109
Figure 3.7 <i>KNOB7</i> negatively regulates lignification in interfascicular fibers.....	111
Figure 3.8 <i>KNOB7</i> is a negative regulator of lignin.....	112
Figure 3.9 <i>KNOB7</i> is a negative regulator of interfascicular fiber wall thickness.....	113
Figure 3.10 Wall-bound hydroxycinnamic acids are increased in <i>knob7-1</i> and <i>knob7-3</i> mutant lines.....	114
Figure 3.11 <i>KNOB7</i> mutant alleles have increased S lignin content.....	115
Figure 3.12 Neutral sugar analysis of <i>knob7-1</i>	116

CHAPTER 1

TANSLEY REVIEWS: GRASS SECONDARY CELL WALLS, *BRACHYPODIUM DISTACHYON* AS A MODEL FOR DISCOVERY.

1.1 Introduction to the secondary cell wall

The secondary plant cell wall provides mechanical strength that allows plants to stand upright, resist pest and pathogen invasion, and transport water over long distances. Both plants and humans have found this abundant matrix of crosslinked polymers useful as durable building material, with timber featuring in human construction around the world for generations. The secondary wall is distinct from other cell wall types in composition as well as the developmental timing and tissue types where it is deposited. Secondary walls form in thick layers, rich in cellulose, hemicelluloses, and lignin. Cellulose microfibrils have a tensile strength rivaling steel, and form crystalline structures. Hemicelluloses include a variety of polysaccharides, but in grass secondary walls these are mostly mixed linkage glucans and heteroxylans, a defining aspect of this plant lineage. Finally, lignin is a recalcitrant and heterogeneous mixture of randomly polymerized phenolic monolignols that is interspersed and cross linked with wall polysaccharide polymers. Lignification is a hallmark of secondary walls, and unique chemistry and synthesis of this polymer continues to be uncovered (Fig. 1.1).

Following cell expansion of cells surrounded by a primary wall, secondary walls are deposited in a highly specific spatio-temporal manner in certain cell types over development. Unlike eudicots, grass stem growth is a result of iterative division and

elongation events from stacked intercalary meristems called nodes (Esau, 1977; Langer, 1979). New cells generated from the node elongate, pushing up the nodes above with the final node transitioning to the flowering meristem. Thus, the internode regions are most mature at the bottom of the stem, while cells within an internode are most mature at the top of that region, just before the next node (Langer, 1979). Secondary wall deposition occurs between cell elongation and senescence, with cellulose, lignin, and hemicellulose content increasing with maturity (Rancour *et al.*, 2012; Matos *et al.*, 2013; Kapp *et al.*, 2015). Grass stems account for the majority of secondary wall forming sclerenchyma tissues. The interfascicular fibers develop thick secondary walls and provide mechanical strength for the upright stem. Grasses form discrete vasculature with the xylem and phloem contained by bundle sheath cells, unlike eudicots where a cambium separates colateral xylem and phloem (Fig. 2). Depending on the species, stem vascular bundles can be arranged in peripheral rings or dispersed throughout the stem (Esau, 1977). Xylem develops strong secondary walls that can tolerate the high pressures caused by evapotranspiration. Phloem cells do not have secondary walls. Besides phloem, grass stem parenchyma tissue can be found in the pith and in cortex pockets, which have been shown to function as carbon storage tissues during development (Jensen & Wilkerson, 2017). While this review focuses on secondary cell walls in *B. distachyon* and other grasses, wall synthesis has also been investigated using *B. distachyon* as a model system for callus tissue, young vegetative growth, and endosperm development (Christensen *et al.*, 2010; Guillon *et al.*, 2011a; Liu *et al.*, 2016; Betekhtin *et al.*, 2018; Francin-Allami *et al.*, 2019).

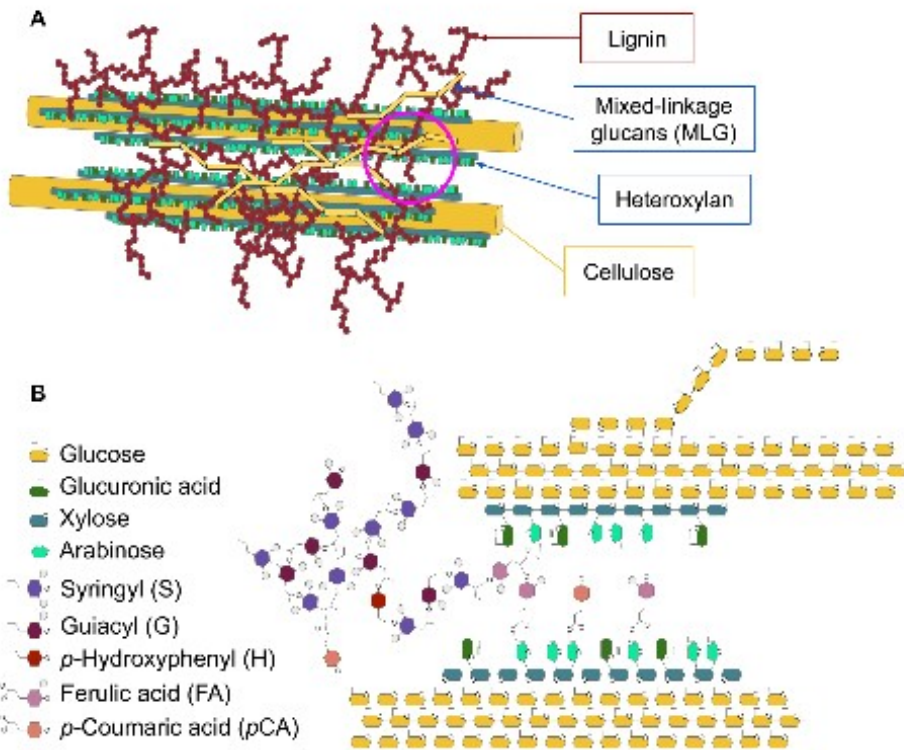


Figure 1.1. General schematic of grass secondary cell wall matrix. The grass secondary cell wall matrix is made up of cellulose microfibrils, mixed-linkage glucans, heteroxylans, and lignins. (a) A generalized cartoon of grass secondary wall polymer interactions. (b) Schematic fine structure of the pink circled region in (a). Cellulose microfibrils consist of multiple, organized, $\beta(1,4)$ -linked glucose chains. Mixed-linkage glucans are also glucose chains, but include $\beta(1,3)$ linkages. Heteroxylan has a xylose backbone that is decorated with sugar and phenolic side chains of xylose, arabinose, glucuronic acid, and hydroxycinnamates (FA and pCA). These polysaccharides can be interwoven with lignins, branched phenolic polymers made of three main lignin units, syringyl (S), guaiacyl (G), and *p*-hydroxyphenyl (H). Lignins can also contain ferulic and *p*-coumaric acids.

1.2 *Brachypodium distachyon*, a model grass system.

B. distachyon is a model for cereal crops and temperate grasses because of its small stature, simple growth requirements, short life cycle, relatively small and sequenced genome, and close phylogenetic relation to those species (Scholthof *et al.*, 2018). *B. distachyon* has a ‘finished’ reference genome with the only ambiguity being the placement of some centromeric repeats

(https://phytozome-next.jgi.doe.gov/info/Bdistachyon_v3_1). In addition, there is a growing atlas of gene expression profiles (Trabucco *et al.*, 2013b; Sibout *et al.*, 2017; MacKinnon *et al.*, 2020). It is also remarkable in terms of the resources available for experimental molecular genetics. Genetic transformation protocols are well-developed; current efficiency makes *B. distachyon* a grass highly amenable to transformation (Bragg *et al.*, 2012). Mutant resources consist of 23,000 T-DNA mutants and 1,200 sequenced chemical mutants (Bragg *et al.*, 2012; Granier *et al.*, 2015). Given that these mutations are more-or-less randomly distributed across the genome and chemical mutagenesis typically induces multiple mutations per mutant line, this large collection likely includes loss-of-function mutations in the majority of *B. distachyon* genes and multiple nonsynonymous mutations in virtually every gene (Dalmais *et al.*, 2013). This latter category of mutations may be particularly interesting because it can help elucidate the function of cell wall genes, as well as the importance of specific amino acids and protein domains, information that cannot be inferred from knock-out mutants. A large natural variation population exists for *B. distachyon*, with sequenced genomes for many accessions. These resources have been applied in several studies on growth and biomass related traits (Lee *et al.*, 2012; Tyler *et al.*, 2014; Kapp *et al.*, 2015; Gordon *et al.*, 2017). Thus, *B. distachyon* is well positioned for gaining fundamental insights into cell wall biosynthesis (Coomey & Hazen, 2015). This knowledge can then be leveraged for agronomic gains in more experimentally recalcitrant grass species.

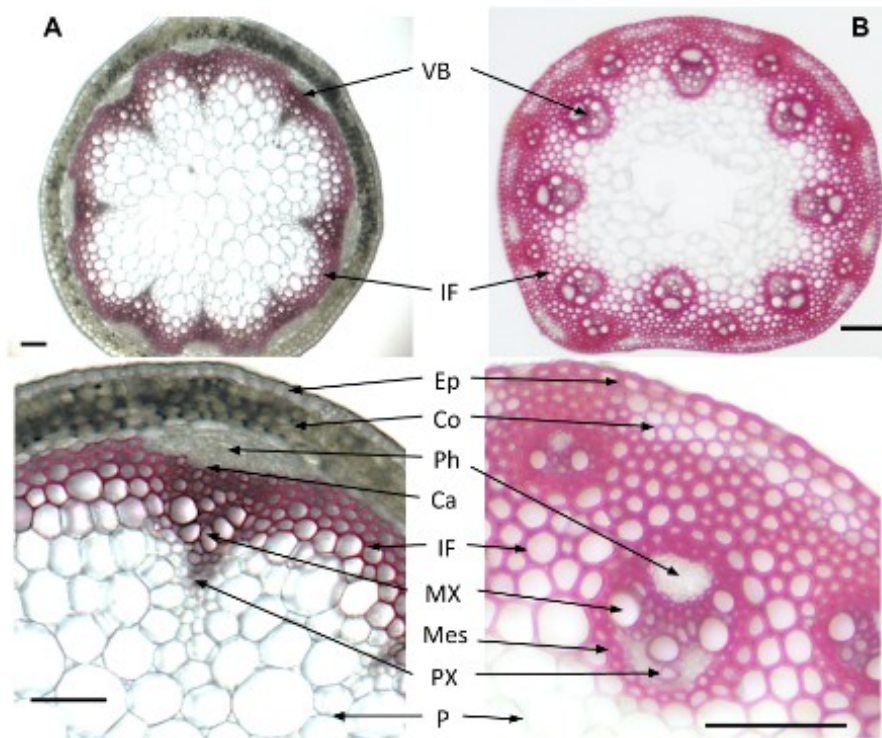


Figure 1.2. Transverse section of *B. distachyon* and *A. thaliana* stems. Transverse stem cross sections of *A. thaliana* (a) and *B. distachyon* (b) stained with phloroglucinol-HCl, a general stain for lignified tissues. Most eudicots, such as *A. thaliana*, have vascular bundles of xylem separated from phloem by cambium layers, and flanked by interfascicular fibers. In *B. distachyon*, the stem vascular bundles also contain xylem and phloem, but there is no cambial layer, and the vasculature is encased by a lignified bundle sheath layer of mestome cells and surrounded by interfascicular fiber cells. In both species, a cortex region of less lignified cells separates the interfascicular region from the epidermis. Abbreviations: vascular bundles (VB), epidermis (Ep), cortex (Co), cambium area (Ca), interfascicular fibers (IF), phloem (Ph), mestome (Mes), metaxylem (MX), protoxylem (PX), parenchyma (P). Scale bar = 100 μm .

1.3 Cellulose

Cellulose is perhaps the most abundant polymer in the world, found in the walls of every plant cell. It is made of β -1-4 linked glucose monomers, and these glucan chains are synthesized at the plasma membrane by the cellulose synthase complex (Fig. 1). Extruded cellulose chains form organized microfibrils with crystalline structure; the degree of this organization impacts wall mechanics, with greater crystallinity resulting in stiffer walls.

The cellulose synthase complex consists of multiple Cellulose Synthase A (CesA) subunits and associated proteins (Pear *et al.*, 1996; Polko & Kieber, 2019). *CesA* genes are a subclade of the cellulose synthase superfamily, along with the *Cellulose Synthase-like (Csl)* clades. Across plant species, seven major lineages have been identified in the *CesA* genes, which separate into the *CesAs* associated with primary or secondary wall synthesis (Little *et al.*, 2018). This distinction between primary and secondary wall synthesis is conserved across most vascular plants. In *B. distachyon*, *BdCesA4*, 7, and 8 have been shown to function in secondary wall synthesis, and these proteins are highly similar to those characterized in other species for secondary wall function, such as *Arabidopsis thaliana* and rice (*Oryza sativa*) (Handakumbura *et al.*, 2013). In *B. distachyon*, loss-of-function in the secondary *CesAs* results in reduced crystalline cellulose content, compromised wall integrity, and reduced plant growth (Handakumbura *et al.*, 2013; Petrik *et al.*, 2016). Interestingly, the secondary *CesA* lineage contains a Poacea-specific clade, which in *B. distachyon* is represented by *BdCesA10*. This *CesA10* group does not contain the canonical UDP-glucose binding motif (D,D,D,QxxRW) found in glucosyltransferases (Handakumbura *et al.*, 2013). While phylogenetic analysis clearly places these proteins in the *CesA* clade, it is not clear what role they play, if any, in cell wall synthesis.

Mutants in maize (*Zea mays*), barley (*Hordeum vulgare*), and rice with defects in cellulose synthesis have been identified through brittle stem phenotypes, aptly named brittle stalk, fragile stem, and brittle culm respectively (Tanaka *et al.*, 2003; Sindhu *et al.*,

2007; Burton *et al.*, 2010b; Kotake *et al.*, 2011). These mutants have been mapped both to genes encoding CesAs and other associated proteins, such as the COBRA-like family of glycosylphosphatidylinositol anchored proteins. While the precise function of these anchored proteins is not fully understood, they may play a role in properly orienting cellulose synthesis.

Cellulose synthase complex dynamics have been studied primarily in *A. thaliana*, but recent work in *B. distachyon* has added to our understanding of the conserved functions of this system. The complex moves along cortical microtubules, depositing cellulose microfibrils perpendicular to the axis of elongation (Paredez *et al.*, 2006). This has been observed in real time for primary CesAs in both *A. thaliana* and *B. distachyon*, which showed similar speeds in *B. distachyon* mesocotyl and root, as in *A. thaliana* hypocotyl. This motility was not affected by latrunculin B treatment, which destabilized actin filaments, but was dampened in both species when microtubules were disrupted (Liu *et al.*, 2017). Missense mutation in *Bdcesa1*, a primary wall cellulose synthase, showed reduced cellulose content and crystallinity, as do *A. thaliana Atcesa1* mutants (Arioli *et al.*, 1998; Persson *et al.*, 2007; Brabham *et al.*, 2019). Unlike *Atcesa1* mutants, *Bdcesa1* did not show reduced plant height. Rather, the *Bdcesa1* mutant had more internodes, giving rise to a plant with normal height despite reduced cellular elongation from compromised cellulose synthesis (Brabham *et al.*, 2019). Overall, the process of cellulose biosynthesis appears to be somewhat conserved between eudicots and grasses.

1.4 Mixed-linkage glucans

One of the salient differences that defines grass secondary cell walls is the composition

and utilization of non-cellulosic polysaccharides. These can generally be thought of as pectins and hemicellulose, but discussion of these polymers is often better suited to classification by backbone structure (Scheller & Ulvskov, 2010; Atmodjo *et al.*, 2013). In eudicots, the predominant polysaccharide polymer after cellulose is xyloglucans, β -1-4-linked glucose chains that contain numerous 1-6 xylose substitutions. The xylose side chains can be further decorated with other sugars such as galactose or fucose (Bauer *et al.*, 1973; Fry, 1989; Scheller & Ulvskov, 2010). In grasses, the role of xyloglucans is largely replaced by mixed-linkage glucans (MLGs) and heteroxylans.

Mixed-linkage glucans are, as their name suggests, β -1-4 linked glucose chains that are interrupted with β -1-3 linkages (Fig. 1 & 3). (1,3)- β -glucans are typically separated either by two or three (1,4)- β -glucans, forming oligosaccharide units of β -cellotriosyl or β -cellotetraosyl (Fig. 3), although longer chains of (1,4)- β -glucans are also observed (Bulone *et al.*, 2019). Almost no evidence of adjacent (1,3)- β -glucan bonds has been found (Buliga *et al.*, 1986). These altered linkages result in the polymer having kinks and bends, unlike the linear glucan chains that form cellulose. As a result, MLG does not form crystalline structures. The relative amounts of β -cellotriosyl and β -cellotetraosyl units strongly relate to the solubility of the overall polymer and are expressed as ratios of degrees of polymerization of tri- and tetrasaccharides (DP3:DP4). Solubility of the polymer decreases at either end of the ratio spectrum. Longer stretches of either β -cellotriosyl or β -cellotetraosyl units increases the overall order of the polymer with more undisturbed regions of (1,4)- β -glucan linkages, and thus decreases solubility. Greater solubility occurs with DP3:DP4 ratios that range from 1:1 to 2.5:1 (Lazaridou &

Biliaderis, 2007; Burton *et al.*, 2010a).

MLGs were once thought to be unique to grass cell walls, but several examples have now been observed outside of the commelinid monocots, and indeed outside of green plants. Polysaccharides containing (1,3;1,4)- β -glucans have been observed in green, red, and brown algae, lichens, fungi, bryophytes, and the monophyletic genus *Equisetum* (Bulone *et al.*, 2019). Genomic data further supports the idea that MLGs are not specific to the Poaceae, with enzymes capable of synthesizing (1,3;1,4)- β -glucan linkages identified across monocots and in isolated cases in other species. MLG has been shown to be synthesized by members of the *CsIF*, *CsIH*, and *CsIJ* families (Bulone *et al.*, 2019). All three of these groups have co-evolved independently in monocots from sister Csl clades (Little *et al.*, 2018). Members of *CsIF/H/J* clades have been shown to be capable of synthesizing (1,3;1,4)- β -glucan when heterologously expressed, but it is not clear whether all of these groups are responsible for native MLG synthesis. By far the best characterized enzyme in MLG synthesis is CslF6, which has been studied in barley, wheat (*Triticum aestivum*), rice, maize, and *B. distachyon* (Nemeth *et al.*, 2010; Vega-Sanchez *et al.*, 2012; Kim *et al.*, 2015, 2018). BdCslF6 protein is localized to the Golgi membrane, with an external catalytic domain (Kim *et al.*, 2015, 2018). Antibody detection of (1,3;1,4)- β -glucan in maize also supports a Golgi localized synthesis of MLG (Carpita & McCann, 2010). However, evidence in other grasses suggests that MLG synthesis occurs at the plasma membrane. In barley and wheat, antibody detection of MLG showed localization at the plasma membrane and cell wall, as did antibody detection of HvCslF6 and TaCslF6 (Trethewey & Harris, 2002; Trethewey *et al.*, 2005;

Wilson et al., 2006, 2015). The N-terminus region of the CslF6 protein in barley, maize, and sorghum (*Sorghum bicolor*) influence total MLG synthesis activity and the C-terminal region appears to influence the ratio of DP3:DP4 linkages (Jobling, 2015; Dimitroff *et al.*, 2016)

The evolution of MLG appears to have been followed by the evolution of hydrolytic enzymes specific to (1,3;1,4)- β -glucan polymers (Høj & Fincher, 1995; Fincher, 2009). Both (1,4)- β -glucan and (1,3)- β -glucan endohydrolases exist across land plant lineages, capable of cleaving (1,4)- β -glucan bonds in both cellulose and MLG. Specific (1,3;1,4)- β -glucan endohydrolases have been well characterized in the metabolism of MLG, and analysis of their amino acid sequence and crystal structure show strong similarity with barley (1,3)- β -glucan endohydrolases, indicating that the ability to cleave (1,3;1,4)- β -glucan polymers was achieved through a modification of (1,3)- β -glucan endohydrolase function (Varghese *et al.* 1994).

The utility of increased MLG as a bioenergy source and the effect of increased MLG on wall content and plant health has been explored in studies overexpressing MLG synthesis in barley and *A. thaliana*. Excess MLG synthesis under constitutive promoters was detrimental to plant health, but tissue or developmentally specific promoters driving MLG synthesis resulted in plants with higher MLG content in grain or stem without such deleterious effects (Burton *et al.*, 2011; Vega-Sánchez *et al.*, 2015) In barley, MLG and starch levels have been shown to be inversely related in the developing coleoptile (Roulin *et al.*, 2002), and MLG levels have been shown to dynamically rise and fall over the course of development in vegetative tissue (Gibeaut *et al.*, 2005). The grain cell walls of

B. distachyon differ from cultivated cereals with exceptionally high levels of MLG and relatively lower starch levels (Guillon *et al.*, 2011b; Opanowicz *et al.*, 2011; Trafford *et al.*, 2013; Burton & Fincher, 2014). This shift in carbon storage suggests that *B. distachyon* may rely on MLG to a greater extent than starch for endosperm carbon storage (Trafford *et al.*, 2013; Burton & Fincher, 2014). It has been suggested that MLG metabolism is enzymatically simpler than starch metabolism, requiring fewer enzymes in more available cellular spaces than the multi-step, amyloplast specific process of starch metabolism (Roulin *et al.*, 2002; Burton & Fincher, 2012; Trafford *et al.*, 2013; Bulone *et al.*, 2019). While this has yet to be explored experimentally, it has been noted that a fast, alternative glucose storage pathway from (1,3;1,4)- β -glucan metabolism may confer an advantage to the grasses, as evidenced by the development of this mechanism in a group with such widespread success.

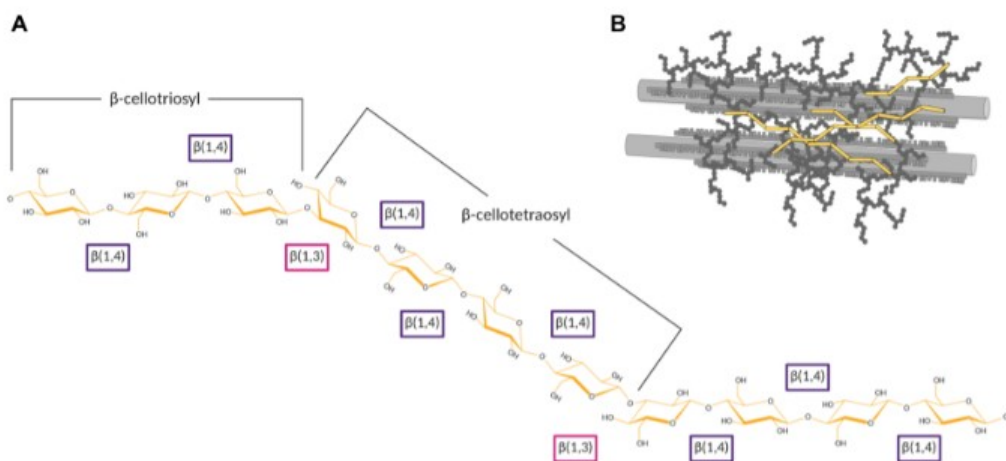


Figure 1.3. Mixed-linkage glucan structure. A) Fine structure of mixed linkage glucan. Glucose monomers (yellow) linked by $\beta(1,4)$ bonds (purple) are occasionally interrupted by $\beta(1,3)$ linkages (pink). The $\beta(1,3)$ bonds do not occur sequentially, but rather separate (1,4)- β -glucans into β -celotriosyl or β -celotetraosyl segments. The relative degree of β -celotriosyl to β -celotetraosyl units relates to the solubility of the overall polymer. (1,3;1,4)- β -glucans are synthesized by Cellulose synthase-like

F6, a Golgi membrane bound protein with cytoplasmically active catalytic sites. (b) Miniature of Fig 1a cell wall schematic highlighting the mixed linkage glucan component.

1.5 Grass heteroxylans

After glucans, xylans are the most abundant polysaccharide in plants. Although present across angiosperms, heteroxylans play a more prominent role in the grasses as the major hemicellulose (Scheller & Ulvskov, 2010). This class of polysaccharide is based on a (1,4)- β -D-xylopyranosyl backbone, with side-chains of arabinose, xylose, glucuronic acid, and hydroxycinnamates (Fig. 1 & 4). The nature and patterning of these side-chains have major impacts on cell wall integrity, mediating xylan-cellulose and xylan-lignin polymer interactions (Simmons *et al.*, 2016; Martínez-Abad *et al.*, 2017). The β -(1,4)-xylan backbone has been shown to be synthesized by members of glycosyltransferase 43 (GT43) and GT47 family proteins in both eudicots and monocots. The *A. thaliana* irregular xylem mutants (*irx*) were some of the first identified xylan synthesis mutants, including *irx9*, *irx14*, and *irx10*, all encoding GT43 and GT47 enzymes in wildtype plants (Brown *et al.*, 2005a, 2009; Lee *et al.*, 2007; Peña *et al.*, 2007). In *B. distachyon*, recent work has shown that a member of the GT43 family is in part responsible for heteroxylan backbone synthesis. Genetic linkage mapping of saccharification rate in a recombinant inbred population identified a QTL (quantitative trait locus) interval containing a *BdGT43A* ortholog of *A. thaliana* *IRX14* (Whitehead *et al.*, 2018). Allelic variation in *BdGT43A* between parental accessions Bd3-1 and Bd21 showed that the Bd3-1 allele encodes an alanine to threonine (A80T) shift that was associated with reduced Bd3-1 saccharification. Knockdown of *BdGT43A* resulted in reduced xylose, arabinose, and ferulic acid deposition in stem tissue. Rice GT43 proteins have similarly been shown

to mediate xylan synthesis, with *OsGT43A* and *OsGT43E* complementing *A. thaliana* *irx9* mutant phenotypes, and *OsGT34J* complementing *irx14* (Lee *et al.*, 2014).

The addition of side chains to the xylan backbone differentiates the various types of heteroxylans. In eudicots, glucuronoxylan is the most prevalent form, in which the side chain is formed by the addition of α -(1,2)-GlcA side chains, sometimes amended with 4-O-Me groups (Scheller & Ulvskov, 2010). Grass cell walls differ from those of eudicots in their abundance of arabinoxylans and glucuronoarabinoxylan.

Arabinoxylans have monomer side chains of α -(1,3)-Araf and β -(1,2)-Xylp, or dimer side chains of α -(1,3)-Araf- α -(1,2)-Araf, α -(1,3)-Araf- β -(1,2)-Xylp, or α -(1,3)-Araf-ferulic acid. Glucuronoarabinoxylans contain the same side chains as arabinoxylans, but also include α -(1,2)-GlcA-4-O-Me additions. Arabinoxylans are the more prevalent form found in endosperm cell walls, while glucuronoarabinoxylan is more common in vegetative tissue. The addition of these sugar side chains to heteroxylans is mediated by xylan arabinosyltransferases (XAT) which are members of the GT61 family. They function in the Golgi to add α -(1,3)-Araf substitutions to the xylan backbone. Two XATs in wheat (*TaXAT1*, *TaXAT2*) and rice (*OsXAT2*, *OsXAT3*) have been characterized both natively and in heterologous systems for arabinosyltransferase activity (Anders *et al.*, 2012; Zhong *et al.*, 2018b). Other GT61 members possess xylosyltransferase activity. Rice xylosyl arabinosyl substitution of xylan 1 (*OsXAX1*) mediates the addition of xylose to arabinose units (Xylp-1,2- β -Araf) (Chiniquy *et al.*, 2012), while rice xylan xylosyltransferase 1 (*OsXYXT1*) adds xylose sidechains to the xylan backbone (Xylp-1,2- β -Xylp)(Zhong *et al.*, 2018b). While much of our understanding of heteroxylan

synthesis comes from rice, a number of *B. distachyon* saccharification mutants identified from a sodium azide mutant population are candidates for characterizing heteroxylan synthesis (Dalmais *et al.*, 2013). The *sac1* GT61 mutant in *B. distachyon* has a phenotype similar to rice mutant *OsXAX1* (Marriott *et al.*, 2014). In *sac1*, plants have reduced xylose content, suggesting that the GT61 candidate, like *OsXAX*, mediates the incorporation of this saccharide component into the wall.

The presence of glucuronic acid (GlcA) side chains differentiates heteroxylans into glucuronoarabinoxylans and arabinoxylans. In *A. thaliana*, GlucUronic acid substitution of Xylan (AtGUX)-1 adds GlcA at evenly spaced intervals of 8-10 xylose residues, although greater spacing has been observed. AtGUX2 appears to preferentially add GlcA more frequently, at 5-7 residue intervals without regard for even spacing (Bromley *et al.*, 2013). The evenly spaced xylan regions form the major xylan domain, and the less organized GlcA spacing populates the minor domain. The major domain has been shown to interact with cellulose microfibrils, an interaction that is also mediated by xylan acetylation. Similar GUX function has yet to be observed in grasses, but presumably a mechanism for adding GlcA to heteroxylan exists. Additionally, 4-O-methylation of GlcA by AtGXMT (glucuronoxylan methyltransferase), a DUF579 protein, has been characterized in *A. thaliana*, but not in any grasses to date (Urbanowicz *et al.*, 2012). The addition of GlcA and its methylation have been implicated in eudicots in mediating xylan interaction with other wall polymers, and this phenomenon is ripe for investigation in grasses.

1.6 Xylan acetylation

Xylan acetylation has long been observed, but only recently has the role of these modifications been revealed. In *A. thaliana*, recent work has shown that acetylation pattern influences xylans-cellulose interaction. Regularly spaced acetylation on every other xylose monomer in regions of the xylan backbone results in the polymer forming a two-fold helix that closely bonds with the hydrophilic side of cellulose microfibrils (Busse-Wicher *et al.*, 2014). The modification of xylan with acetate has strong implications for the solubility of the polymer, as well as the strength of xylan-cellulose interactions. Xylan-O-acetyltransferases (XOATs) are DUF231 family proteins, and carry out 2-O- and 3-O-monoacetylation and 2,3-di-O-acetylation (Fig. 1.4). In *A. thaliana*, 9 XOATs have been identified and genetically characterized, including the Trichome Birefringence protein, TBR-like proteins, and ESKIMO1 (Zhong *et al.*, 2017). In grasses, there has been an expansion of the DUF231 XOATs, with rice containing 14 members. *OsXOAT1* and *OsXOAT7* complement the *A. thaliana esk1* xylan acetylation mutant, and all 14 rice XOATs can acetylate xylohexose *in vitro* (Zhong *et al.*, 2018a)

While the degree of xylan acetylation has been shown to play a critical role in wall integrity, evidence of deacetylation activity has not yet been shown in eudicots.

However, *rice brittle sheath 1 (OsBS1)* encodes a GDSL lipase/esterase that functions as an acylesterase in the Golgi, removing acetyl groups from xylans (Zhang *et al.*, 2017).

Mutation in *OsBS1* results in greater 2-O and 3-O-acetylation, which compromises secondary wall patterning and integrity.

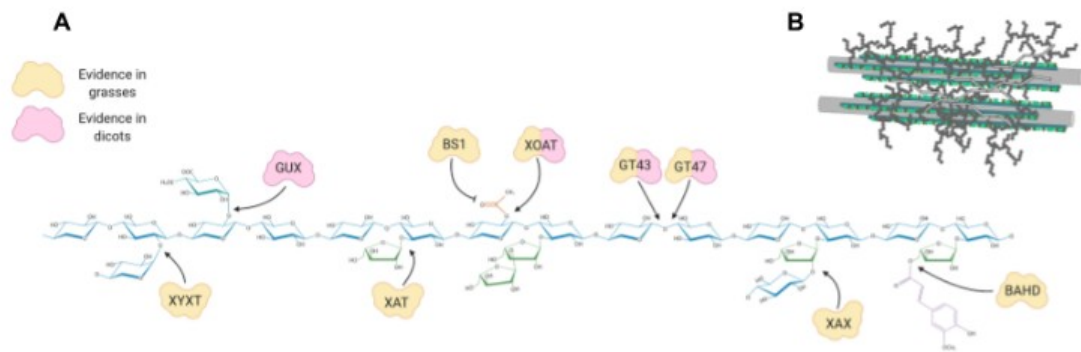


Figure 1.4. Grass heteroxylan structure. (a) Fine structure of heteroxylan and biosynthetic enzymes. The major non-cellulosic polysaccharides in grasses are xylans. A xylose (blue) backbone is decorated with side chains of xylose, arabinose (green), glucuronic acid (teal), and ferulic acid (purple). The enzymes responsible for forming certain linkages on the heteroxylan polymer are depicted in either yellow, pink, or both, having been characterized respectively in grass systems, eudicots, or showing conserved function. (b) Miniature of Fig 1a cell wall schematic highlighting the heteroxylan component.

1.7 Lignins

Lignins are large phenolic polymers mainly deposited in the primary and the secondary cell wall of xylem and sclerenchyma cells. These polymers provide the hydrophobicity and mechanical properties necessary for the development of land plant vasculature.

Lignins embed polysaccharides in the cell wall and are a major barrier for biomass usages such as saccharification for biofuel production (Marriott *et al.*, 2014). Unlike other wall polymers, lignins contain many types of inter-unit bonds (aryl beta-aryl ether, phenyl coumaran, resinol, biphenyl) randomly formed during polymerization, some being more (C-C) or less (C-O-C) resistant to degradation (Mnich *et al.*, 2020). Consequently, lignin structure is not predictable, although the abundance of each monomer seems to influence the occurrence of certain linkages (Stewart *et al.*, 2009).

Lignins are synthesized from three monolignols, *p*-coumaryl alcohol, coniferyl alcohol, and sinapyl alcohol, that differ by their degree of methoxylation. Once incorporated into lignin polymers, these phenolics give rise to *p*-hydroxyphenyl (H), guaiacyl (G), and syringyl (S) units, respectively. In *B. distachyon* stems, lignin content accounts for 18-25% of the dry cell wall residue, and in the wild-type Bd21-3 accession, stem lignin is comprised of about 62% S, 34 % G, and 4 % H units (Bouvier d'Yvoire *et al.*, 2013; Trabucco *et al.*, 2013b). Within the grasses, *B. distachyon* has one of the highest proportions of S units reported (Clarke *et al.*, 1933; Méchin *et al.*, 2014; Herbaut *et al.*, 2018).

Lignin biosynthesis results from a branch of the phenylpropanoid pathway and has long been thought to rely on the aromatic amino acid L-phenylalanine (L-Phe) as a starting substrate (Fig. 5). The standard convention in most studied plant systems has been that L-Phe is first deaminated by phenylalanine ammonia lyase (PAL), yielding cinnamate, which is then C4-hydroxylated by coumarate-4-hydroxylase (C4H) to make coumarate. Coumarate is a common branch point for all three main monolignols. However, this conventional pathway has recently been challenged by work in *B. distachyon* demonstrating that L-tyrosine (L-Tyr) can also serve as an initial substrate for lignin synthesis as it already contains a C4 hydroxylation. Indeed, tyrosine ammonia lyase (TAL) activity in grasses (Higuchi *et al.*, 1967) suggests that C4H activity can be bypassed to produce coumarate (Fig. 1.5). In grasses, PAL and TAL activities are controlled by the same protein, but clear evidence for a genuine PTAL activity in the phenolic pathway was poorly documented until recently. In plants expressing a *BdPAL* RNAi

hairpin construct to knock down expression of multiple *BdPAL* genes, both PAL and TAL activities were affected and plants contained 43% less lignin (Cass *et al.*, 2015; Barros *et al.*, 2016). Only one predicted PTAL (PTAL1) was identified in this family and nearly half of the total lignin deposited in *B. distachyon* occurs via TAL activity (Barros *et al.* 2016). Interestingly, *BdPTAL1* is mainly involved in the biosynthesis of S units and cell wall linked coumarates, with less effect on G units as revealed by plants fed with C13-labelled L-Phe or L-Tyr. A biological role for PTAL has only been shown in *B. distachyon* to date, but putative orthologs to *BdPTAL1* have been identified in several other grasses (Barros *et al.* 2016). Further characterization is needed to confirm whether this alternate initiation of lignin synthesis is shared broadly amongst grasses, or indeed present in other groups.

Other recent discoveries are further changing our understanding of lignin biosynthesis in grasses. Very recently, (Barros *et al.*, 2019) proposed that a cytosolic ascorbate peroxidase with genuine 4-coumarate 3-hydroxylase (C3H) activity oxidizes coumarate into caffeate in the phenylpropanoid pathway. Decreased expression of this novel C3H in *B. distachyon* results in significantly reduced lignin content and structure. This “acid” route to caffeic acid and thus to caffeoyl CoA through the activity of 4-hydroxycinnamate:CoA ligase (4CL) would be complementary to the C3’H pathway where 4CL, 4-hydroxycinnamoyl CoA:shikimate / quinate hydroxycinnamoyltransferase (HCT), 4-coumaroyl shikimate/quinate 3’-hydroxylase (C3’H), function sequentially to convert coumarate to caffeoyl CoA (Fig. 5). Feruloyl-CoA produced by the methoxylation of caffeoyl CoA by Caffeoyl CoA O-methyl transferase (CCoAOMT) is a

substrate of cinnamoyl-CoA reductase (CCR). The proposition of an alternate “acid” route to monolignol synthesis is not new, and but the discovery of a cytosolic ascorbate peroxidase with 4-coumarate 3-hydroxylase activity *in planta* was lacking until now. Interestingly, Barros et al. 2019 showed this is not unique to grasses, as the null allele of the *Arabidopsis* C3H ortholog is lethal. The lignin pathway that involves the membrane bounded C3H also plays a critical role in grass lignin synthesis. Indeed, C3H knockout rice mutants were severely affected in their development and displayed typical C3H phenotypes with lignins largely enriched in H units at the expense of G and S units (Takeda *et al.*, 2018). Interestingly, caffeoyl shikimate esterase (CSE) activity was not detected in *B. distachyon* stem crude extract and this result is supported by the absence of close orthologs of *AtCSE* in *B. distachyon* (Ha *et al.*, 2016). CCR is a cornerstone step to monolignol biosynthesis. CCR activity converts CoA-conjugated intermediaries into the aldehyde precursors of monolignols. While *ccr* mutants with decreased lignin and increased monolignol conjugates were studied in maize there are no reports on cell wall properties of CCR deficient lines in *B. distachyon* (Tamasloukht *et al.*, 2011; Cass *et al.*, 2015).

The last enzyme in the monolignol pathway, the cinnamyl alcohol dehydrogenase (CAD) reduces cinnamaldehyde into alcohols. Mutants and transgenics lines affected in CAD have been well characterized in *B. distachyon* (Bouvier d’Yvoire *et al.*, 2013; Trabucco *et al.*, 2013b). Lignin content of *Bdcad1* mutants was drastically enriched in aryl β -aryl ether and diaryl ether-coupled S units, as well as resistant inter-unit bonds and free phenolic groups, a result previously observed in maize and sorghum *brown-midrib*

mutants (Pillonel *et al.*, 1991; Barriere *et al.*, 2004). By contrast, there was little increase in coniferaldehyde-end groups in the *Bdcad1*, suggesting that another CAD gene specific to coniferyl alcohol is involved in lignification. As observed in CAD-deficient eudicot plants, sinapic acid esters linked to the cell wall were detected in *Bdcad1* (Bouvier d'Yvoire *et al.*, 2013).

As stated above *B. distachyon* lignin is relatively enriched in S units. Their precursor, sinapyl alcohol is produced through the C5 hydroxylation of coniferaldehyde by the P450 enzyme ferulate-5-hydroxylase (F5H) and methoxylation by caffeoyl-*O*-methyl transferase (COMT). When *F5H* was overexpressed in *B. distachyon*, cell wall analysis revealed an average increase of 25% in the content of S units in these lines, leading to an increase in S/G ratio from 2.3 in wild type to 8.1, with a modest increase of 5 hydroxy guaiacyl units and 30% higher saccharification yield (Sibout *et al.*, 2017). Several *B. distachyon* mutants affected in COMT activity were identified in a sodium azide-induced mutant collection by TILLING (Dalmais *et al.*, 2013). As observed in maize *comt* mutants, *B. distachyon* mutants showed the accumulation of 5-OH-G units in their lignin and significantly altered lignin content, (Piquemal *et al.*, 2002; Bouvier d'Yvoire *et al.*, 2013; Dalmais *et al.*, 2013; Trabucco *et al.*, 2013b).

Once exported into the apoplast by an unknown mechanism, monolignols are oxidized by peroxidases and/or laccases (Vanholme *et al.*, 2012; Wang *et al.*, 2013; Perkins *et al.*, 2019; Vermaas *et al.*, 2019). Laccases are multi-copper oxidases that use oxygen as an electron acceptor, while peroxidases use H₂O₂. Once oxidized, the monolignols radically

polymerize into the branched lignin polymer with multiple bond types resulting from the various positions of the oxygen radical on the monolignol subunit. There are 17 laccases in *A. thaliana* and 29 in *B. distachyon* (Berthet *et al.*, 2011; Le Bris *et al.*, 2019). *B. distachyon* LACCASE 5 and 8 were identified as orthologs of *AtLAC17* and were shown to be responsible for lignification in interfascicular fibers (Wang *et al.*, 2015; Le Bris *et al.*, 2019). A laccase gene from sugarcane (*SofLAC*) also genetically complemented an *A. thaliana lac17* mutant (Cesarino *et al.*, 2013). Lignin content decreased by 30% in the double *lac5lac8* mutant, and saccharification increased by 140% compared to the wild type. Lignin deposition was less affected in vascular bundles compared with fibers suggesting that different laccases or peroxidases are recruited for lignification of these tissues.

1.8 Hydroxycinnamic acids

The presence of hydroxycinnamic acids, namely ferulic acid (FA) and *p*-coumaric acid (*p*CA), in the cell wall is a defining feature of grass secondary cell walls (Ralph *et al.*, 1994; Hatfield *et al.*, 2009). FA is predominantly linked to heteroxylan through an ester bond. The oxidation of FA in the cell wall, probably by peroxidases, generates esterified dehydrodiferulates which serve as linkages between two arabinoxylan polymers. In lignified tissues, xylan-esterified ferulates can be etherified to G units of lignin and thus serve as a covalent linkage between hemicelluloses and lignins (Hatfield *et al.*, 2016; Lapiere *et al.*, 2019). An esterified ferulate on arabinoxylan is considered as a nucleation site of lignification in grasses and thus an important mechanism for cell wall reinforcement (Ralph *et al.*, 1995, 1998). *p*CA is esterified on arabinoxylan to a lesser

extent than FA and tends to be found esterified to S units in *B. distachyon* lignins. Plant-specific acyl-CoA dependent acyltransferases of the BAHD (BEAT, AHCT, HCBT, and DAT) family are the enzymes responsible for the acylation of the arabinose side chains of heteroxylans and monolignols with hydroxycinnamates (D'Auria, 2006; Mitchell *et al.*, 2007). An expanded grass-specific BAHD clade (also called the "Mitchell clade") was identified by bioinformatic analysis in rice as candidates for hydroxycinnamate transfer (D'Auria, 2006; Mitchell *et al.*, 2007; Bartley *et al.*, 2013). Consequently, BAHD enzymes with feruloyl transferase activity were first explored in rice and have also been investigated in *B. distachyon* (Piston *et al.*, 2010; Bartley *et al.*, 2013). BAHD01 in *B. distachyon* and *Setaria viridis* appear to be involved in feruloylation of arabinoxylans (de Souza *et al.*, 2018). Downregulation of *SvBAHD01* significantly reduced FA on arabinoxylan, with an increase in *pCA-Araf* acylation and no substantial change in lignin content while in *B. distachyon* only a moderate decrease in FA-arabinoxylan was observed (de Souza *et al.*, 2018). Interestingly, *BdBAHD01* downregulation lines showed increased saccharification efficiency, despite unchanged lignin content, highlighting the role of FA in maintaining cell wall integrity. Overexpression of *BdBAHD05* (also called *BdAT1*) caused a moderate increase in FA content and downregulation showed a moderate decrease (Buanafina *et al.*, 2016; de Souza *et al.*, 2018). Analysis in sugarcane revealed six *BAHD* genes, one of which is homologous to *SvBAHD01*, and downregulation of *SacBAHD01* similarly reduced stem FA content and increased biomass digestibility (de Souza *et al.*, 2019).

FA acylated monolignols were detected in several species, including willow (*Salix* sp.) and poplar (*Populus trichocarpa*), although in much lower amounts than *pCA* acylated

monolignols in grasses (Karlen *et al.*, 2016). In rice, feruloyl monolignol transferase (OsFMT) was identified through homology with other BAHD acyltransferases that act on monolignols (Wilkerson *et al.*, 2014; Karlen *et al.*, 2016). *OsFMT* overexpression resulted in higher levels of FA on lignin. FA from heteroxylan, released through mild alkaline hydrolysis, was unchanged by altered *OsFMT* expression. Furthermore, there was no change in the levels of *pCA* acylated monolignols, suggesting specificity of this enzyme for monolignol feruoylation.

In *B. distachyon*, *p*-coumaryl-CoA:monolignol transferase (PMT) acylates lignin with *pCA*, but not heteroxylan (Petrik *et al.*, 2014). While OsPMT has a high affinity for coumaryl alcohol *in vitro*, BdPMT preferentially acylates sinapyl alcohol with *pCA* *in planta* (Withers *et al.*, 2012; Sibout *et al.*, 2016). Lines overexpressing *BdPMT* showed lower total lignin despite an increase of *pCA* content (Petrik *et al.*, 2014). This may be a consequence of redirecting *p*-coumaric acid CoA for acylation rather than monolignol synthesis, or the inhibition of the monolignol polymerization by excessive *p*-coumaroylation (Sibout *et al.*, 2016). Interestingly, when *BdPMT* was overexpressed in *A. thaliana*, which does not natively produce *pCA* acylated lignin, a significant amount of *pCA* was found on lignins (Karlen *et al.*, 2016). More surprising, when *BdPMT* was expressed under a specific *C4H* promoter in a *ccr* deficient *A. thaliana* mutant background, lignin was esterified with both *pCA* and FA. Mutants in *CCR* accumulate high levels of feruloyl CoA, and BdPMT activity in this mutant suggests that not only is BdPMT functional in eudicots, but it is also able to use feruloyl-CoA as a substrate when available in sufficient quantities (Withers *et al.*, 2012; Sibout *et al.*, 2016). In maize, *ZmPMT* loss-of-function lines had less *pCA* and modified lignin structure, but not

reduced total lignin content (Marita *et al.*, 2014). Overall, BAHD proteins have a related set of functions in decorating cell wall components; feruloylation of arabinoxylan (BAHD01), feruloylation of lignins (FMT), and coumaroylation of lignins (PMT). An enzyme responsible for the coumaroylation of arabinoxylan remains to be discovered.

1.9 Tricin

As evidenced by their *pCA* and FA content, grasses are remarkable in their capacity to incorporate phenolic compounds other than the typical coumaryl, coniferyl, and sinapyl alcohols into lignin. Tricin, an O-methylated flavone, was first characterized in wheat straw lignin (del Río *et al.*, 2012). Tricin is incorporated into grass lignin in varying amounts across grass species, with oat (*Avena sativa*), wheat, and *B. distachyon* straw being particularly enriched in this compound (Lan *et al.*, 2016). Tricin is incorporated in lignin polymers via 4'-O- β coupling (Lan *et al.*, 2018). Biomimetic radical coupling reactions give evidence that triclin may serve as a possible nucleation site for lignification, as has been suggested for ferulate (Ralph *et al.*, 1995, 1998; Lan *et al.*, 2015). Tricin and monolignols come from two different branches of the phenylpropanoid pathway, and consequently their synthesis shares some common enzymes. This is particularly true for enzymes involved in the metabolic flux upstream of *p*-coumaric acid synthesis.

CHALCONE SYNTHASE, a pivotal enzyme for flavonoids production, uses malonyl-CoA and *p*-coumaryl-CoA as substrates. Silencing this enzyme in maize resulted in strongly reduced levels of apigenin- and triclin-related flavonoids, and also strongly reduced incorporation of triclin into the lignin polymer (Eloy *et al.*, 2017). The impact of the flavonoid pathway on the production of cell wall triclin content was also demonstrated in rice (Lam *et al.*, 2017, 2019). It is also possible that some of the cell wall changes

observed in *BdPMT* overexpression lines may stem from the depletion of *p*-coumaroyl-CoA pool, as both chalcone synthase and PMT act on this substrate. O-methyltransferases involved in the O-methylation of 5-hydroxy-coniferaldehyde to produce sinapyl alcohol were also shown to be involved in the methylation of triclin in rice, maize, and sorghum (Fornalé *et al.*, 2017; Eudes *et al.*, 2017; Lam *et al.*, 2019). The bi-functionality of COMT in the lignin and flavonoid pathways is not unexpected since an COMT involved in lignification of *A. thaliana* stems also O-methylates isorhamnetin, a flavonoid structurally similar to triclin (Do *et al.*, 2007). There is now abundant evidence that other molecules, called “nontraditional monomers” like triclin or hydroxycinnamic acids, can be incorporated into the lignin polymer (del Río *et al.*, 2018; Vanholme *et al.*, 2019). The biological role of these novel lignin components remains to be determined.

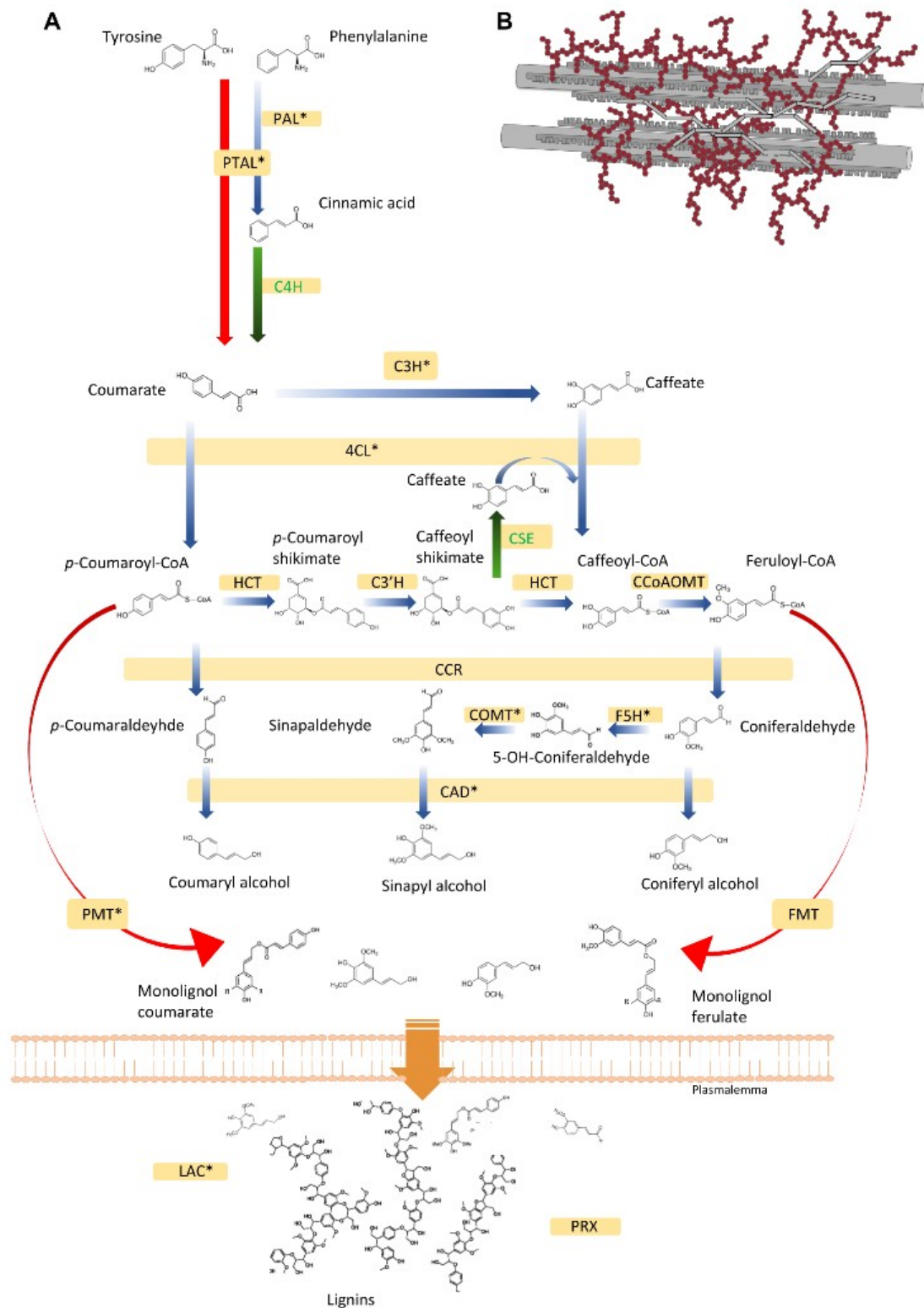


Figure 1.5. Alternative routes to lignin biosynthesis. (a) In some grasses, phenylalanine tyrosine ammonia lyase (PTAL) can bypass cinnamic acid 4-hydroxylase (C4H) activity and thus directly produce p-coumarate from tyrosine.

An ascorbate peroxidase-like gene with coumarate 3-hydroxylase (C3H) activity can directly synthesize caffeate from coumarate. Red arrows illustrate a grass specific lignin pathway unique from other lignin pathways identified in most studied eudicots. Green arrows show routes potentially bypassed or absent in *B. distachyon*, such as caffeoyl shikimate esterase (CSE). Blue arrows are paths believed to be common to eudicots and grasses. Asterisks highlight enzymes characterized in *B. distachyon*. The mechanism for monolignol export across the plasma membrane remains unclear. Phenylalanine ammonia lyase (PAL), , 4-hydroxycinnamoyl CoA ligase (4CL), hydroxycinnamoyl CoA:shikimate hydroxycinnamoyl transferase (HCT), p-coumaroyl shikimate 3'-hydroxylase (C3'H), , caffeoyl CoA O-methyltransferase (CCoAOMT), hydroxycinnamoyl CoA reductase (CCR), ferulic acid 5-hydroxylase (F5H), caffeic acid/5-hydroxyferulic acid O-methyltransferase (COMT), cinnamyl alcohol dehydrogenase (CAD), laccase (LAC), peroxidase (PRX). R- in the monolignol hydroxycinnamics could be substituted by a hydrogen or methyl group. (b) Miniature of Fig 1a cell wall schematic highlighting the lignin component.

1.10 Silicon

Poaceae accumulate high quantities of silicon in the cell wall of their shoots. This phenomenon is particularly remarkable in rice (Ma & Yamaji, 2006). The main role of silicon is to provide plant resistance to many biotic and abiotic stresses (Hattori *et al.*, 2005; Deshmukh *et al.*, 2017). However, silicon may interact with polysaccharides, which consequently impact plant biomass processing in biorefineries (Perry & Lu, 1992; Kido *et al.*, 2015). For biofuel production, there is a tradeoff between soil amendment with silicon that can increase polysaccharide yield with a negative effect on the conversion of biomass into biofuels (Głazowska *et al.*, 2018b). Silicon content in rice and maize can be modulated by changing the expression of silicon transporters (Ma *et al.*, 2007; Mitani-Ueno *et al.*, 2016; Bokor *et al.*, 2017). The analysis of different silicon transporter mutants showed that silicon availability may impact the morphology and patterning of stem and leaf macrohairs (Głazowska *et al.*, 2018b). The *Bd low silicon 1* (*Bdlsi1*) mutant is impaired in silicon transporter function and has reduced silicon uptake, with 93% less silicon present in the shoot. Mixed-linkage glucan content is drastically

modified in *Bdlsi1* ((Kido *et al.*, 2015; Głazowska *et al.*, 2018a). This result is in agreement with previous studies suggesting that (1;3,1;4)- β -glucan is involved in silicon-dependent strengthening of the rice cell wall (Kido *et al.*, 2015). The *Bdlsi1* mutant also displayed an altered degree and pattern of homogalacturonan methyl esterification. Despite the relatively low amount of pectins found in grasses, this change in homogalacturonan represents a significant alteration to the wall matrix. Lastly, *Bdlsi1* mutant FA extractability was lower with only minor changes in lignin content (Kido *et al.*, 2015; Głazowska *et al.*, 2018a). These data highlight the important role silicon plays in cell wall integrity in *B. distachyon* and grasses in general, and presents interesting avenues for further study.

1.11 Transcriptional regulation of secondary cell wall thickening

Canonical transcription factors that directly bind DNA play a prominent role in the regulation of plant secondary cell wall thickening. The *cis*-regulatory regions of genes associated with cellulose, hemicellulose, and lignin biosynthesis interact directly with numerous MYB and NAC family transcription factors (Fig. 6)(Nakano *et al.*, 2015). Many of the R2R3-MYB protein family subgroups appear to bind a similar sequence motif, the AC element, also known as the M46RE (MYB46 responsive *cis*-regulatory element) and the SMRE (secondary wall MYB-responsive element) (Kim *et al.*, 2012; Zhong & Ye, 2012; Zhao & Bartley, 2014; Handakumbura *et al.*, 2018). In *A. thaliana*, *AtMYB46* and the close paralog *AtMYB86* activate the expression of cellulose, hemicellulose, and lignin biosynthetic genes, as well as other MYBs capable of activating secondary cell wall related genes (Zhong *et al.*, 2007b; Zhong & Ye, 2007). Some of the

downstream MYB activators, among them *AtMYB58/63* and *AtMYB42/85*, activate only lignin genes (Rao & Dixon, 2018; Zhang *et al.*, 2018a). However, in sorghum, rice, and switchgrass (*Panicum virgatum*), ectopic expression of *OsMYB58/63*, *PvMYB58/63*, and the sorghum ortholog *SbMYB60* results in the activation of cellulose and hemicellulose genes as well as lignin (Noda *et al.*, 2015; Scully *et al.*, 2016; Rao *et al.*, 2019). A potential ortholog to *OsMYB42/85*, *ZmMYB167*, was overexpressed in maize and heterologously in *B. distachyon* to similar effect (Bhatia *et al.*, 2019). Similar functions have been resolved for the *A. thaliana* and rice orthologs *AtMYB61* and *OsMYB61* as well as *AtMYB103* and *OsMYB103* (Hirano *et al.*, 2013; Huang *et al.*, 2015; O'Malley *et al.*, 2016; Zhao *et al.*, 2019). These downstream MYBs bind the AC element and activate both lignin and wall polysaccharide biosynthesis genes. Overall, there are few distinctions in the transcription factor targets for these genes between grasses and *A. thaliana*. Those that have been observed may be the outcome of low-resolution experimental designs that sample one tissue type at one time point for a limited number of outputs.

The expression of cell wall associated genes is often highly correlated (Brown *et al.*, 2005a; Persson *et al.*, 2005). Co-expression analysis of a *B. distachyon* gene expression atlas resolved a cluster of 96 genes that is enriched for cell wall biosynthetic processes with numerous cellulose, hemicellulose, and lignin associated genes (Sibout *et al.*, 2017). Among the identified genes, two primary and two secondary wall *CESAs*, as well as *COBRA*, *KORRIGAN*, *CS11*, *CSLF2*, numerous glycosyltransferases and glycosylhydrolases, fasciclin-like family, and numerous lignin associated genes. The

MYB transcription factor *SECONDARY WALL ASSOCIATED MYB 1* (*SWAM1*) is one of two canonical transcription factors that are part of the wall gene enriched cluster, making it a candidate for a regulator of genes in the cluster (Fig. 6). Similarly, analysis of *B. distachyon* leaf, root, and stem microarray gene expression data identified *SWAM1/2/3* and MYBs that are part of six other prominent subgroups orthologous to *AtMYB46/83*, *AtMYB103*, *AtMYB58/63*, *AtMYB52/54*, *AtMYB42/85*, and *AtMYB4/32* that are highly correlated with secondary *CESA* and lignin biosynthetic gene transcriptional targets (Handakumbura *et al.*, 2018). Interestingly, the *SWAM1* gene and its two closest homologs, *SWAM2* and *SWAM3*, are conspicuously absent from genomes in the *A. thaliana* family Brassicaceae but present in other eudicots and monocots (Handakumbura *et al.*, 2018). Like the other described secondary cell wall regulating R2R3-MYBs, *SWAM1* interacts with the AC element and is an activator of secondary cell wall genes. Based on amino acid similarity with characterized genes in other systems and their expression pattern, all of the *B. distachyon* identified MYBs are excellent candidates for a role in cell wall biosynthesis.

The same promoters that interact with the secondary cell wall regulating MYB transcription factors often interact with NAC transcription factors collectively referred to as the *SWN* (*SECONDARY WALL NACs*) or the *VNS* (*VND*, *NST/SND*, *SMB* related) (Ohtani *et al.*, 2011; Zhong *et al.*, 2011). This group of proteins are generally classified into four clades, all binding the similarly named VNS element in *in vitro* assays (O'Malley *et al.*, 2016; Olins *et al.*, 2018), which is consistent with independently identified TERE and SNBE binding sites for the same proteins (Pyo *et al.*, 2007; Valdivia

et al., 2013). In *A. thaliana*, three of the clades that include the *VASCULAR-RELATED NAC-DOMAINS* (*VND*s), activate cell wall thickening directly and by activating the previously described downstream MYBs (Kubo *et al.*, 2005). The *VND*s can induce vascular cells differentiation, induce further thickening, and initiate programmed cell death (Kubo *et al.*, 2005; Zhong *et al.*, 2008b). They function in xylem rather than fibers where thickening is activated by the clade IV NACs: *NAC SECONDARY WALL THICKENING FACTOR 1* (*NST1*), *NST2*, and *NST3* (also known as *SECONDARY WALL-ASSOCIATED NAC-DOMAIN PROTEIN 1* (*SND1*)) (Zhong *et al.*, 2006a; Mitsuda *et al.*, 2007). Uniquely, programmed cell death is not activated by clade IV NACs. Such cell type specific functions have not been resolved in grasses. The function of the *SWNs* is well conserved between *A. thaliana* and grasses where grass genes can complement mutants in *A. thaliana* (Zhong *et al.*, 2011, 2015; Rao *et al.*, 2019). In *B. distachyon*, members of all four clades induced the formation of secondary walls when ectopically expressed in tobacco leaves and the *VND*-type *SWNs* also activated programmed cell death (Valdivia *et al.*, 2013). Together with the MYBs, the NACs form feed-forward loops (Nakano *et al.*, 2015; Taylor-Teeples *et al.*, 2015). In general, all of the transcription factor proteins can bind to genes that encode cell wall structural enzymes and they also have the function of activating other activating transcription factors.

The finger like protuberance formed by a zinc-finger protein domain can interact with DNA, RNA, and proteins. Tandem CCCH zinc finger (TZF) proteins modulate gene expression transcriptionally by interactions with DNA or post-transcriptionally by interactions with mRNA (Bogamuwa & Jang, 2014). *A. thaliana C3H14* is a direct

activator of lignin, cellulose, and hemicellulose biosynthesis genes and may be a repressor of MYB cell wall activators (Ko *et al.*, 2009; Kim *et al.*, 2012). On the other hand, the *INDETERMINATE* family C2H2-type zinc finger transcription factor in rice, OsIDD2, interacts with the ID motif to repress the expression of lignin associated genes (Huang *et al.*, 2018). Analysis of mutants and transgenic plants suggests that OsIDD2 directly represses lignin associated gene expression and indirectly secondary wall *CESA* genes. By yet another possible mechanism of gene regulation, the rice TZF protein ILA1-interacting protein 4 (IIP4) functions as a repressor of secondary wall thickening through protein-protein interaction with OsSWN2 (NAC29) and SWN3 (NAC31) (Zhang *et al.*, 2018b). The association with the SWNs is attenuated by phosphorylation of IIP4 protein, which results in translocation to the cytosol. Thus, zinc-finger proteins influence the thickening of grass secondary walls through multiple mechanisms.

While the regulatory network is dominated in number by MYB and NAC transcription activators, several repressors have also been described; namely TALE (Three Amino acid Loop Extension), zinc-fingers, HD-ZIP III, WRKY, LATERAL ORGAN BOUNDARY (LBDs) and some MYBs. Among the many types of cells that do not have secondary cell walls are pith, which reside inside the stem and among the cells in the plant with the thickest walls. A WRKY transcription factor, *WRKY12*, is a repressor of wall thickening in pith and other cells. It can directly bind the promoters of *AtNST2* and poplar *C4H* and broadly repress wall thickening in *A. thaliana*, poplar, and switchgrass (Wang *et al.*, 2010; Yang *et al.*, 2016; Rao *et al.*, 2019). The five class III HD-ZIPs in *A. thaliana* (*REVOLUTA*, *PHABULOSA*, *PHAVOLUTA*, *CORONA*, and *HB8*) and some orthologs in

poplar have been shown to play a role in cambium cell initiation and vascular bundle organization (Floyd & Bowman, 2006). However, to our knowledge, there are no reports describing a function for this group of genes in grasses. Several LBD family transcription factors, *AtLBD15/18/30*, can activate the expression of *AtVND7* and induce wall thickening and differentiation into tracheary cells (Soyano *et al.*, 2008; Ohashi-Ito *et al.*, 2018). *AtLBD29*, on the other hand, is a repressor of stem secondary wall thickening and is activated by the phytohormone auxin (Lee *et al.*, 2019a). Repression is also supplied by the MYB G4 clade and are the best characterized in grasses. These include *ZmMYB11/31/42*, *PvMYB4/32*, and *OsMYB108*, which are orthologous to *AtMYB4/32* (Zhao & Bartley, 2014; Rao & Dixon, 2018; Miyamoto *et al.*, 2019). These were first described in a grass as direct repressors of lignin gene expression (Fornalé *et al.*, 2006; Sonbol *et al.*, 2009). In switchgrass, *PvMYB4* is a direct repressor of lignin associated genes (Shen *et al.*, 2012; Rao *et al.*, 2019). The MYB31/42 MYBs in sorghum, rice, and maize directly bind to the *cis*-regulatory regions of various lignin biosynthetic gene, but there appears to be variation in phenylpropanoid gene expression and protein-DNA interactions across species (Agarwal *et al.*, 2016). Wounding induced lignification occurs in maize by the degradation of *ZmMYB11/31/42* protein and a protein interacting partner *ZML2* (Vélez-Bermúdez *et al.*, 2015). Thus, wounding and the subsequent activation of MeJA signaling will remove MYB G4 clade repression in maize and induce lignin gene expression. The repressing MYB G4 clade interacts with AC-like sequence motifs, similar to the wall activating MYBs (Fornalé *et al.*, 2010; Shen *et al.*, 2012; Agarwal *et al.*, 2016). The exact targets of the phenylpropanoid pathway vary across system and study, which suggests there may be some transcription factor sub-functionalization.

Members of two different classes of the TALE super family, KNOX and BEL, have been shown to regulate secondary wall synthesis. The class II KNOX gene *KNOTTED OF ARABIDOPSIS THALIANA 7* (*AtKNAT7*) was initially identified as an irregular xylem mutant (*irx11*) (Brown *et al.*, 2005a). *KNAT7* orthologs are generally described in the literature as repressors, and while there is substantial evidence for this, there are also some outstanding issues raised by data indicating a role as an activator of wall deposition. *Atknat7* mutants have thicker interfascicular fiber walls, as expected for a repressor mutant, but this mutant also shows collapsed xylem (Brown *et al.*, 2005a; Li *et al.*, 2012). *Atknat7* mutants have greater lignin content, but reduced xylan, suggesting that *AtKNAT7* may differentially regulate aspects of wall polymer synthesis. In conflicting reports, one group has shown xylan biosynthetic genes upregulated in *Atknat7* lines, while another shows downregulation (Li *et al.*, 2012; He *et al.*, 2018). *AtKNAT7* protein can bind to the *AtIRX9* promoter, a gene responsible for xylan backbone synthesis.

The rice ortholog of *KNAT7*, *OsKNOR1* (also known as *OsKNAT7*), can negatively regulate cell wall synthesis in interfascicular fiber cells (Zhao *et al.*, 2019; Wang *et al.*, 2019). *Osknor1* mutants have thicker interfascicular fiber walls, with no reported xylem phenotype. However, *OsKNOR1* analysis revealed other functions unique to *AtKNAT7* (Wang *et al.*, 2019). *OsKNOR1* protein interacts with *OsSWN3* (also known as *OsVND7* and *OsNAC31*) and *OsGRF4* proteins and transient gene expression analysis showed that *OsKNOR1*-*OsSWN3* jointly regulated *OsMYB61* and *OsMYB103* expression, with the addition of *OsKNOR1* reducing the positive regulation of *OsSWN3* targets. Similarly,

OsGRF4 is known to activate expression of expansin genes *OsEXPB3*, *OsEXPB17*, and *OsEXPA6*, and addition of *OsKNOR1* also repressed that effect. This suggests that *OsKNOR1* regulates wall thickening and cell expansion by decreasing the transcriptional activation of *OsSWN3* and *OsGRF4*, respectively. This was validated by the observation of wall thickening in stem internodes and cell elongation along the panicle in relation to the expression of *OsKNOR1*, *OsSWN3*, and *OsGRF4* (Wang *et al.*, 2019).

Among the genes co-expressed with *B. distachyon* *CSLF6*, a predominant MLG synthase, was a trihelix family transcription factor (*BdTHX1*) (Kim *et al.*, 2018; Fan *et al.*, 2018). This is the first THX protein associated with cell wall biosynthesis and the first shown to bind directly to a *CSLF* gene. *In planta* and *in vitro* assays showed that *BdTHX1* protein binds to the GT element in the second intron of *BdCSLF6* and the 3' region of glycoside hydrolase family 61 endotransglucosylase/hydrolase 8 (*BdXTH8*), a grass-specific enzyme that uses MLG as a substrate (Fan *et al.*, 2018). Attempts to recover viable transgenic plants were unsuccessful and suggest a strong selection against the perturbation of *BdTHX1*; thus, it is uncertain if it is a transcriptional activator or repressor.

The presence of phytohormone gibberellin results in the induction of secondary wall CESA genes in rice, and *OsMYB103* is necessary for that activation (Ye *et al.*, 2015). Similarly, the function of *OsSWN2* (also known as *OsNAC29*) and *OsSWN3* protein can be activated by gibberellins. The mechanism for activation is to degrade a protein interaction with the rice DELLA protein SLENDER RICE1 (*SLR1*) (Huang *et al.*, 2015).

SLR1 protein is degraded in the presence of gibberellins and subsequently, wall gene expression is activated (Fig. 5). A similar mechanism for gibberellin signaling in eudicots has not been reported and the role of hormone in the regulation of wall thickening is not well resolved.

There is nearly complete overlap between the regulatory network components between eudicots and grasses. The distinctions between grass and eudicot walls are difficult to assign to differences in varying functions or members of the regulatory network. While no LBD, BLH, or HD-ZIP III have been described as regulators of cell wall biosynthesis in grasses, it is possible that they have simply not been studied or reported. Additionally, *THX1* is likely unique to grasses since it regulates a hemicellulose gene not present in eudicots. Meta-analysis of microarray gene expression data, to make a combined mutual ranked network for rice and *A. thaliana*, has revealed differences in the relative importance of each regulator (Zhao *et al.*, 2019). The degree of connectivity among genes, which is the number of edges for each network node, can suggest the importance of each transcription factor. Some highly connected genes in *A. thaliana*, including *VND1/2/6/7* and *AtMYB46/83* have a two to five-fold decrease in connectivity in rice. On the other hand, transcription factors with considerably more connections in rice than *A. thaliana* are *OsSND2/3*, the rice ortholog of *KNAT7*, *KNOR1* as well as *OsSWN1*, the ortholog of *AtNST1*.

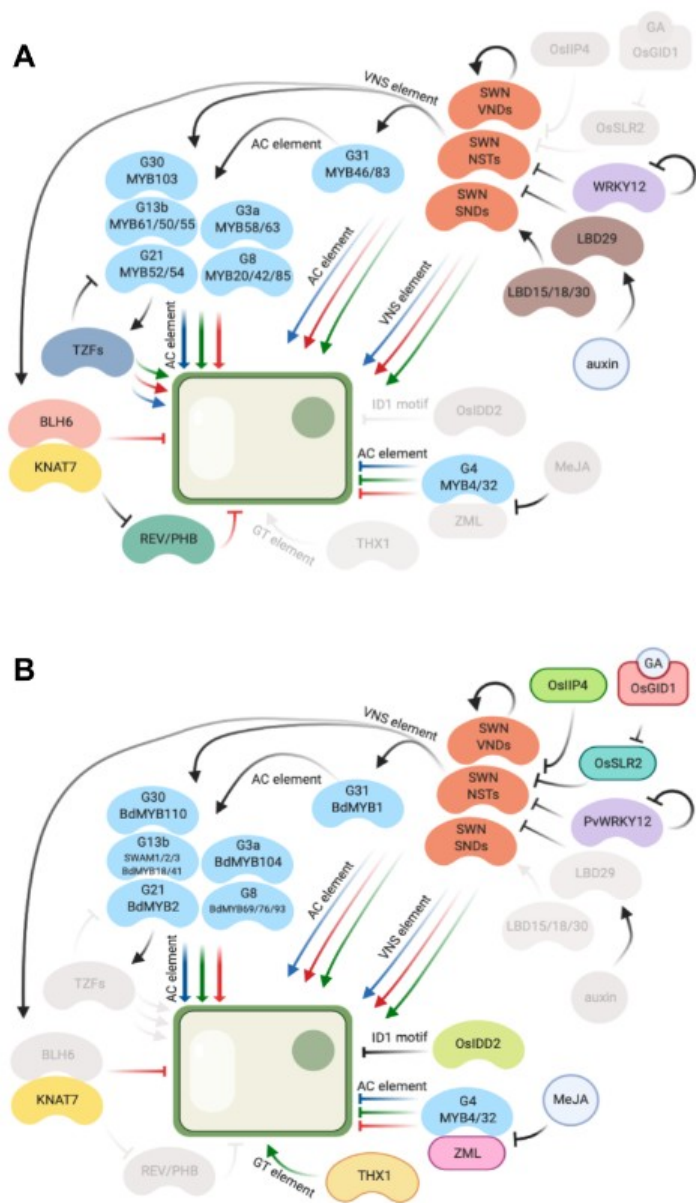


Figure 1.6. Transcriptional regulation of secondary cell wall deposition. Secondary cell wall transcription regulatory network in *A. thaliana* (a) and grasses (b). Bean shape indicates DNA binding transcription factors. Ovals indicate protein interactors. Circles are hormones. Orthology between *A. thaliana* and grasses is denoted by color. Blue, red, and green arrows indicate regulation of cellulose, lignin, and hemicellulose, respectively. Arrows indicate activation and bars repression. Grey shaded items have not been described in both systems.

1.12 Conclusions

Much progress has been made in recent years to better understand grass cell wall composition and regulation, in large part thanks to the numerous genetic and genomic resources that have been developed. A case in point, *B. distachyon* as a model grass system has been central to these efforts, and provides fertile ground for future studies. The unique features of grass cell walls, such as MLG synthesis and the integration of hydroxycinnamates into lignin and xylan are beginning to be uncovered in detail. Elements that were thought to be more common between grasses and eudicots, such as lignin synthesis, continue to show evidence that there is yet unexplored diversity in plant cell wall chemistry, with alternate lignin biosynthetic pathways and atypical monomers components. Regulation remains an area of much overlap, but rather than playing catch-up with eudicots, grass networks now offer new insights of their own that expand the cell wall network. Uncovering grass specific functions, such as *BdTHX1* regulation of MLG, highlight the opportunities to advance this important area of plant biology.

CHAPTER 2

SECONDARY WALL INTERACTING BZIP (SWIZ) IS A TOUCH-SENSITIVE REGULATOR OF PLANT HEIGHT AND CELL WALL THICKENING

2.1 Introduction

2.1.1 Mechanosensing and thigmomorphogenesis

Forces both internal and external to a cell influence growth. Turgor pressure in conjunction with anisotropic cell wall dynamics maintain a cell's physical shape and direction of growth. Force perception between neighboring cells plays a critical role in the development and maintenance of tissue form and function, such as in the lobed, interlocking pavement cells on the leaf epidermis, or the developmental hotspots in the apical meristem (Hamant *et al.*, 2008; Uyttewaal *et al.*, 2012; Bidhendi *et al.*, 2019). Specific inter-cell forces result in dynamic remodelling of the cortical cytoskeleton, with subsequent changes in cellulose microfibril alignment and alterations to other cell wall components such as pectin methyl esterification (Hamant *et al.*, 2008; Uyttewaal *et al.*, 2012; Bidhendi & Geitmann, 2018; Bidhendi *et al.*, 2019; Altartouri *et al.*, 2019). Beyond cell to cell response to force, whole plants perceive and respond to mechanical force through thigmomorphogenesis (Jaffe, 1973; Jaffe *et al.*, 1980, 2002). The classic hallmarks of touch responsive growth include reduced plant height, increased radial growth in plants with a cambial meristem, increased branching, and delayed flowering time (Jaffe, 1973; Braam, 2004). These attributes have been leveraged by farmers for hundreds of years, with the mugifumi tradition documented in Japan in 1680. Farmers tread on young wheat and barley seedlings to elicit increased branching and seedset, along with stronger roots, a practice that still continues today with mechanized rollers

(Iida, 2014). The molecular and genetic mechanisms in plants that perceive and translate force into remain somewhat poorly understood. Touch induced gene expression has been studied for some time, identifying numerous transcripts upregulated by mechanical stimulation. The first *touch-induced (TCH)* genes identified in *A. thaliana* were found to encode calmodulin (*AtTCH1 / AtCaM2*), calmodulin -like proteins (*AtTCH2 / AtCML24*, *AtTCH3 / CML12*), and a xyloglucan endotransglucosylase/hydrolase (*AtTCH4 / AtXTH*) (Braam & Davis, 1990). Subsequent studies identified numerous other genes with touch responsive expression, often showing overlap with induction from other stimuli such as dark, cold, and hormones (Polisensky & Braam, 1996; Lee *et al.*, 2005). Together, around 600 genes were found to be upregulated by touch, primarily coding for proteins involved in calcium binding and signaling, cell wall modification, and a variety of transcription factors and kinases. The nucleus plays a key physical role in mechanoperception (Fal *et al.*, 2017). In animal cells, the nucleus participates in force perception through interactions between the cytoskeleton and nucleoskeleton. Microtubules and actin filaments interact with nuclear membrane Linker of Nucleoskeleton and Cytoskeleton (LINC) complexes, composed of Klarsicht/ANC-1/Syne-1 homology (KASH), and Sad1p and UNc-84 (SUN) domain proteins that internalize force applied to the cytoskeleton to the lamin protein nucleoskeleton (Chambliss *et al.*, 2013; Fal *et al.*, 2017). In this way, forces applied to the exterior of the cell are translated to the nucleus, where modulation of nuclear shape and chromatin structure are related to gene expression events. In plants, similar molecular players have been implicated, but fewer have been experimentally validated. KASH and SUN domain complexes exist in plants, similarly connecting the cytoskeleton and nucleoskeleton (Graumann *et al.*, 2014; Fal *et al.*, 2017).

Mechano-sensitive ion channels are capable of cellular mechanoperception (Monshausen & Haswell, 2013; Leblanc-Fournier *et al.*, 2014; Basu & Haswell, 2017). These membrane embedded complexes dynamically open and close in response to lateral membrane tension, allowing ions to flow across the membrane. When force is applied to a cell, such as through tissue bending or cell expansion, the membrane tension increases and opens the ion channel. These types of mechanically gated signalling events have been best described in animal and bacterial systems, but plants also contain genes encoding similar channels, *AtMCA1&2* and *AtMsl1-10*, that have been implicated in sensing mechanical signals such as gravity, osmotic pressure, pathogen invasion, and touch (Haswell *et al.*, 2008; Peyronnet *et al.*, 2008; Leblanc-Fournier *et al.*, 2014; Hamilton *et al.*, 2015b). *AtMsl* family proteins are localized not only to the plasma membrane, but to mitochondrial and chloroplast membranes as well, and these organelles have been shown to function in mechanoperception signaling and osmotic shock protection (Hamilton *et al.*, 2015a; Lee *et al.*, 2016, 2019b; Basu *et al.*, 2019). The function of these membrane channels strongly implies that ions play a role as mechano-signalling molecules, of which calcium is at the forefront. Cytosolic Ca²⁺ fluxes have been observed in roots following mechanical bending (Monshausen *et al.*, 2009), is required for lateral root formation (Richter *et al.*, 2009), and a maize calcium dependent protein kinase, *ZmCPK11*, has been shown to be activated rapidly following mechanical stimulation (Szczegieliński *et al.*, 2012). Additionally, *AtTCH1*, 2, and 3 are all calmodulin and calmodulin like proteins, rapidly upregulated in expression following touch (Braam & Davis, 1990; Braam, 2004; Lee *et al.*, 2005). Despite these many observations, it is not yet known where Ca²⁺ fluxes originate from or by what mechanism they cross the membrane. The

dynamic control of bioactive cellular gibberellic acid (GA) has been linked to mechanoperception as well as cytosolic calcium levels. GA has also recently been shown to control the cytosolic accumulation of Ca²⁺ following mechanical stress, and perhaps more interestingly, that this Ca²⁺ accumulation occurred even in a *della* quintuple mutant line (Okada *et al.*, 2017). This suggests that GA levels mediate cytosolic calcium flux in response to mechanical stress independent of DELLA mediated pathways. Furthermore, it has been demonstrated in *A. thaliana* that mechanical force application inactivates cellular GA (Lange & Lange, 2015). The addition of exogenous bioactive GA to mechanically stressed plants remedies their height phenotype, and mutants in *Atga20ox*, an enzyme that inactivates cellular GA, do not show thigmomorphogenic phenotypes under mechanical stress treatment (Lange & Lange, 2015). Recent work studying the translocation dynamics of several bZIP family transcription factors has provided new links for calcium and GA signalling in mechanoperception signalling.

2.1.2 bZIPS

In plants, the basic leucine zipper (bZIP) proteins family is a relatively large group of transcription factors. In *B. distachyon* there are 96 bZIPS, divided into 9 groups, compared to *A. thaliana* with 78 bZIPS placed into 13 groups (Jakoby *et al.*, 2002; Liu & Chu, 2015; Dröge-Laser *et al.*, 2018). Group I bZIPS in *A. thaliana* function pleiotropically in aspects of biotic and abiotic responses, as well as plant development. The best characterized Group I bZIP is *A. thaliana* *VirE2-interacting protein 1* (*AtVIP1*), which was identified for its role in agrobacterium mediated T-DNA transfer (Djamei *et al.*, 2007). *AtVIP1* also regulates leaf growth, as does *bZIP29* and *30* (Van Leene *et al.*, 2016; Lozano-Sotomayor *et al.*, 2016). Other Group I bZIPS have been shown to play

roles in anthocyanin synthesis in response to abiotic stress, pollen fertility, and vascular development (Torres-Schumann *et al.*, 1996; Yin *et al.*, 1997; Ringli & Keller, 1998; Dai *et al.*, 2004, 2008; Van Oosten *et al.*, 2013; Gíbalová *et al.*, 2017). All of these bZIPs are also implicated in mechanosensing, in the form of osmosensing. AtVIP1 and other Group I bZIPs have been shown to translocate from the cytoplasm to the nucleus in response to a variety of biotic and abiotic stimuli, including hypoosmotic conditions (Tsugama *et al.*, 2012, 2014, 2016). This translocation appears to be dependent on protein phosphorylation, either from mitogen activated protein kinase 3 (MPK3) during pathogen invasion, or via calcium dependent protein kinase (CDPK). AtVIP1 has recently been shown to interact with calmodulins, the calcium binding proteins involved in many calcium signalling events. Calcium dynamics have long been implicated in touch response signalling, but as mentioned above, the connection between stimulus, calcium fluctuation, and biological response has remained elusive. AtVIP1 translocation was found to depend on cytosolic calcium levels. Treatment with ion scavengers such as EDTA and EGTA strongly limited AtVIP1 nuclear translocation (Tsugama *et al.*, 2018). Looking further upstream in the touch signalling cascade, calcium ion flux across the membrane may be controlled by membrane pore complexes, a number of which have been shown to be mechanically responsive. *AtMCA1* and *AtMCA2* mutants were tested for impact on AtVIP1 translocation, but no effect was shown, indicating that other ion channels may be responsible for touch mediated Ca²⁺ import (Tsugama *et al.*, 2018). The Group I bZIP *Nt REPRESSOR OF SHOOT GROWTH* (*NtRSG*) in tobacco has been implicated in playing a GA homeostasis maintenance role and has been shown to translocate from the cytoplasm to the nucleus in response to cellular GA levels. When

GA levels are nominal, NtRSG is largely in the cytoplasm, and to some extent in the nucleus. At nominal GA levels when NtRSG was partially localized to the nucleus, it directly activates expression of *NtEnt-kaurene oxidase (NtKO)*, an enzyme at an early step in the GA biosynthesis pathway. After cellular GA levels were reduced, NtRSG translocated to the nucleus and also activated *NtGA20oxidase1 (NtGA20ox1)*, an enzyme further down the GA biosynthesis pathway that is in part responsible for converting GA species to their bioactive form (Fukazawa *et al.*, 2010, 2011). This suggests that NtRSG acts to promote bioactive GA synthesis in response to low GA conditions. As with AtVIP1, NtRSG translocation relies on CDPK mediated phosphorylation (Ishida *et al.*, 2008; Ito *et al.*, 2017). Both AtVIP1 and NtRSG associate with 14-3-3 proteins in the cytoplasm while phosphorylated (Ishida *et al.*, 2004; Ito *et al.*, 2014, 2017; Tsugama *et al.*, 2018). Phosphatase activity causes NtRSG to dissociate from the 14-3-3 protein and enters the nucleus, with PP2A complexes implicated in this process for AtbZIP29 in (Van Leene *et al.*, 2016). *NtRSG* is named due to the dwarf phenotype observed when a dominant negative form of the protein is over expressed. In the dwarf plants, there are reduced levels of bioactive GA and reduced elongation of stem internode cells (Fukazawa *et al.*, 2000). These phenotypes were later explained by the work described above on *NtRSG* positive regulation of GA synthesis. Transverse sections of the *NtRSG* dominant negative mutant do not show obvious cell wall phenotypes (Fukazawa *et al.*, 2000). Two rice bZIP genes, *OsRF2a* and *OsRF2b*, have also been shown to regulate GA levels and impact elements of cell wall synthesis and vascular development. The role of these genes in vascular development has been described in the context of rice tungro bacilliform virus. This double stranded DNA badnavirus contains a promoter region with vascular

tissue-specific cis-elements, particularly phloem-specific elements, that *OsRF2a/b* were found to bind and activate (Yin *et al.*, 1997; Dai *et al.*, 2003, 2004, 2008). Similar to *NtRSG*, dominant negative forms of *OsRF2a/b* cause stunted growth. A *OsRF2a* dominant negative transgene in tobacco is reported to have altered phloem development and reduced xylem lignification (Dai *et al.*, 2003). In rice leaf vasculature, overexpression and knockdown of *OsRF2a* resulted in more sclerenchyma development around the vascular bundle, and the presence of large air pockets flanking the vascular bundle. The vasculature itself was somewhat smaller in both cases (Yin *et al.*, 1997).

2.1.3 Summary

Thigmomorphogenesis is a widely observed phenomenon that results in reduced height, increased radial growth, and increased branching. The mechanisms behind this form of growth are not yet fully understood, but involve aspects of hormone regulation, Ca²⁺ signalling, Group I bZIP intracellular translocation, and changes in gene expression. Here I describe the function of a *B. distachyon* bZIP transcription factor, SECONDARY WALL ASSOCIATED bZIP and its role in touch response and cell wall biosynthesis.

2.2 Methods

2.2.1. Plasmid construction

Overexpression constructs were built using the Invitrogen Gateway cloning system. PCR amplified coding sequences were cloned into the pENR-D-TOPO or appropriate pDONR vector for multisite recombination, and further subcloned into a modified pOI001 destination vector (Vogel *et al.*, 2006). Artificial microRNA constructs were built by sequential PCR amplification from the pNW55 plasmid, replacing the native rice microRNA *osaMIR528* with the target sequence of interest, and later subcloned into a

modified pOL001 destination vector (Vogel *et al.*, 2006; Warthmann *et al.*, 2008). Target sequences were derived from the Web MicroRNA Designer platform (<http://wmd3.weigelworld.org>).

Sequence confirmed clones for all destination vectors were electroporated into *Agrobacterium tumefaciens* strain AGL-1.

2.2.2. Plant transformation

Transformation was performed according to Vogel & Hill 2008 (Vogel & Hill, 2008). Immature seeds were collected from ~6 week old plants, deglumed, and surface sterilized with a solution of 1.3% NaClO and 0.01% Triton-X100 for four min. Sterilized seeds were rinsed three times in sterile water. Embryos were dissected from the seeds and placed on callus initiation media (CIM) for four weeks, then subcultured to fresh CIM for two more weeks, then subcultured a final time onto fresh CIM for one week. Seven week old calli were co-cultivated in a suspension of *A. tumefaciens* for ~5 min, then thoroughly dried on sterile filter paper for 3-5 days at 22C in the dark. Calli were moved onto CIM media containing 50 mg/L hygromycin B and 150 mg/L timentin, where they were grown for 3-5 weeks with selective subculture of healthy callus at week 4. After selection, healthy calli were moved to Linsmaier and Skoog media supplemented with 50 mg/L hygromycin B, 150 mg/L timentin, and kinetin to promote shoot growth. Calli that produced green tissue within 3-5 weeks were moved to Murashige and Skoog media supplemented with 50 mg/L hygromycin B and 150 mg/L timentin to allow root growth. After 1-3 weeks, calli that established roots were transplanted to soil and grown as described below.

2.2.3. Plant growth

Brachypodium distachyon line Bd21-3 was used for all experiments. Seeds were stratified on wet paper towel wrapped in foil to exclude light for 10 days at 4°C before being planted in Promix BX potting mix in SC10 Ray Leach Cone-tainers (Stuewe & Sons Inc, <https://www.stuewe.com/products/rayleach.php>). Plants were grown in a Percival PGC-15 growth chamber with day/night conditions of 20h light at 24°C and 4h dark at 18°C respectively.

2.2.4. Transverse stem sections, histology

The main stem of senesced plants was taken and the internode of interest removed and embedded in 8% agarose. Samples were sectioned using a Leica VT1000 Vibratome, making 55µm thick sections. Multiple sections of each internode were collected and stored in water at 4°C. Histochemical staining was carried out using toluidine blue, phloroglucinol-HCl, and Maule reagent as described in Mitra & Loque (2014)(Pradhan Mitra & Loqué, 2014). Images were obtained at 4, 10, and 20x using a Nikon Eclipse E200MV R light microscope and PixeLINK 3 MP camera.

2.2.5 Measuring cell wall thickness

Transverse sections imaged at 20x were used for cell wall thickness measurements. Interfascicular fiber cells separated by one cell layer from the mestome cells on the phloem side of major vascular bundles were targeted for measurement. Using ImageJ, lines were drawn across two walls of adjoining cells. The resulting line length was divided by two to give one cell wall width. ~15 measurements were made for each plant.

2.2.6. Translocation assay

2.2.6.1. Plant growth

Seeds were deglumed and surface sterilized in an aqueous solution of 1.3% NaClO and 0.1% Triton-X100 for 4 min with agitation. The sterilization solution was removed and seeds were washed three times in aseptic conditions with sterile water. Using sterile forceps, the seeds were placed on agar containing 1X MS salts, pH 5.7, without sucrose. The seeds were placed in a row across the upper third of the plate, convex side up, with the embryo oriented down when the plates were held vertically. 8-12 seeds were placed per plate. The plates were wrapped in foil to exclude all light and incubated vertically at 28°C for 6 d.

2.2.6.2. Pharmacology treatments

After the 6 day growth period, seedlings were moved to segmented petri plates with four quadrants. Each quadrant contained 1x MS media, pH 5.7, without sucrose, plus a different concentration of the pharmacological agent being tested, including a no-treatment control quadrant. GA4 and paclobutrazol treatment concentrations of 10 mM, 50 mM, and 100 mM were used. After transfer to the treatment media, roots were gently pressed into the media so that they were completely covered, and positioned close to the bottom of the plate in an even plane for better imaging. Plants were left in the treatment media for 6h to acclimate from the touch stimulus of movement, and to allow for chemical uptake of the treatment compound.

2.2.6.3. Confocal microscopy

All observations were made on a Nikon A1R scanning confocal microscope using a 10x objective. Plates were fixed to the microscope stage with tape and their lid removed. Root

areas to be observed were located by eye and then confirmed under confocal conditions. The coordinate stage locations of each region were programmed into the Nikon NIS Elements Advanced Research V6 software package for automated imaging. After all target regions were programmed, 30 min of imaging began pre-treatment, with images captured every 2 min.

2.2.6.4. Touch treatment

To elicit the touch response, the time lapse capture program was paused and the microscope switched back to the eyepoint. Each observed root region was gently probed for 5 sec with a blunt metal probe while observing through the eyepiece, as one would with a dissecting scope. After all regions were probed, each field of view was quickly refocused under confocal to assure the root had not moved in the x, y, z planes, repositioning the stage and reencoding the location if necessary, and then resuming time lapse capture every 2 min. From start to finish, the touch treatment takes no more than 5 min. Images are captured for 60-90 min post treatment. For experiments with multiple stimulus events, the timelapse sequence was paused and roots were probed as described for the relevant stimulus events.

2.2.6.5. Analysis

Analysis of GFP signal was done using the Nikon NIS Elements Advanced Research V5 software package. For each time series of images for one root, the frame showing maximal nuclear signal was selected and used as a reference point. Using the General Analysis tool, a channel for GFP signal was established and thresholded for intensity and particle size to identify the nuclear regions. These regions were added to the timelapse image series as a binary layer and then converted to static regions of interest (ROIs) for

quantification. The GFP intensity under each nuclear ROI was calculated for the course of the timelapse and the average signal from each nucleus was plotted for intensity over time.

2.2.7. Cell wall material insoluble in alcohol (MIA)

The main stem of mature, senesced plants was collected and cut into small pieces (~2cm) into a 2ml tube. Two metal beads were added and the stem was ground to a fine powder using a Retsch 440 bead beater. Ground material was transferred to a glass screw cap tube. Cell wall material was washed with 5ml of water in an 80°C water bath for 10 min with agitation. The cell wall material was pelleted by centrifugation at 3700 rpm for 10 min and the supernatant aspirated by vacuum. This was repeated for a second water wash. The cell wall material was then washed three times with 100% ethanol at 80°C for 15 min per wash, with collection by centrifugation and aspiration of the supernatant between washes as described above. The cell wall material was then washed twice with acetone for 15 min per wash at room temperature, then left to dry under a fume hood overnight. Modified from INARE protocols.

2.2.8. ABSL quantification

Beginning with dry cell wall MIA samples, 4.5-5.5mg of each sample was weighed into a 2mL glass vial using a precision balance. 1ml of acetyl bromide solution(25% acetyl bromide, 75% acetic acid) was carefully added to each vial under a fume hood. The vials were capped and inverted several times to mix. Samples were incubated in a drying oven at 55°C for 2h 30 min, with mixing by gentle inversion every 30 min to ensure full sample solubilization. The samples were cooled to room temperature before proceeding. 0.1 ml of sample was diluted into 1.2ml of acidified 2M NaOH, then mixed with 0.3ml of

0.5M hydroxylamine chlorhydrate and 1.4ml of acetic acid. Using a glass pipette, air was bubbled through the sample to ensure full homogenization of the reaction mixture. Absorbance at 280nm was measured on a SpectraMaX M6 plate reader, and the lignin content was calculated using the following equation: %lignin= $100 \times (A_{280} \times \text{Vol reaction} \times \text{Vol dilution}) / (20 \times \text{Vol sample solution} \times \text{Mass sample (mg)})$. Modified from INARE protocols.

2.2.9. Thigmomatic construction and operation

The Thigmomatic is a very basic robotic device that sweeps a flat of plants with a metal bar at regular intervals to elich a touch response (Fig 2.1). The device was constructed from aluminum V-Slot linear rail (<https://openbuildspartstore.com/linear-rail/>) and bracket joints for the upright supports (20x20 mm), cross bars (20x20 mm), and tracks (20x40mm).

Two gantry carts (<https://openbuildspartstore.com/v-slot-gantry-kit-20mm/>) ride along the 20x40mm V-Slot linear rails, connected by a metal rod bolted to the carts. Their movement is powered by a belt driven linear actuator system using a NEMA 17 stepper motor (<https://openbuildspartstore.com/v-slot-nema-17-linear-actuator-bundle-belt-driven/>) with a 12V 18W AC/DC power supply (<https://www.digikey.com/product-detail/en/triad-magnetics/WSU120-1500/237-1393-ND/3094919>).

The stepper motor provides fine spatial control over the gantry cart position with bi-directional motion. Motor function is controlled by a Raspberry Pi 3B microcomputer equipped with a stepper motor HAT (<https://www.adafruit.com/product/2348>). The Thigmomatic was programmed to cover a specified distance in one direction once every 90 min.

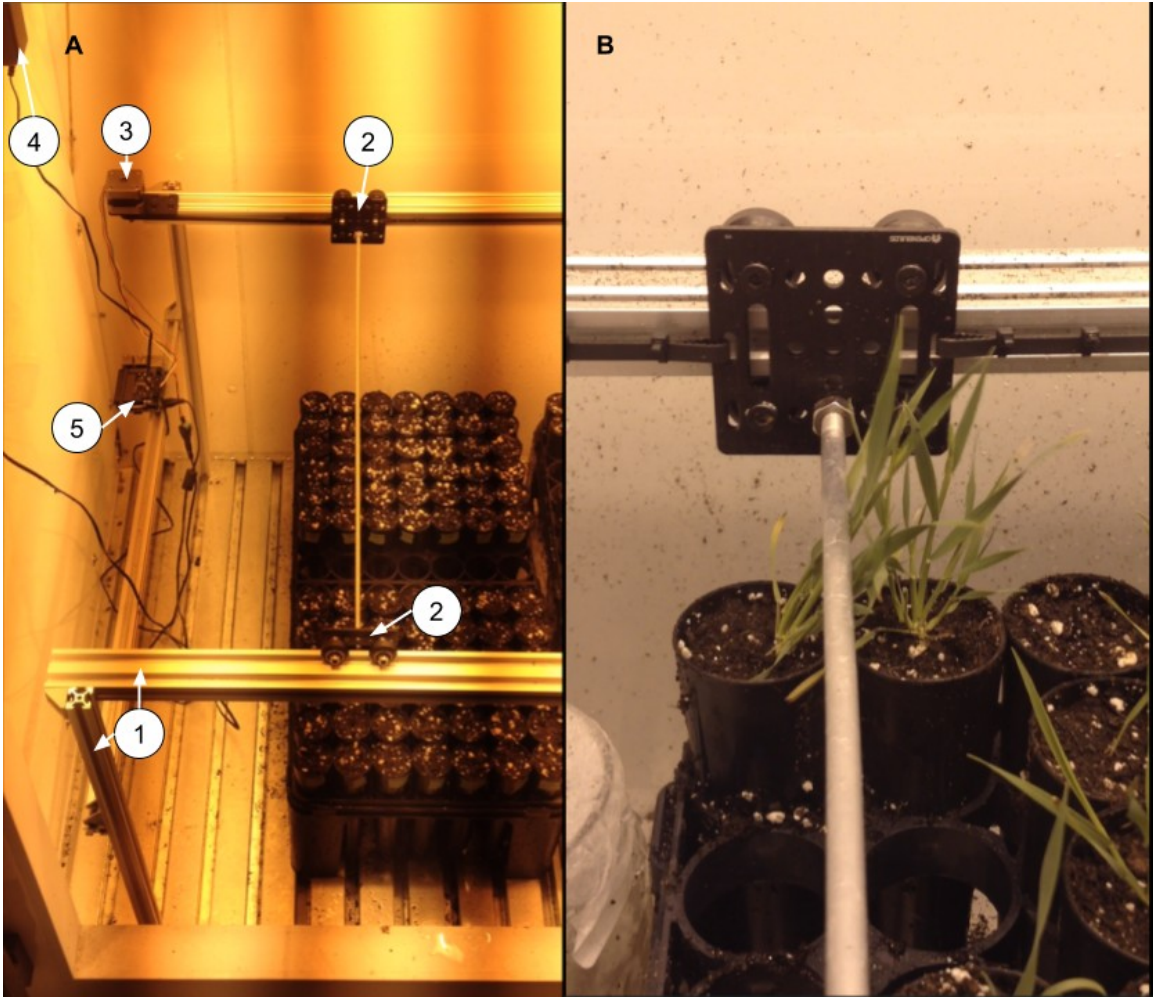


Figure 2.1 Thigmomatic. (A) Overview of Thigmomatic setup inside a Percival PGC-15 growth chamber, showing linear rail based frame (1), gantry carts (2), NEMA17 stepper motor (3), 12V 18W AC/DC power supply (4), and Raspberry Pi 3b microcomputer (5). (B) Thigmomatic in action, making contact with *B. distachyon*.

2.2.10. DAP-seq

DNA affinity purification was carried out by collaborators at the JGI according to the protocol established by O'Malley et al 2016 (O'Malley *et al.*, 2016). In brief, transcription factor coding sequences were HALO tagged and mixed with Bd21 genomic DNA for in vitro binding. Protein-DNA was crosslinked, fragmented, immunoprecipitated using the HALO tag, barcoded, and sequenced. Reads were mapped

back to the Bd21 genome to identify binding target loci. The nearest annotated gene to a bound peak was used for GO analysis.

2.2.11. HOMER identification of motifs

HOMER v4.10 (Heinz *et al.*, 2010) was used to compute enrichment scores for transcription factor binding motifs previously identified using DNA-affinity-purified sequencing (DAP-seq) (O'Malley *et al.*, 2016) among each group of cycling transcripts. Motif enrichment was calculated against the hypergeometric distribution; the significance threshold was set to $p < 0.05$. Similar motifs were determined using the compareMotifs.pl function of HOMER against the global list of known motifs with the default threshold cutoff of 0.6. Modified from MacKinnon et al 2020 (MacKinnon *et al.*, 2020).

2.2.12. GO analysis

NCBI BLAST and Phytozome (Altschul *et al.*, 1990; Goodstein *et al.*, 2011) were used to find orthologs for all *B. distachyon* v3.1 genes as the reciprocal best match to *A. thaliana* TAIRv10 protein sequences. Genes that did not significantly match a corresponding gene in *A. thaliana* were discarded from this analysis. *Arabidopsis thaliana* biological process gene ontology (GO) annotations were obtained from <http://ge-lab.org/gskb/>. For Kuiper's test, the distribution of GO terms was compared with an empirically-determined background distribution. Gene identifiers were submitted to g:Profiler (Raudvere *et al.*, 2019) for KEGG and Wiki pathway enrichment analysis. Modified from MacKinnon et al 2020 (MacKinnon *et al.*, 2020).

2.2.13. Yeast one-hybrid assay for protein DNA interaction

In a yeast one-hybrid assay, the interaction between a transcription factor (TF) of interest

and a DNA sequence of interest are assayed by measuring the activation of a reporter gene in a heterologous yeast system.

The DNA sequence of interest is usually the promoter region of a gene representing approximately 1kb of sequence upstream from the gene's start codon. This sequence is cloned and tested in three overlapping fragments for approximately 400bp each. The promoter sequence fragment is cloned upstream of a reporter gene, in this case encoding a B-galactosidase reporter. The finished vector is linearized by restriction digest, and then stably transformed into YM4271 yeast to generate reporter lines. Homologous recombination of the linearized vector targets the insertion to a specific locus in the yeast genome, controlling for transcriptional effects based on insertion point. A number of these lines are grown on selective media and then tested for reporter activity. Lines that do not show reporter activity without an effector added are selected for use in testing protein-DNA interaction.

The coding sequence for the TF of interest is cloned into the pDEST22 expression vector in frame with the Gal4 activation domain (Gal4AD), which induces transcriptional activity when bound to DNA. This vector is then transformed into the yeast reporter lines. If the Gal4AD:TF fusion protein binds to the promoter fragment being tested, the Gal4AD will activate transcription of the luciferase gene. B-galactosidase activity is measured by adding ONPG, a substrate that the B-galactosidase enzyme cleaves, causing a colorimetric change from clear to yellow. Protein-DNA interactions were tested in triplicate, with a positive/negative determination made for colorimetric change after a 3 h incubation period.

2.2.14. Genomic DNA Extraction

Tissue samples were collected in 1.5ml tubes with two metal beads and flash frozen in liquid nitrogen. They were ground to a fine powder in frozen blocks in Retsch 440 bead beater. 600ul of DNA extraction buffer (100mM NaCl, 50mM Tris, 25mM EDTA pH8, 1% SDS, a 10mM 2-mercaptoethanol) was added to each sample while still frozen, then vortexed vigorously to mix. Samples were incubated at 65°C for 10 min. 250ul of potassium acetate was added, the samples were mixed by inversion and then incubated on ice for 20 min. Tubes were centrifuged at 12,000 rpm for 10 min and the supernatant was carefully removed and placed in a new tube containing 600ul of isopropanol. The samples were incubated on ice for 20 min to precipitate the nucleic acids, then centrifuged at 10,000rpm. The supernatant was removed and the pellet was washed once with 300ul of 70% ethanol followed by a centrifugation at 15,000rpm for 1 min. The supernatant was removed and the pellet was dried under a fume hood for 1h before resuspending in 30ul of DNase free water.

2.2.15 RNA extraction and RT-qPCR

RNA was extracted from the main stem of plants one day after flowering using the Qiagen RNeasy Plant Mini Kit with on-column DNA digestion with RNase-free DNase I (Qiagen). First strand cDNA synthesis was performed using 500ng of total RNA with the Invitrogen SuperScript™ III First-Strand Synthesis SuperMix for qRT-PCR. cDNA samples were diluted by a factor of 10 with RNase-free water. Quantitative PCR was done in 10ul reactions with 1ul of diluted cDNA using the Qiagen QuantiFast SYBR Green PCR Kit. Reactions were run in triplicate on an Eppendorf RealPlex2 Mastercycler.

2.3 Results

2.3.1 SWIZ is a Group I bZIP transcription factor and candidate cell wall regulator.

To identify genes potentially involved in cell wall regulation, microarray analysis of transcript abundance was conducted on RNA extracted from *B. distachyon* leaf, root, and stem tissue (Trabucco *et al.*, 2013a). A gene annotated as a bZIP transcription factor, *Bradi1g17700* was highly expressed in root and stem relative to leaf (Fig 2.2).

Additionally, expression was highly correlated with other genes associated with wall biosynthesis, including secondary wall cellulose synthases and members of the lignin biosynthesis pathway. Phylogenetic analysis of the *Bradi1g17700*, henceforth referred to as *SECONDARY WALL INTERACTING bZIP (SWIZ)*, amino acid sequence shows it to be an ortholog of the *A. thaliana* Group I bZIPs (Jakoby *et al.*, 2002; Dröge-Laser *et al.*, 2018), and most closely related to *AtbZIP18/52* (Figure 2.3).

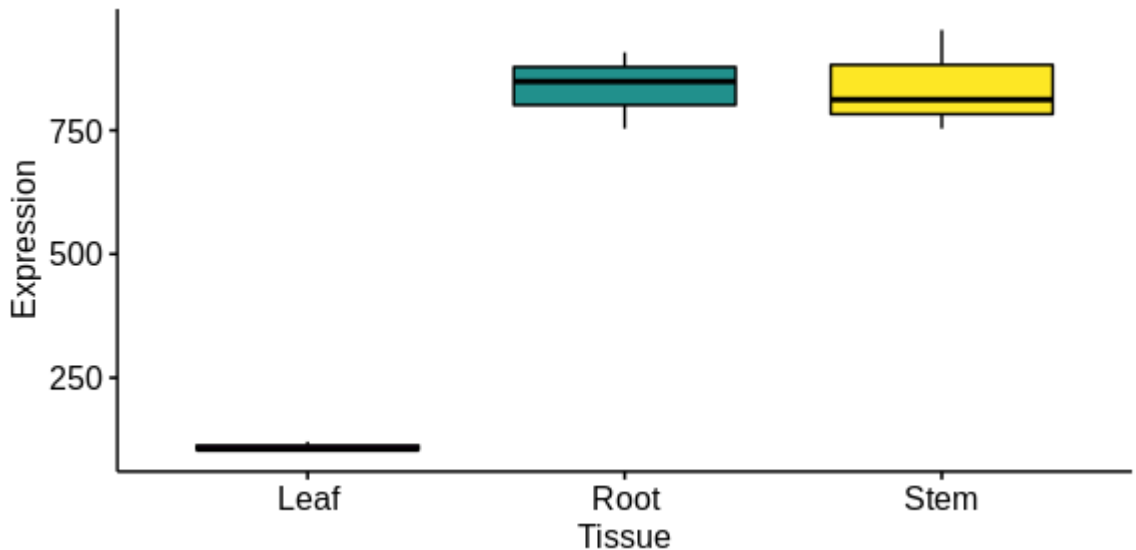


Figure 2.2. SWIZ is highly expressed in maturing stem and root. SWIZ transcript measured by microarray from *Brachypodium distachyon* leaf, root, and stem tissue. Mean +/- standard deviation of three biological replicates.

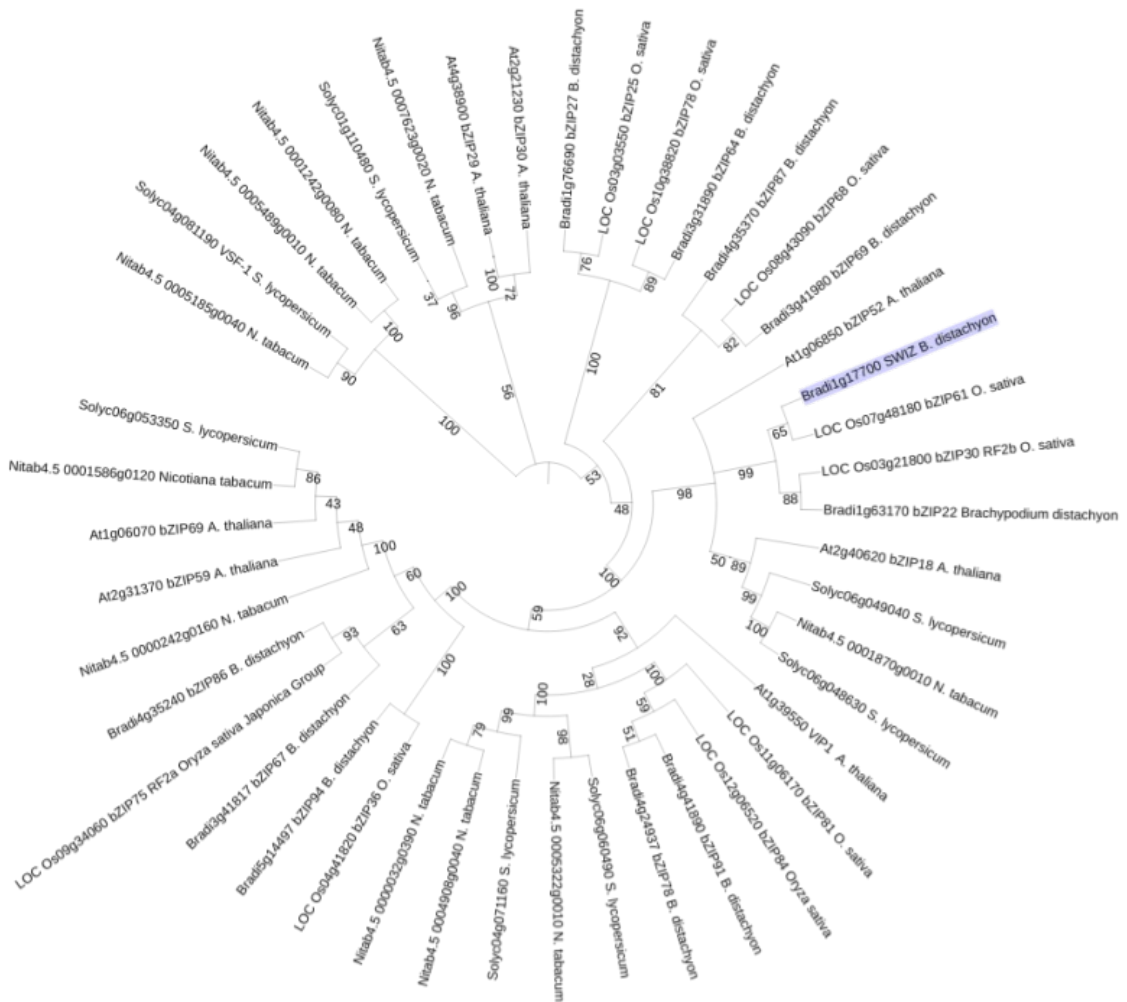


Figure 2.3 SWIZ phylogeny. Comparison of amino acids sequences from *B. distachyon*, *O. sativa*, *A. thaliana*, *N. tabacum*, and *L. solanum* shows SWIZ (blue) is similar to *A. thaliana* Group I bZIPs.

To further support the candidacy of SWIZ as a potential secondary cell wall regulator, it was screened for interaction with cell wall gene promoters by a yeast one-hybrid assay. Regulatory regions ~1000 bp upstream of the start codon of genes involved with cell wall biosynthesis were divided into three ~400 bp overlapping fragments. These regions were cloned upstream of the *B-galactosidase* reporter gene and stably integrated into yeast. The SWIZ coding sequence was cloned in frame with a Gal4 activation domain and transformed into the reporter lines. Interaction of SWIZ protein with the DNA region

being tested would allow the Gal4 activation domain to promote transcription of the reporter gene. B-galactosidase activity was determined by colorimetric assay as either a positive or negative interaction (Fig 2.4A). SWIZ interacted positively with one fragment of *CAFFEIC ACID 3-O-METHYLTRANSFERASE 6* (*COMT6*) promoter, two fragments of *CINNAMYL ALCOHOL DEHYDROGENASE 1* (*CAD1*) promoter, and one fragment of *CELLULOSE SYNTHASE A4* (*CESA4*) promoter (Fig 2.4B, full sequences listed in Appendix). *CAD1* and *COMT6* are members of the lignin biosynthetic pathway, while *CESA4* is a secondary cell wall cellulose synthase.

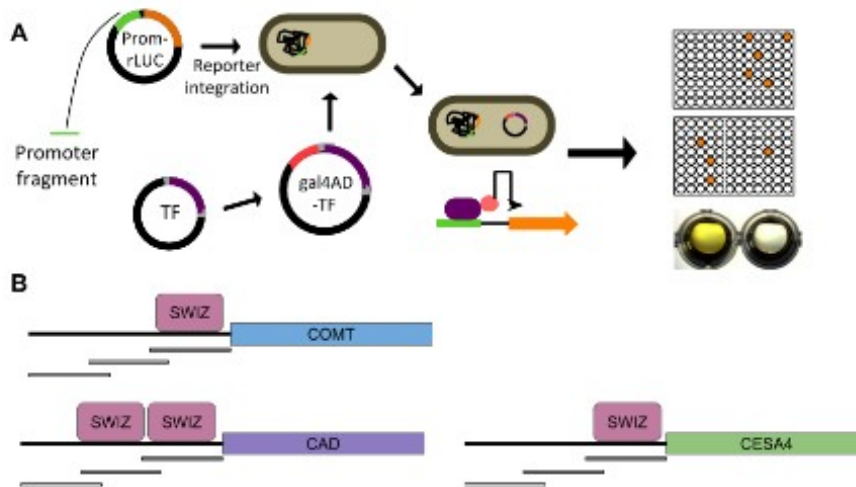




Figure 2.4. SWIZ protein interacts with cell wall gene regulatory regions. Yeast one-hybrid assay of protein-DNA interaction using a B-galactosidase colorimetric reporter. SWIZ coding sequence fused with the Gal4 activation domain was transformed into yeast lines containing promoter:reporter constructs of cell wall promoter fragments driving B-galactosidase expression. A) Schematic of the yeast one-hybrid assay. Reporter lines were tested for self activity prior to screening, with two non-self active lines of each construct chosen for assay. Activation of the reporter was measured in triplicate, with positive/negative determination for colorimetric change. B) Schematic showing SWIZ positive interactions with promoter regions from *CAD1*, *COMT6*, and *CESA4*.

2.3.2 SWIZ binds a conserved motif

In determining the direct and indirect effects of transcription factor activity, assaying the targets directly bound by the protein of interest is of immense value. DNA affinity purification sequencing (DAP-seq) is an *in vitro* approach to identifying genome wide binding sites of a protein of interest. Collaborators at the Joint Genome Institute performed DAP-seq for SWIZ protein with Bd21 genomic DNA. Based on statistically significant enrichment of sequences purified with SWIZ protein, we identified 3,302 loci across the genome. The genes downstream of the binding sites were identified for further analysis (Supplemental File 1). From the bound DNA sequences, the HOMER program was used to identify binding motif sequences enriched in these fragments compared to the genomic background. From *de novo* analysis, nine sequence motifs were identified as significantly enriched above the background. The two most significant motifs were found in 24% and 17% of the enriched regions, and strongly resemble an *A. thaliana* Group I bZIP binding motifs (O'Malley *et al.*, 2016) (Table 1). Gene ontology (GO) analysis was performed on both the full set of binding targets identified genome wide (Table A1), as well as the subset of 812 genes containing the top two binding motifs (Supplemental File 2), essentially CAGNCTG and CAGCTG (Table A2).

Table 1. SWIZ binding motifs identified by DNA affinity purified sequencing. Motif analysis using the HOMER program identified conserved sequences between regions interacting with SWIZ. Motif column displays the binding motif logo with nucleotide size depicting conservation at that position. p-value represents significance of enrichment in bound sites compared to the genomic background

Weighted matrix motifs	p-value	% of bound targets	% of background
	1e-1357	23.93	0.21
	1e-737	16.98	0.36

2.3.3 SWIZ genetic reagents

To investigate the role of *SWIZ* in plant growth and secondary cell wall development, transgenic lines with enhanced or perturbed *SWIZ* function were generated.

Overexpression lines were created using the maize ubiquitin promoter to drive expression of the *SWIZ* coding sequence as well as the *SWIZ* coding sequence fused with engineered green fluorescent protein (*GFP*), hereafter referred to as *SWIZ-OE* or *SWIZ:GFP-OE* (Figure 2.5A). Two independent events of *SWIZ-OE* and three independent events of *SWIZ:GFP-OE* were isolated and analyzed. Knockdown of *SWIZ* transcript abundance was done by expressing an artificial microRNA construct with homology to the first exon of the *SWIZ* mRNA, hereafter referred to as *swiz-miRNA* (Fig 2.5B). Two independent events were isolated and analyzed. Transcript abundance analysis by RT-qPCR showed that *SWIZ* was significantly over expressed in the *SWIZ-OE* lines compared to wildtype ($p < 0.05$, Fig 2.5C). *SWIZ* expression was reduced in the *swiz-miRNA* line, but not significantly at the $p < 0.05$ threshold ($p=0.065$, Fig 2.5D).

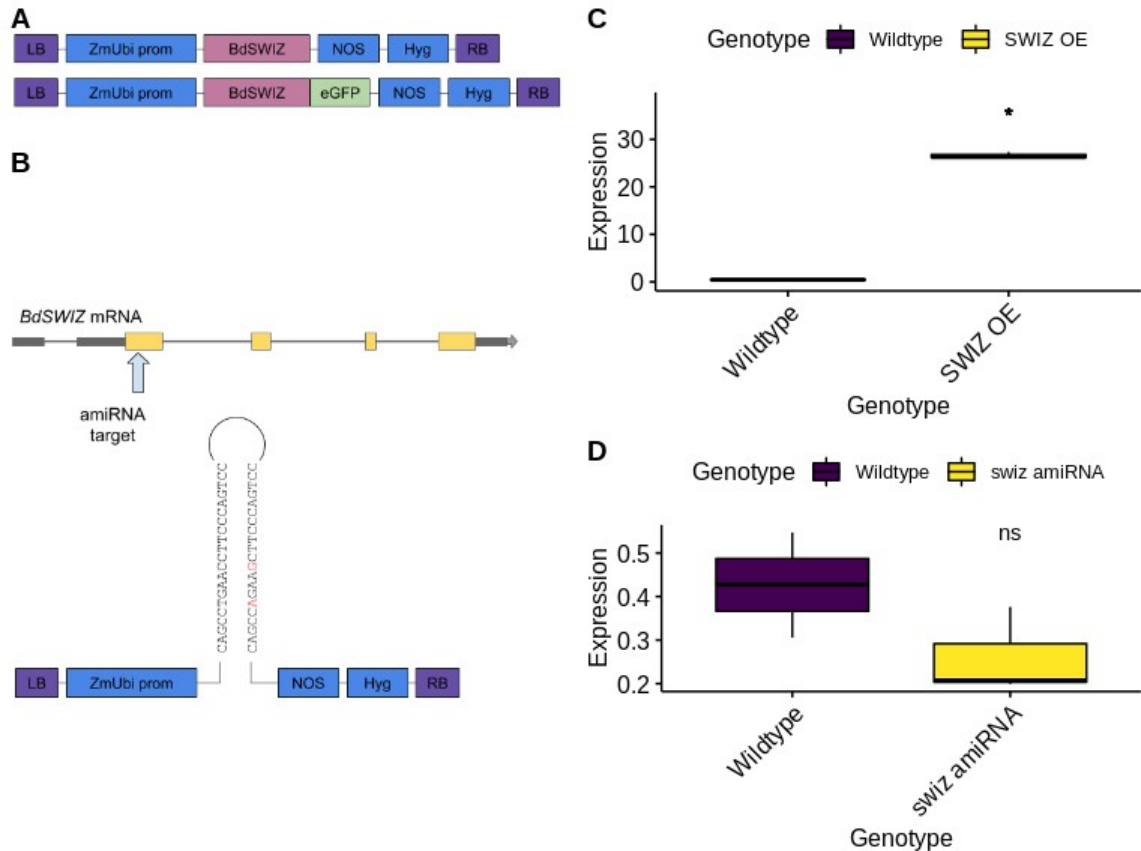


Figure 2.5. Diagram of SWIZ transgenic reagents. A) Constructs for SWIZ overexpression. The maize ubiquitin promoter was used to drive expression of the SWIZ coding sequence, either alone or fused in frame with *eGFP*. **B) Artificial microRNA construct for SWIZ knockdown.** The SWIZ mRNA schematic (exons - yellow blocks, introns - grey lines, UTR - gray blocks) shows the target site for amiRNA interference, indicated by the arrow in the first exon. Below is a diagram of the amiRNA construct used for SWIZ knockdown. The maize ubiquitin promoter was used to drive expression of an amiRNA that has homology with SWIZ exon 1, and forms a hairpin after transcription. The 21-mer nucleotide sequence used for target specificity is listed, with red positions showing hairpin mismatches that are predicted to interact with the DICER complex. **C) and D) Relative level of SWIZ gene expression measured by RT-qPCR in SWIZ-OE (C) and *swiz-amiRNA* (D) lines.** Whole stem tissue was collected 1 day after inflorescence emergence. LB, left border; *ZmUbi prom*, maize ubiquitin promoter; Hyg, hygromycin phosphotransferase gene; NOS, nopaline synthase terminator; RB, right border. ns: $p > 0.05$, *: $p \leq 0.05$.

2.3.4 SWIZ effects cell wall thickness, lignification, and plant morphology

Wildtype, *SWIZ-OE*, and *swiz-amiRNA* plants were grown and phenotyped for plant morphology, stem biology, and cell wall deposition. Transverse sections were taken from the second elongated internode of the main stem and stained for lignin using phloroglucinol-HCl. *SWIZ-OE* and *swiz-amiRNA* plants had dramatic interfascicular fiber phenotypes (Fig 2.6A-C). Compared to wildtype, (Fig 2.6A), *SWIZ-OE* plants (Fig 2.6B) had comparable intensity of phloroglucinol staining, but with an uneven distribution of color between neighboring fiber cells. The walls also appeared to be thicker than those of wildtype, again with an uneven pattern of thickening among cells. Some epidermal cells in the *SWIZ-OE* lines were also aberrantly thickened. The *swiz-amiRNA* plants (Fig 2.6C) also showed thicker interfascicular fiber walls, but in a more even distribution. These fiber cells also stained far more lightly for lignin compared to wildtype (Fig 2.6C). Interfascicular fiber wall thickness was quantified in fiber cells, two layers distal from the major vascular bundle sheath layer, and showed significantly thicker walls in both *SWIZ-OE* and *swiz-amiRNA* compared to wildtype (Fig 2.6D). Lignin content was measured by the acetyl bromide soluble lignin (ABSL) method, which showed no change in lignin between wildtype and *SWIZ-OE*, but a significant reduction in *swiz-amiRNA* plants (Fig 2.6E). This quantification is in agreement with the visual measure of lignification observed by phloroglucinol-HCl staining, which showed lighter staining and thus less lignin in *swiz-amiRNA* plants. Additionally, both *SWIZ-OE* and *swiz-amiRNA* lines were significantly shorter in height than wildtype plants (Fig 2.6F).

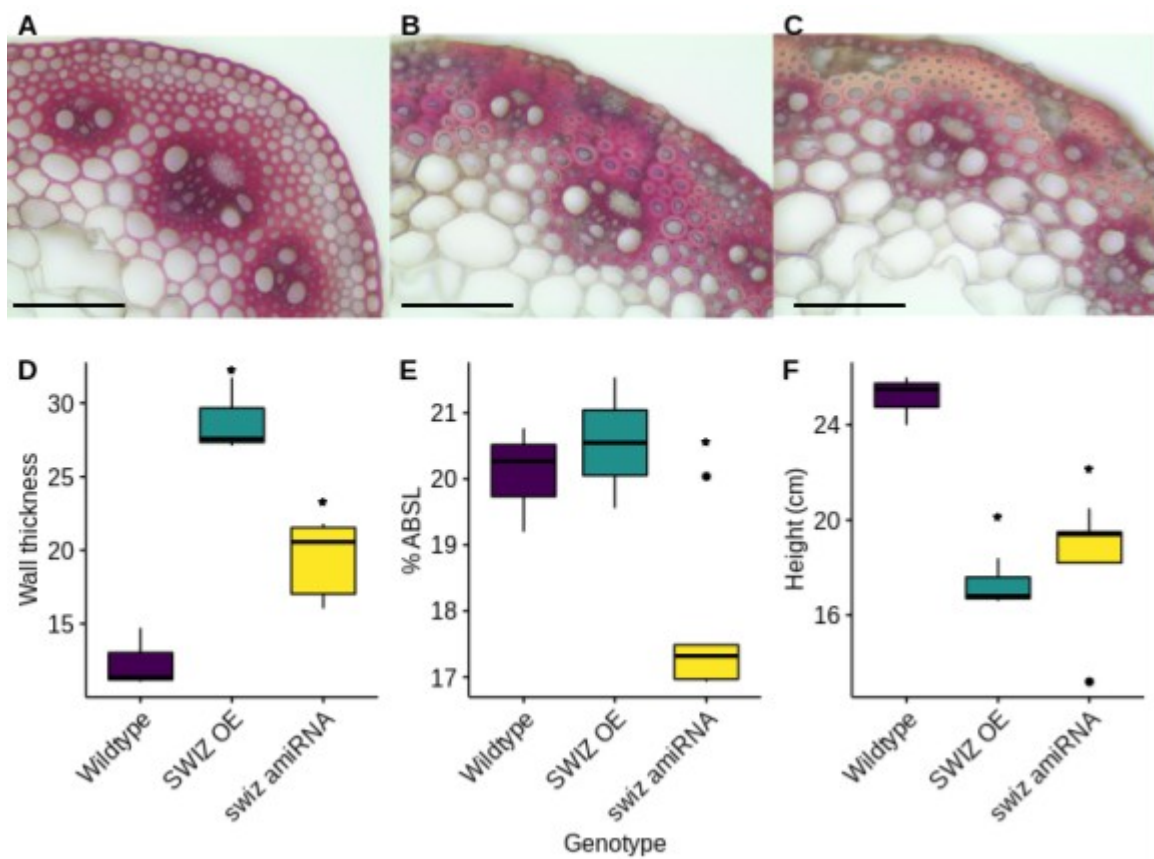


Figure 2.6. *SWIZ* reagent phenotypes. Plants were grown in standard long day conditions without consideration for mechanical stimuli. Wildtype Bd21-3 (A), *SWIZ-OE* (B), and *swiz-amirRNA* (C) stems were sectioned in the second elongated internode after senescence and stained with phloroglucinol-HCl to show lignin deposition in pink-red hues. (D) Cell wall thickness was quantified for interfascicular fiber cells. (E) Acetyl bromide soluble lignin measured in extractive free cell wall material prepared from the main stem after senescence. (F) Plant height measured at senescence. Scale bar = 100 μm. ns: $p > 0.05$, *: $p \leq 0.05$. $n = 4-6$ plants per genotype.

2.3.5 SWIZ translocates into the nucleus in response to mechanical stimulus and cellular GA levels

Some Group I bZIP proteins have been described as mechano- and osmosensing (Tsugama *et al.*, 2014, 2016). I hypothesized that SWIZ protein may translocate within the cell in response to mechanical force. To test this, *SWIZ:GFP-OE* and *GFP-OE* plants were grown on tilted MS plates for 6 d in the dark and GFP localization was observed in their roots following a mechanical stimulus. The nuclear localized GFP signal was tracked and quantified over a 75 min period following the application of mechanical force with a metal probe (Fig 2.7A). *GFP-OE* signal was present in both the cytosol and nucleus, and nuclear accumulation remained static over the imaging period. The GFP protein was mostly observed in the cytosol in *SWIZ:GFP-OE* plants, but following mechanical force treatment, nuclear GFP signal increased substantially, reaching a peak around 30 min post stimulus (Fig 2.7B). The nuclear signal then decreased, returning to near starting levels by the end of imaging period (Fig 2.7A).

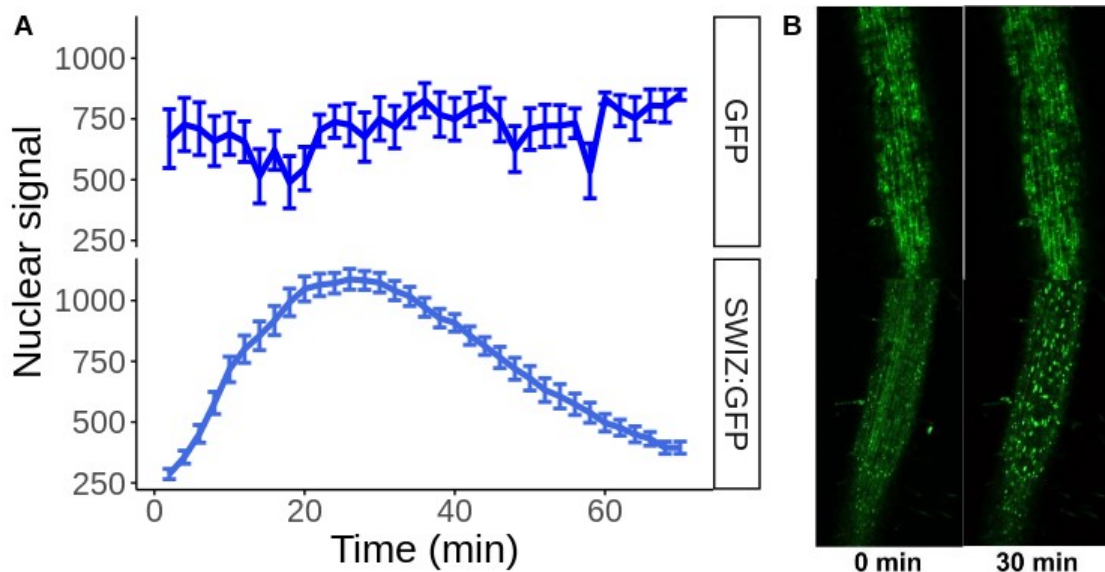


Figure 2.7. SWIZ translocates to the nucleus in response to mechanical stress. (A) Roots of *SWIZ:GFP-OE* and *GFP-OE* were observed after mechanical stress application. Images were taken every 2 min. Nuclear GFP signal was quantified in selected nuclei at each time point. The average nuclear GFP signal is represented by the trend line, with error bars indicating standard deviation of the mean. (B) Still image of *SWIZ:GFP-OE* and *GFP-OE* roots at 0 min (pre-stimulus) and 30 min (post stimulus). $n=14-20$ nuclei.

The dynamics and repeatability of SWIZ nuclear translocation were further investigated by sequential stimulus events. Touch response to stimulus can saturate at a certain number of treatments (Martin *et al.*, 2010; Leblanc-Fournier *et al.*, 2014; Moulia *et al.*, 2015). To see if SWIZ translocation dynamics varied after repeated treatments, I applied mechanical force to *SWIZ:GFP-OE* roots as described above. A second stimulus was given 80 min after the first stimulus was applied, and again at 160 min. Following each mechanical stimulation, SWIZ translocated from cytoplasm to nucleus with maximum nuclear signal achieved in about 30 min post stimulus (Fig 2.8). The maximum intensity of each of these three translocation events did not differ significantly from each other, nor did the time between reaching maximum intensity or returning to pre-stimulus levels.

This suggests that SWIZ translocation dynamics are not impacted by repeated stimulus events, at least not over ~3 h.

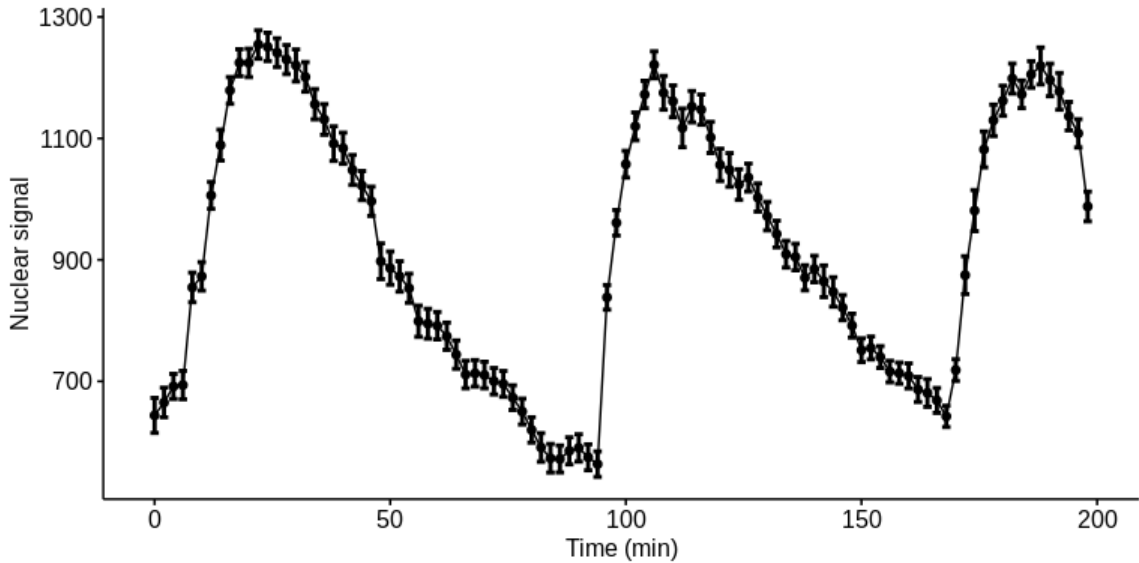


Figure 2.8. SWIZ translocation dynamics are similar in amplitude and timing following repeated stimuli. *SWIZ:GFP -OE* roots were imaged by confocal microscopy with stimulus applied to the field of view at 0, 90, and 180 min. Images were taken every 2 min. Nuclear GFP signal was quantified in selected nuclei at each time point. The average nuclear GFP signal is represented by the trend line, with error bars indicating standard error of the mean. n=124 nuclei.

When conducting these translocation assays, root in the field of view was treated with mechanical force and all nuclei in that region were tracked and quantified for fluorescence. To determine if the mechanically stimulated SWIZ translocation signal is transferable to regions outside of the specific tissue that receives the force, two regions of the same *SWIZ:GFP-OE* root were imaged over the same timespan. The two regions were separated by 3 cm of undisturbed tissue. After a 45 min acclimation period, where nuclear GFP signal was static, the upper root region was given a mechanical stimulus (Fig 2.9A). The upper stimulated region showed typical SWIZ:GFP nuclear signal accumulation. At the same time, the lower root region was also imaged, and no translocation was observed (Fig 2.9B). The nuclear signal in the lower region remained

constant at the acclimation period levels. At 120 min, the treatments were reversed, with the lower root region receiving a stimulus while the upper region was unperturbed. The lower region showed the expected SWIZ:GFP nuclear translocation while the upper region did not. These results suggest that the signal that triggers SWIZ nuclear translocation following a mechanical force event is localized to the cells that directly receive that stimulus.

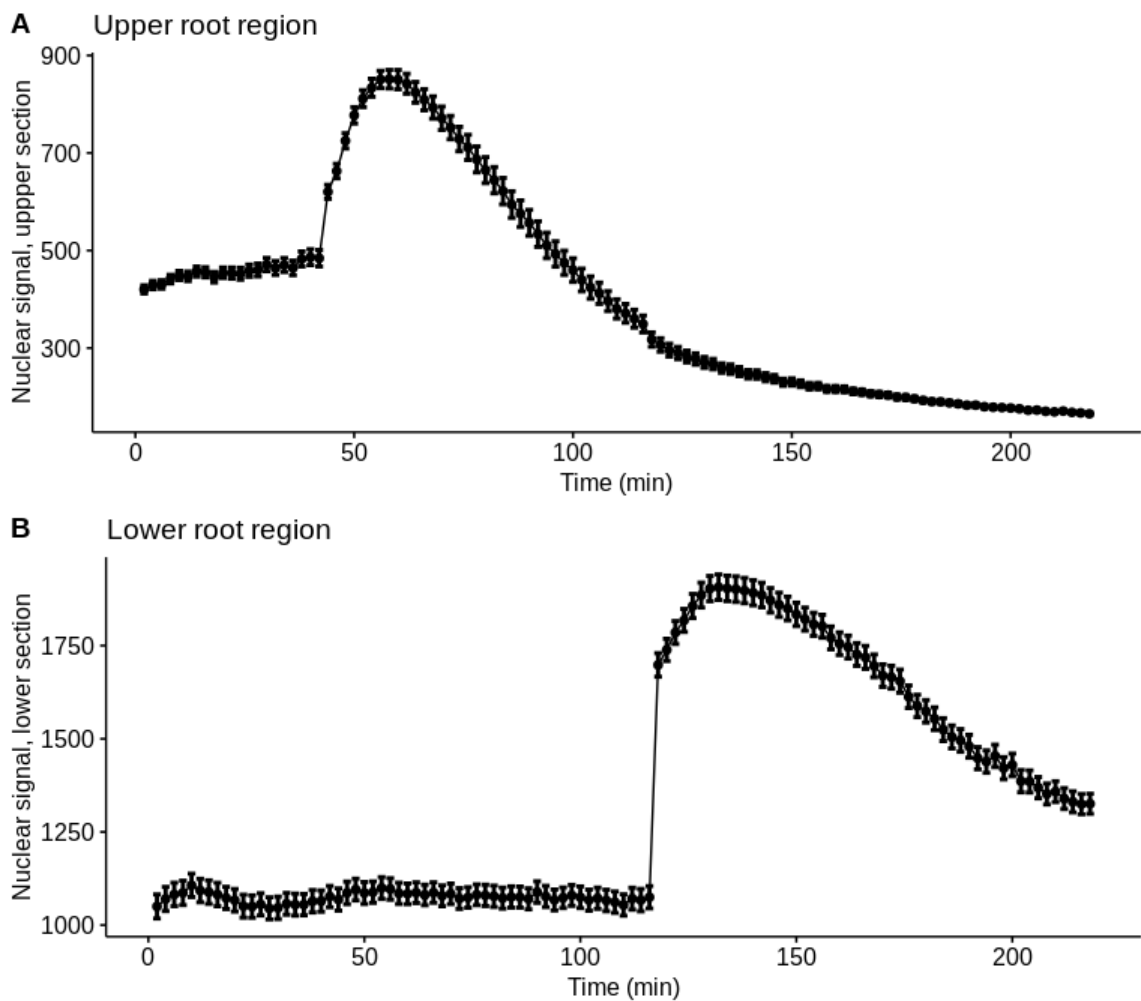


Figure 2.9 SWIZ translocation is localized to the region of tissue that experiences mechanical stimulus. *SWIZ:GFP-OE* roots were imaged by confocal microscopy with stimulus applied to the field of view at 30 and 120 min. At 30 min, stimulus was applied to the upper section of the root, while at 120 min it was applied to the lower section. SWIZ:GFP translocation was monitored in the upper section in (A) and the lower section in (B). Upper and lower regions were separated by ~3 cm of root tissue. Images were taken every 2 min. Nuclear GFP signal was quantified in selected nuclei at each time point. The average nuclear GFP signal is represented by the trend line, with error bars indicating standard error of the mean. n=109, 184 nuclei respectively for upper and lower regions.

SWIZ translocation dynamics were further investigated in response to cellular gibberellic acid (GA) levels. Mechanical forces have been shown to inactivate cellular GA, and that cellular GA levels dictate cytosolic versus nuclear localizations of *A. thaliana* Group I bZIPs similar to SWIZ in amino acid sequence (Fukazawa *et al.*, 2010; Lange & Lange, 2015). To test if SWIZ translocation following mechanical force application was dependent on bioactive GA levels, *SWIZ:GFP-OE* roots were grown on MS media for 6 d before being transferred to GA treatment plates. Seedlings were transferred to media plates containing MS + 0 mM (control), 10 mM, 50 mM, or 100 mM bioactive GA (GA4) and were incubated on this media for 6 h prior to imaging. After a 10 min acclimation period, in which no nuclear translocation was observed, a mechanical force was applied and nuclear signal tracked. SWIZ:GFP signal amplitude was reduced in roots treated with GA, particularly at the 50 and 100 mM level. After 60 min the nuclear signal had returned to near pre-stimulus levels, and a second stimulus was applied (Fig 2.10). This time all the GA treated roots showed a similar reduction in nuclear signal, nearly half of the untreated control. These results suggest that the addition of exogenous GA4 reduces SWIZ translocation to the nucleus following mechanical force application.

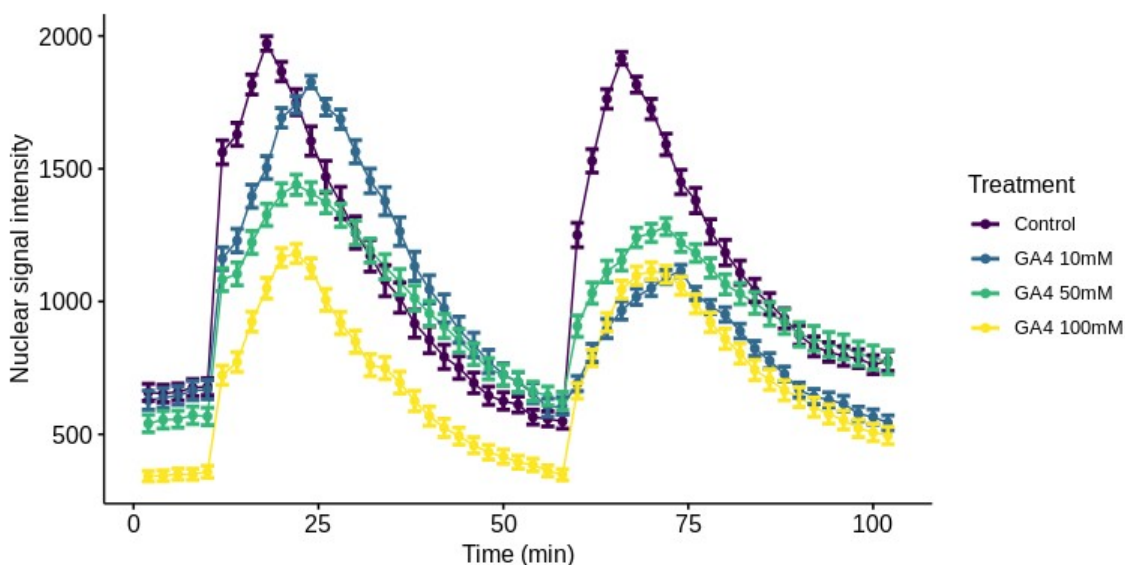


Figure 2.10. SWIZ translocation to the nucleus is dampened by the addition of exogenous GA4. *SWIZ:GFP-OE* roots were grown on MS media for 6 d then moved to media supplemented with 10, 50, or 100 mM of GA4. Plants were left on supplemented media for 6 h then imaged following stimulus at 10 and 60 min. Images were taken every 2 min. Nuclear GFP signal was quantified in selected nuclei at each time point. The average nuclear GFP signal is represented by the trend line, with error bars indicating standard deviation of the mean. n= 85-125 nuclei per treatment

The effect of reduced GA levels on SWIZ translocation was also investigated.

Paclobutrazol is an inhibitor of GA synthesis, and is known to reduce the level of bioactive GA in treated cells. *SWIZ:GFP-OE* roots were grown on MS media for 6 d before being transferred to GA treatment plates. Seedlings were transferred to media containing MS + 0 mM (control), 10, 50, or 100 mM paclobutrazol and were incubated on this media for 6 h prior to imaging. After a 10 min acclimation period, in which no nuclear translocation was observed, a mechanical force was applied and nuclear signal tracked. Roots treated with 10 mM of paclobutrazol did not show altered translocation dynamics compared to the untreated control, but roots treated with 50 or 100 mM

paclobutrazol showed greater SWIZ:GFP nuclear localization to begin with, even prior to mechanical stimulus (Fig 2.11). Following stimulus, the nuclear GFP signal in the 100 mM paclobutrazol treated roots did increase to a similar maximum as the control, 10, and 50 mM treated roots, but the net degree of translocation was far less. SWIZ:GFP signal in the 100 mM paclobutrazol treated roots was high prior to treatment and remained high even after the other nuclear signals diminished. This suggests that pharmacological reduction of bioactive GA levels triggers SWIZ nuclear translocation even without the application of mechanical force.

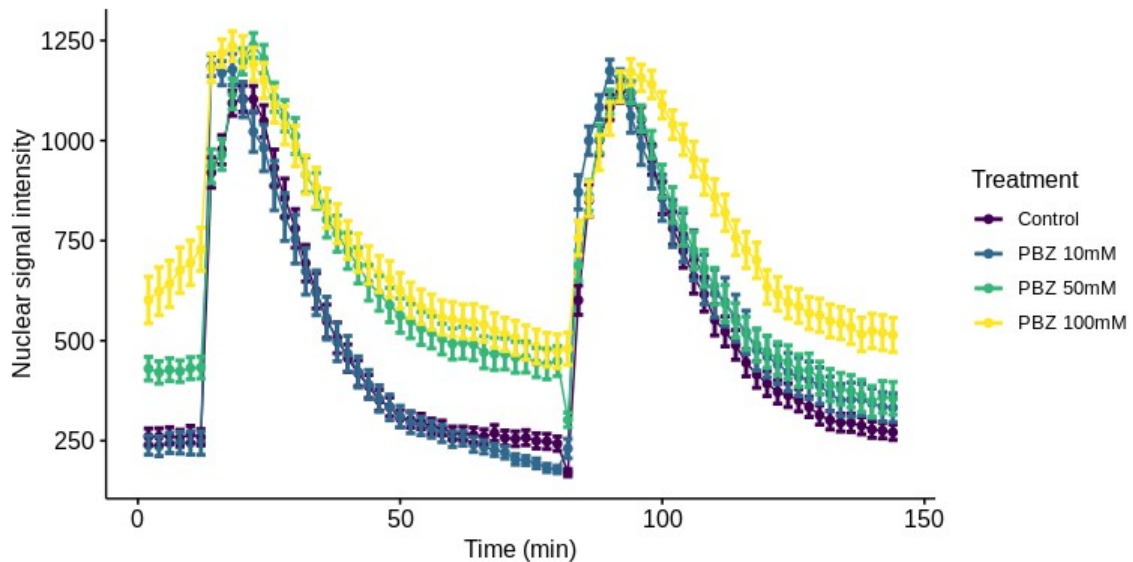


Figure 2.11. SWIZ translocation to the nucleus is enhanced by the addition of paclobutrazol (PBZ), a GA synthesis inhibitor. *SWIZ:GFP-OE* roots were grown on MS media for 6 d, then moved to media supplemented with 10, 50, or 100 mM of PBZ. Plants were left on supplemented media for 6 h, then imaged by confocal microscopy with stimulus at 10 and 60 min. Images were taken every 2 min. Nuclear GFP signal was quantified in selected nuclei at each time point, and then normalized to their value at t=0 min. The average normalized nuclear GFP signal is represented by the trend line, with error bars indicating standard deviation of the mean. n= 64-142 nuclei per treatment

2.3.6 Thigmomorphogenesis in *B. distachyon*

The thigmomorphogenic response in *B. distachyon* was assessed by treating plants with regular mechanical force for two or three weeks during development. Wildtype Bd21-3 plants were grown for 7 d and then either grown without mechanical perturbation as controls or brushed with a metal bar once every 90 min for two or three weeks. After two weeks, a subset of the treated plants were removed from stress and allowed to recover. Another set of plants remained under the treatment for an additional week, totalling three weeks of mechanical force application (Fig 2.12A). After the stress period, all plants were allowed to recover and grow without intentional mechanical perturbation until senescence, after which they were phenotyped. Two week stressed plants were significantly shorter than controls, and three week stressed plants were shorter still (Fig 2.12B). Despite this difference in height, there was not a significant difference between the groups in terms of aboveground biomass (Fig 2.12C). Three week stressed plants had significantly more branches, with an increase also observed in two week stressed plants that was not statistically significant (Fig 2.12D).

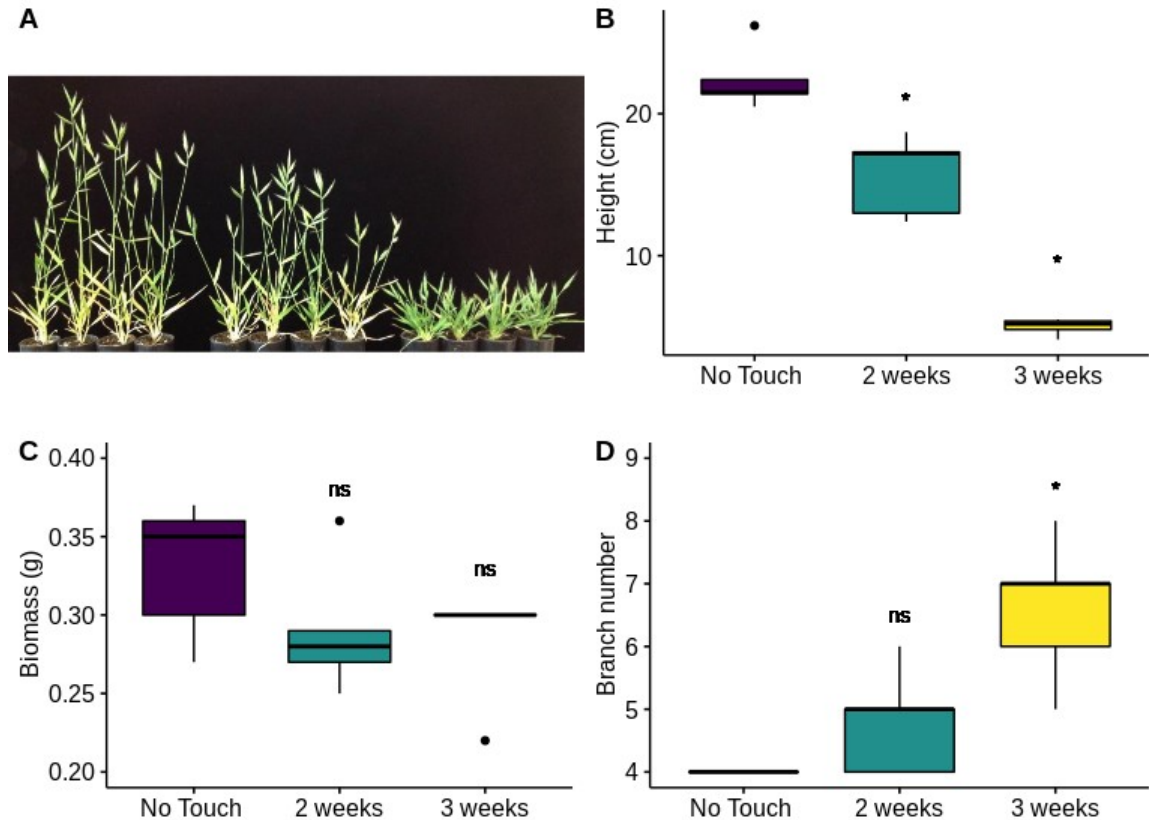


Figure 2.12. *B. distachyon* displays classic thigmomorphogenic phenotypes. Wildtype Bd21-3 was grown for one week prior to treatment and then brushed once every 90 min with a metal bar for two or three weeks, then allowed to grow without mechanical stimulus until senescence. (A) Left to right, no stress, two weeks stress, three weeks stress. Height (B), (C) aboveground non-grain biomass, and (D) branch number were measured at senescence. ns: $p > 0.05$, *: $p \leq 0.05$. $n = 5$ plants per treatment. $n = 5$ plants per treatment.

The effect of repeated mechanical stress on stem biology and interfascicular fiber cell walls was assessed by making transverse sections of the peduncle (Fig. 2.3.13A-C) and the third internode (Fig. 2.3.13D-F) of control plants (Fig. 2.3.13A,D) or plants treated with two (Fig. 2.3.13B,E) or three weeks (Fig. 2.3.13C,F) of mechanical perturbation. Sections were stained with phloroglucinol HCl to detect secondary cell walls, with reddish-pink coloration identifying lignification. The degree of staining and stem morphology in the third internode did not appear to be impacted by mechanical treatments, but the peduncle showed distinct morphological changes in the three week

stressed plants (Fig 2.13C). Interfascicular fiber cell walls stained lighter for lignin, and large parenchyma pockets were evident around the stem periphery, between the minor bundles. These parenchyma pockets contain starch granules, as evidenced by staining with Lugol's iodine (Fig 2.14). There was no significant difference in fiber wall thickness between the internode regions or from differing touch treatments (Fig 2.13G).

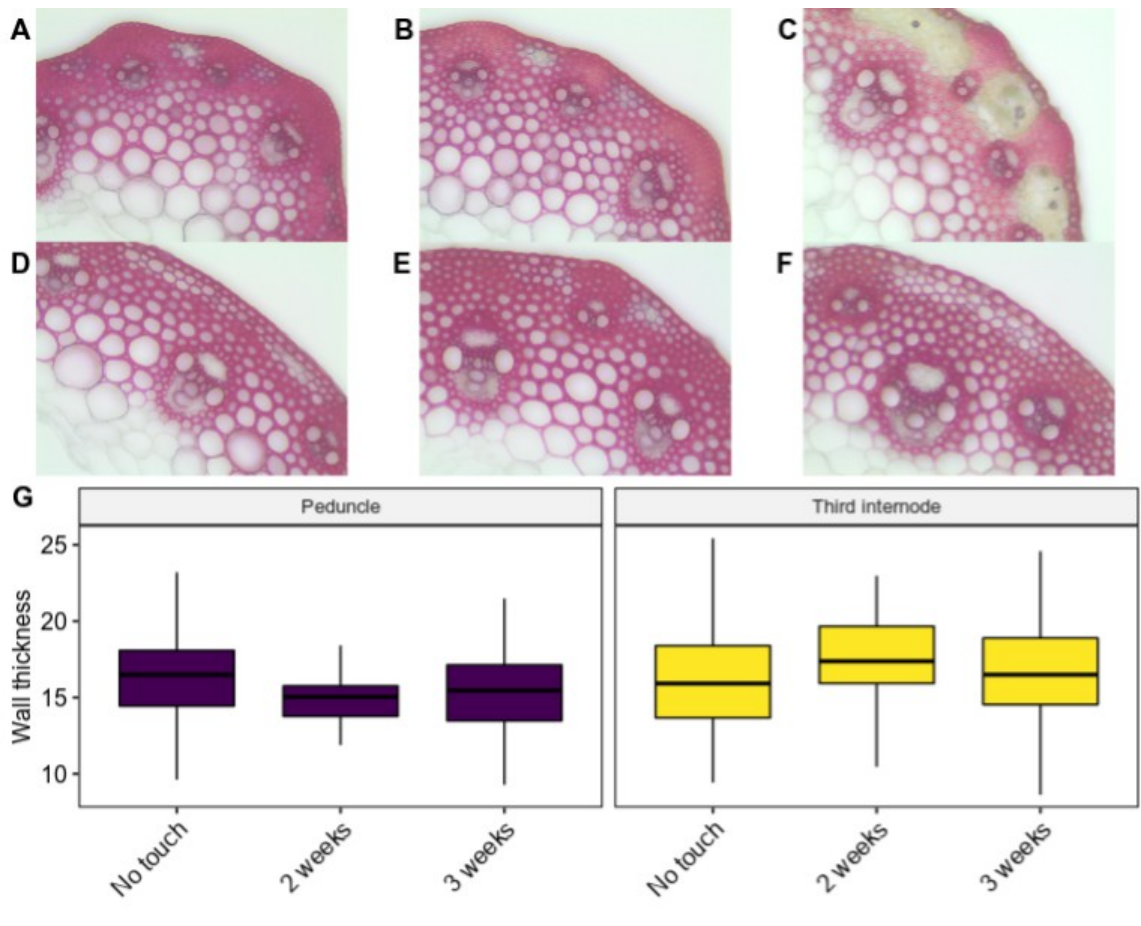


Figure 2.13. *B. distachyon* stem biology under mechanical stress conditions. Wildtype Bd21-3 was grown for one week prior to treatment and then brushed once every 90 min with a metal bar for two or three weeks. Transverse sections of the peduncle (A-C) or 3rd internode (D-F) were taken from control (no stress) (A, D), 2 week stressed (B, E), and 3 week stressed (C, F) plants and stained with phloroglucinol-HCL to identify lignin. (G) Quantification of interfascicular fiber wall thickness. Scale bar = 100µm. ns: $p > 0.05$, *: $p \leq 0.05$. $n = 3$ plants per treatment.



Figure 2.14. Stem parenchyma pockets contain starch granules. Lugol's iodine staining of *B. distachyon* peduncles after three weeks of mechanical stress (Fig 15C) detects starch granules in parenchyma pockets around the stem periphery. Red arrow indicates an example starch granule. Scale bar = 100 μ m.

2.3.7 Thigmomorphogenesis in *SWIZ* genetic reagents

Given the nature of *SWIZ* translocation in response to mechanical stimulus, and the aberrant wall phenotypes observed in *SWIZ-OE* and *swiz-amiRNA* lines, I wanted to test the hypothesis that *SWIZ* translocation in response to mechanical stimulus was responsible for the observed cell wall and plant growth phenotypes. Wildtype Bd21-3, *SWIZ-OE*, and *swiz-amiRNA* were established for one week then placed under mechanical stress as described above for two weeks, or grown carefully without mechanical stimuli as a control group. After senescence, plant height (Fig 2.15A), branching (Fig 2.15B), and aboveground biomass (Fig 2.15C) were measured. In control conditions, there was no difference in these traits. In mechanically stressed conditions, both *SWIZ-OE* and *swiz-amiRNA* were significantly shorter than wildtype, and *swiz-amiRNA* also showed a significant increase in branching.

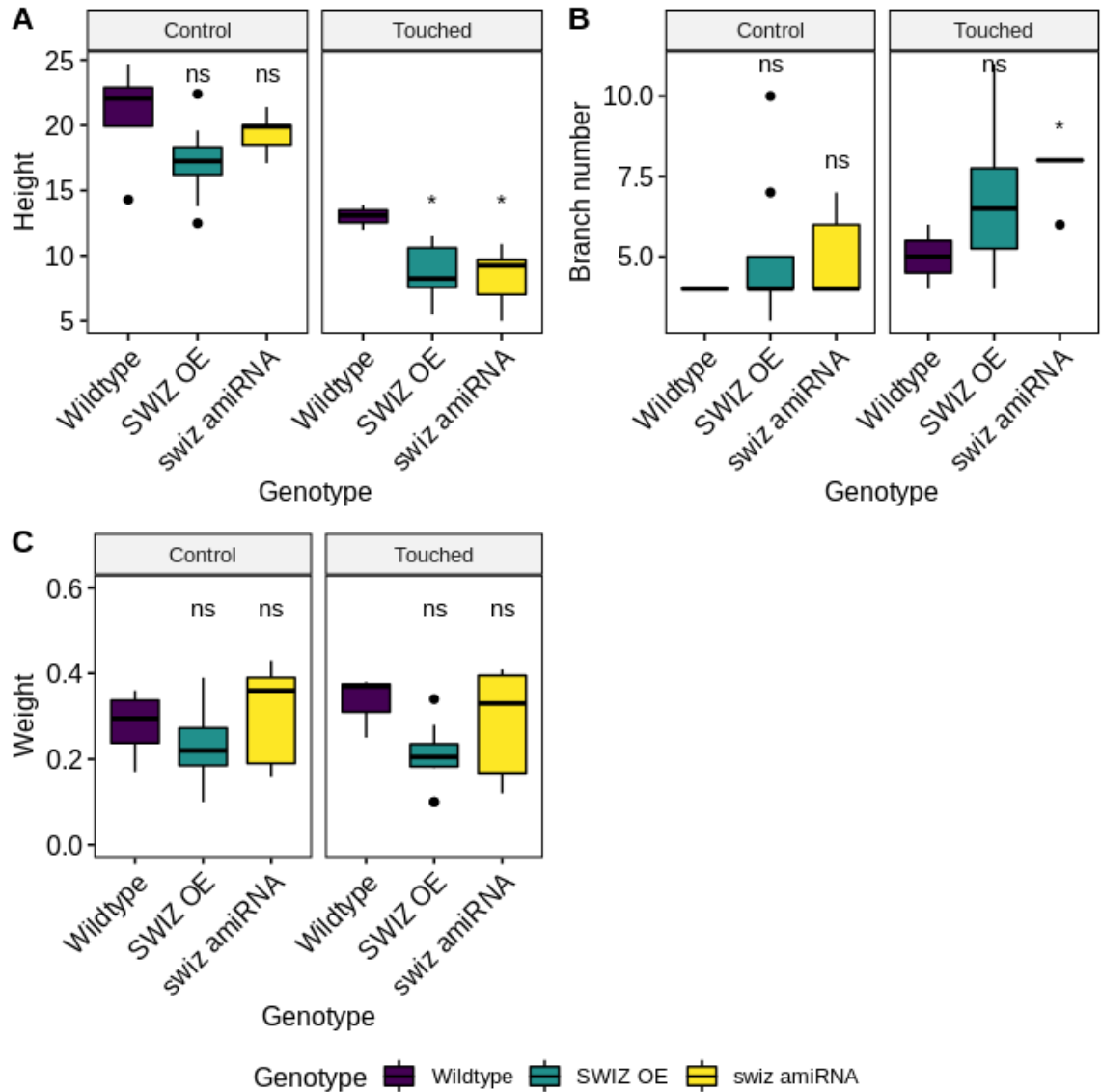


Figure 2.15. Thigmomorphogenic whole plant phenotypes are enhanced in SWIZ reagents under mechanical stress. Wildtype Bd21-3, SWIZ -OE, and swiz-amiRNA plants were grown for one week and then placed under control conditions or two weeks of mechanical stress with metal bar contact once every 90 min. After senescence, plants were phenotyped for (A) height (cm), (B) branch number, and (C) aboveground biomass (g). ns: $p > 0.05$, *: $p \leq 0.05$. $n = 5$ plants per treatment.

Transverse sections of the stem were made in the third elongated internode and the peduncle for wildtype, *SWIZ-OE*, and *swiz-amiRNA* plants in control and touch conditions, and stained with phloroglucinol-HCl (Fig 2.16). The largest effect was seen in the peduncle (Fig 2.16). Control *SWIZ-OE* and *swiz-amiRNA* plants showed lighter lignin staining compared to wildtype. In mechanically stressed conditions, both showed an increase in phloroglucinol-HCl staining, particularly in *swiz-amiRNA*. *SWIZ-OE* interfascicular fiber walls also appear thicker in the stressed peduncle. In the third internode, *SWIZ-OE* and *swiz-amiRNA* both showed less lignin staining than wildtype in control and stressed conditions (Fig 2.16). Interfascicular fiber wall thickness was quantified, showing that thickness increased with mechanical stress treatment in the peduncle of *SWIZ-OE* compared to wildtype. In the third internode there was no difference in *SWIZ-OE* compared to wildtype, although *SWIZ-OE* walls were thicker in the touched plants compared to the control. *swiz-amiRNA* fiber cells did not show a significant difference in touched versus control conditions, or compared to wildtype.

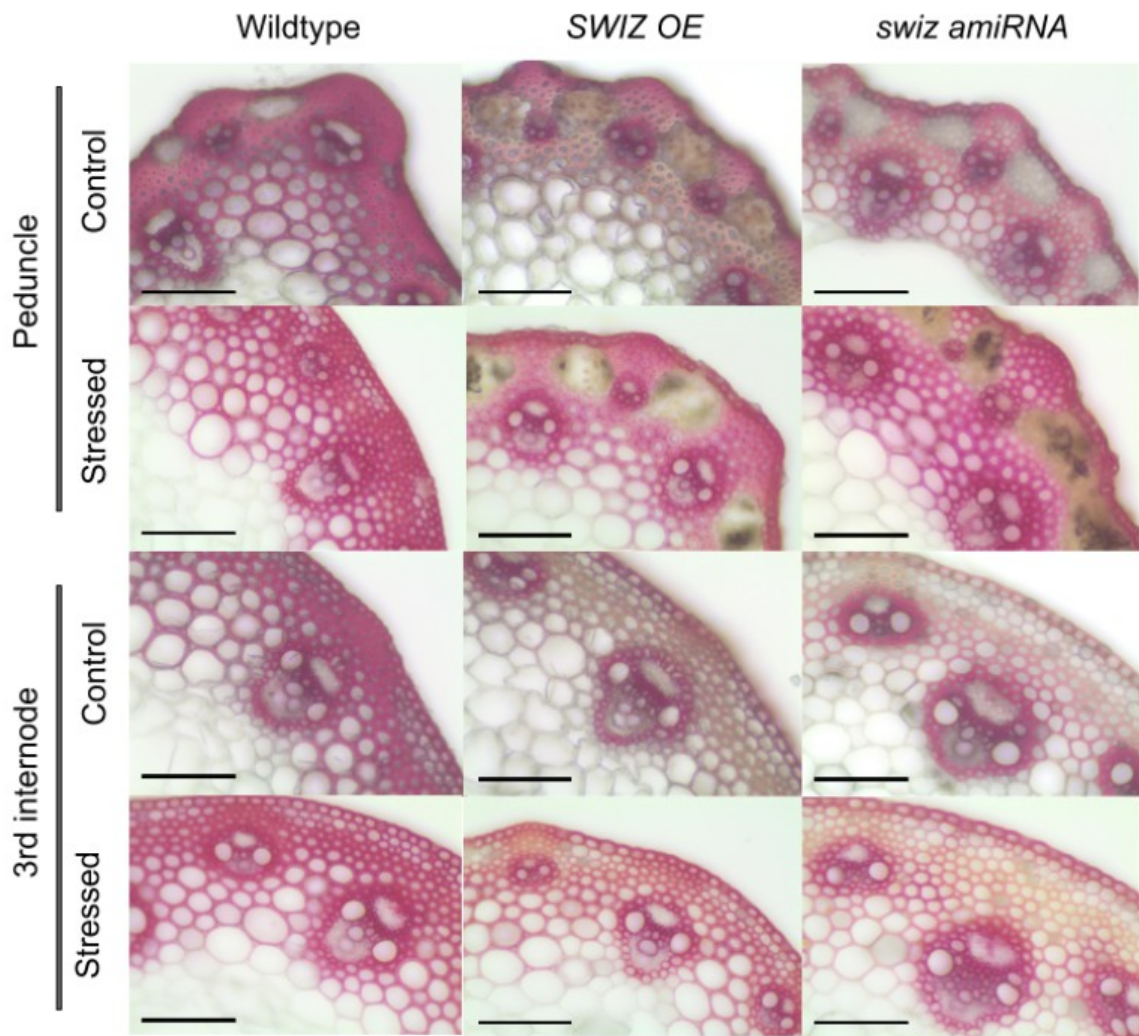


Figure 2.16. Stem biology of *SWIZ* transgenic reagents under touched conditions. Wildtype Bd21-3, *SWIZ-OE*, and *swiz-amiRNA* plants were grown for one week and then placed under control conditions or two weeks of mechanical stress with metal bar contact once every 90 min. After senescence, the main stem was collected and transverse sections made of the peduncle and third elongated internode. Sections were stained with phloroglucinol-HCl. Scale bar = 100 μ m.

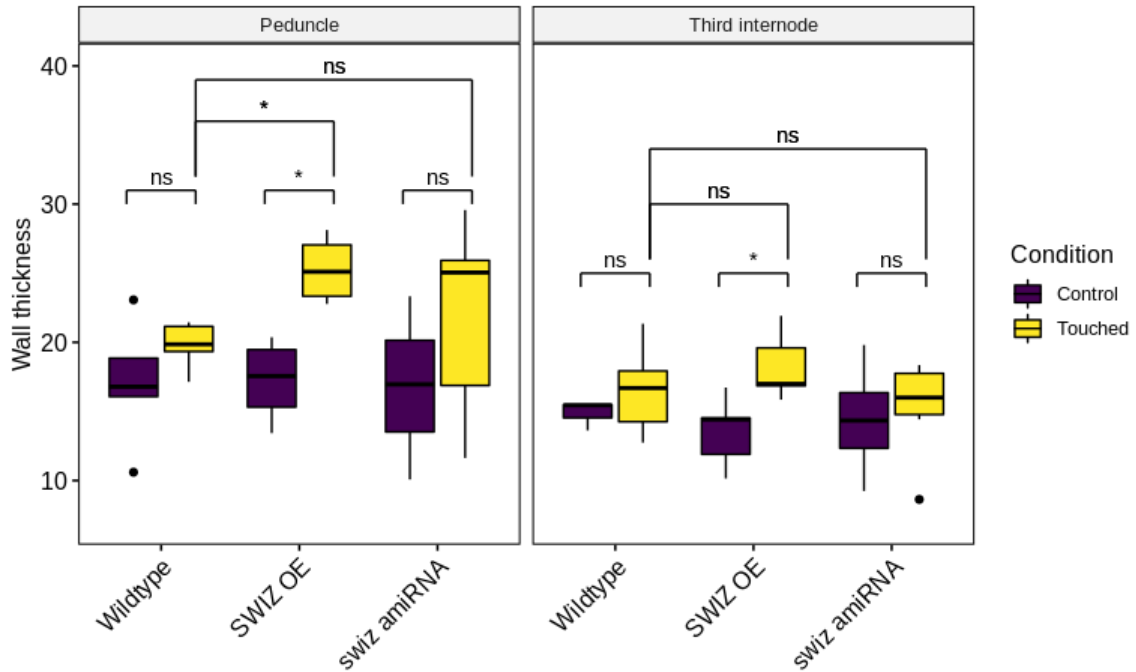


Figure 2.17 Quantification of interfacicular fiber wall thickness under touch and control conditions in SWIZ genetic reagents. n=4-6 plants per genotype, per treatment.

The changes observed in cell wall thickening and staining in *SWIZ-OE* and *swiz-amiRNA* lines under touched conditions, coupled with the protein binding of cell wall associated promoters in the yeast one hybrid prompted me to investigate cell wall gene expression in *SWIZ* transgenic plants in response to touch stimulus. The entire main stem from wildtype, *SWIZ-OE*, and *swiz-amiRNA* plants in control and mechanically stimulated conditions was collected one day after flowering, and approximately 20 min following mechanical stimulus. Relative expression of cell wall biosynthesis genes was measured for *CAD1*, *COMT6*, and *CESA4* (Fig 2.18). While not statistically significant, *COMT6* expression decreased in both *SWIZ-OE* and *swiz-amiRNA* with a larger decrease in *swiz-amiRNA* when touched.

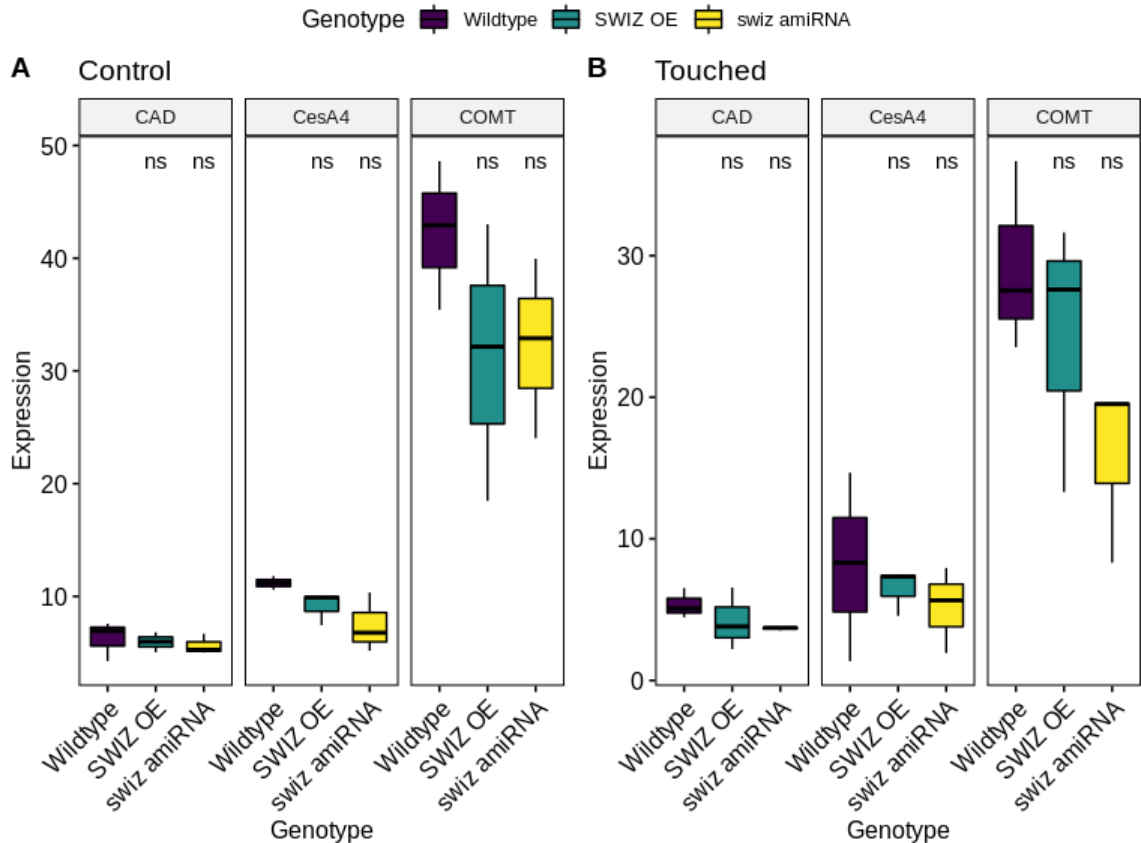


Figure 2.18. Cell wall gene expression in SWIZ transgenic plants following mechanical stimulus. Wildtype Bd21-3, SWIZ-OE, and *swiz-amiRNA* plants were grown for one week and then placed under control conditions or two weeks of mechanical stress with metal bar contact once every 90 min. One day after flowering, the entire main stem was collected approximately 20 min after a touch stimulus event. Transcript abundance measured by RT-qPCR relative to ubiquitin conjugating enzyme 18 expression. ns: $p > 0.05$, *: $p \leq 0.05$. $n = 3$ plants per genotype.

2.4 Discussion

2.4.1 SWIZ is a likely cell wall regulator

SWIZ was first identified as a candidate regulator of secondary wall synthesis based on gene expression pattern and subsequently by protein-DNA interactions with cell wall associated cis-regulatory regions. *SWIZ* is clearly a Group I bZIP transcription factor, and is the closest *B. distachyon* ortholog to *A. thaliana bZIP18/52* and *O. sativa bZIP61*, closely related to *OsRF2b* (Jakoby *et al.*, 2002; Liu & Chu, 2015; Dröge-Laser *et al.*, 2018). Several families of transcription factors are known to directly regulate secondary wall thickening, chief among them are NAC and MYB proteins (Coomey *et al.*, 2020). As with *SWIZ*, many of these genes were first identified based on their expression patterns being correlated with secondary wall biosynthetic enzymes. Recent studies in *A. thaliana*, *B. distachyon*, and *O. sativa* have shown protein-DNA interactions with the promoters of secondary wall associated genes, as I have demonstrated for *SWIZ* and *CAD1*, *COMT6*, and *CESA4* (Zhong & Ye, 2007; Taylor-Teeple *et al.*, 2015; Handakumbura *et al.*, 2018).

Surprisingly, I observed a similar phenotypic response in both gain and loss of function lines with reduced height and thicker interfascicular fiber walls. *SWIZ* gain-of-function mutants were generated constitutively expressing *SWIZ* transcript and loss-of-function was achieved by knockdown of *SWIZ* expression using an artificial microRNA construct targeting *SWIZ* transcript. After confirming the presence and expression of the transgenes, *SWIZ-OE* and *swiz-amirNA* were assayed for growth and cell wall defects. The *swiz-amirNA* lines had lower lignin content in fiber cells compared to wildtype, while *SWIZ-OE* was unchanged. These data suggest a role for *SWIZ* in activating lignin

deposition. Furthermore, the decrease of lignin in *swiz-miRNA* supports a role as a direct regulator of *CAD1* and *COMT6*. Given the unusual pattern of wall thickening seen in *SWIZ-OE* sections and the reports of Group I bZIPs translocating in response to hypo-osmotic stress (Tsugama *et al.*, 2014, 2016), I hypothesized that SWIZ may respond to mechanical stimuli to regulate aspects of growth and secondary wall deposition.

2.4.2 SWIZ translocation dynamics are consistent with reported bZIP dynamics in response to mechanical stimulus and GA

I began to test this hypothesis by investigating the cellular localization of SWIZ protein in response to mechanical stimulus. Consistent with reports of Group I bZIPs in root tissue (Tsugama *et al.*, 2014, 2016), SWIZ translocated from the cytosol to the nucleus in response to mechanical stimulus. In *A. thaliana*, translocation was stimulated by treatment with a hypo-osmotic solution, which proved technically challenging on our confocal microscope platform. Since hypo-osmotic pressure simulates external force on the cell, I opted to apply force directly to the root by light contact with a metal probe. Prior to touch, SWIZ was mostly localized to the cytosol, with some nuclear localization. Following touch, SWIZ translocated to the nucleus quite rapidly, with peak nuclear signal intensity around 30 min after stimulus. By 75 min post-stimulus, the nuclear signal had returned to pre-stimulus levels. This timing is consistent with the observations made for *A. thaliana* Group I bZIPs (Tsugama *et al.*, 2014, 2016), although those reports only provide information at 0, 30, and 120 min post-treatment, rather than the measurements taken every 2 min for SWIZ translocation. I also investigated the repeatability of SWIZ translocation following sequential stimuli. The timing of touch response has been investigated in various systems on the order of min to days, and have shown acclimation of the touch response to successive stimuli (Coutand *et al.*, 2009; Martin *et al.*, 2010;

Leblanc-Fournier *et al.*, 2014). For SWIZ, the translocation dynamics are consistent at least over three successive cycles of stimulus and return to baseline. The dynamics observed in *SWIZ-OE* suggest that SWIZ translocation is not dampened by subsequent stimulus. While the kinetics of touch response acclimation have not been studied in *B. distachyon*, we may consider at least that input from SWIZ remains consistent for multiple stimulus events.

2.4.3 Thigmomorphogenesis in *B. distachyon*.

Before testing the idea that SWIZ functioned in touch responsive growth, I first wanted to examine thigmomorphogenesis in *B. distachyon* to establish a mechanical stimulus assay and provide a baseline of phenotypic response in wildtype plants. In light of the timing and repeatability of SWIZ translocation dynamics, regular stimulus at 90 min intervals was chosen for the treatment. Touch stimulus is generally an inhibitor of plant elongation growth, but promotes branching and radial growth (Jaffe, 1973; Braam, 2004; Chehab *et al.*, 2009). In eudicots, this radial growth occurs in the cambium meristem, a cell type that is not present in grasses. Therefore, they do not undergo such changes in radial growth. Our study of wildtype *B. distachyon* plants with two or three weeks of regular touch revealed a decrease in plant height similar to that previously reported (Gladala-Kostarz *et al.*, 2020). We also observed an increase in branching with increasing touch treatment. However, we did not observe a change in total biomass at senescence, perhaps due to compensation by increased branching.

2.4.4 SWIZ touch responsive phenotypes

SWIZ gain- and loss-of-function transgenic lines were subjected to two weeks of touch stimulus alongside control groups that were treated carefully to minimize possible

sources of mechanostimulation from watering and handling. In touch conditions, both *SWIZ-OE* and *swiz-miRNA* plants were shorter than wildtype, while in control conditions they were not different. Total biomass was not affected by genotype or touch, but *swiz-miRNA* did show increased branching under touched conditions. While the touch treatment did affect wildtype plants similar to control conditions, the influence of touch was greater in the *SWIZ* transgenics.

Under touched conditions, the peduncle of *SWIZ-OE* had thicker interfascicular fiber walls compared to wildtype, while in the control there was no difference. In the third internode there was no difference in fiber wall thickness between lines. The peduncle also showed a difference in lignin staining in touched conditions compared to control, with *SWIZ-OE* and *swiz-miRNA* showing an increase in staining intensity. The prevalence of phenotypic changes in the peduncle but not the third internode is attributed to the nature of the touch treatment. The metal bar passed over the plants at a set height that was above the position of the third internode, but came into contact with the peduncle. Thus, the entire plant did not experience the mechanical stimulus evenly, and the touch induced response was limited to the contacted tissue. This is consistent with how *SWIZ* translocation is restricted to the stimulated region. In *A. thaliana*, *AtVIP1* translocation was limited to just a few cells perturbed by contact with a pin (Tsugama *et al.*, 2014). *SWIZ* translocation was similarly specific to the cells that experienced direct mechanical stimulus. Regions of the root 3 cm away from a touched section did not show translocation. Given this specificity, I assume that the peduncle cells of touched plants experienced *SWIZ* translocation while lower internodes did not.

2.4.5 Bioactive GA status may act in SWIZ mechanosignaling and explain touch responsive height phenotypes.

Several lines of evidence implicate bioactive GA status as part of the mechanoperception pathway that modulates SWIZ translocation, and may help explain the SWIZ touch responsive phenotypes. Dominant negative *NtRSG* transgenic tobacco has a dwarf phenotype due to misregulation of GA synthesis that inhibits cell elongation (Fukazawa *et al.*, 2000). In tobacco protoplasts, NtRSG translocates into the nucleus in response to low bioactive GA, where it then promotes the synthesis of bioactive GA (Ishida *et al.*, 2004; Fukazawa *et al.*, 2010, 2011). Lange & Lange (2015) demonstrated that touch inactivates cellular GA (Lange & Lange, 2015). Together, these observations can provide a model relating touch, GA, and cell elongation. Touch inactivates GA, a hormone that promotes elongation, and in response bZIP proteins translocate into the nucleus and act to re-establish bioactive GA and elongation. SWIZ translocation is consistent with these observations. When *SWIZ-OE* roots were treated with exogenous bioactive GA, the nuclear translocation following touch was dampened. When *SWIZ-OE* roots were treated with paclobutrazol to chemically inhibit bioactive GA synthesis, SWIZ protein localized to the nucleus even in the absence of touch.

Applying this model to *SWIZ-OE* and *swiz-amiRNA* provides possible mechanisms for the reduction in height observed in both types of transgenic plant under touch treatment. If *SWIZ* is indeed an activator of wall synthesis, the large influx of protein to the nucleus following touch may trigger activation of cell wall thickening, resulting in reduced cellular elongation. If *SWIZ* regulates GA synthesis genes similarly to *NtRSG*, then the reduced *SWIZ* population in *amiRNA* lines may not be able to restore proper GA levels following touch, resulting in an inability to continue elongation. This sort of activity in

the *swiz-miRNA* lines would be consistent with the dwarf phenotype observed in *NtRSG* dominant negative mutants (Fukazawa *et al.*, 2000). Similar dwarfing is also seen from expression of an *OsRF2a* dominant negative mutant (Dai *et al.*, 2003).

2.4.6 SWIZ touch responsive cell wall phenotypes may depend on interacting partners

In touched peduncles, *SWIZ-OE* and *swiz-miRNA* showed increased lignin staining in interfascicular fiber cells compared to untouched controls, while the third internode of both mutants stained more lightly in both touched and control conditions. Gene expression analysis did not show a significant difference in *COMT6*, *CAD1*, or *CESA4* expression in stems of either *SWIZ-OE* or *swiz-miRNA* in touched or control conditions. *COMT6* expression did appear to be somewhat reduced in the *SWIZ* transgenics, which would be consistent with the lighter staining seen in the third internode. However, this experiment was conducted on whole stems prior to my understanding of the specific nature of *SWIZ* translocation in directly contacted regions. It is possible that the gene expression signal in the touched cells was diluted by homogenization with the entire stems, and thus we did not observe a change in touched conditions.

SWIZ may regulate wall thickening by directly binding upstream of genes associated with secondary wall biosynthesis. We identified a sequence motif commonly reported for bZIP-DNA interactions (O'Malley *et al.*, 2016). Yeast one-hybrid data shows *SWIZ* protein interacting with regulatory regions of *CAD1*, *COMT6*, and *CESA4*, yet none of these appear in the *in vitro* DAP-seq binding results. Interestingly, one of the top two binding motifs from DAP-seq is present in the overlapping region of two *CAD1* promoter fragments that *SWIZ* interacted in yeast. One explanation for why this and perhaps other

cell wall relevant genes do not appear in the DAP-seq results comes from the homo and heterodimerization of bZIP proteins. The leucine zipper domain of bZIPs has been shown to dictate the interactions between dimerizing partners (Schütze *et al.*, 2008), and in *A. thaliana* the combinatorial interactions of different bZIP groups has been fairly well defined (Deppmann *et al.*, 2004; Grigoryan & Keating, 2006; Ehlert *et al.*, 2006; Weltmeier *et al.*, 2006; Schütze *et al.*, 2008). Group I bZIPs are known to interact with one another as well as with Group E members (Schütze *et al.*, 2008; Van Leene *et al.*, 2016). These interactions can have a synergistic effect on transcriptional activity, and can result in unique binding interactions (Schütze *et al.*, 2008; Van Leene *et al.*, 2016). A study of *AtbZIP29* showed heterodimerization specifically within a subset of seven Group I bZIPs that are orthologous to bZIPs implicated in cell wall synthesis and remodelling in other systems, including *NtRSG*, *OsRF2a*, *OsRF2b*, and *SIVSF-1* (Yin *et al.*, 1997; Ringli & Keller, 1998; Fukazawa *et al.*, 2000; Dai *et al.*, 2003, 2004; Van Leene *et al.*, 2016). SWIZ is part of the same clade of protein, and SWIZ's role in cell wall synthesis may also rely in part on interaction with other bZIP partners, a role that would not be identified through the *in vitro* DAP-seq assay.

2.4.7 SWIZ *in vitro* binding targets relate to hormone cross talk and mechanoperception pathways

Despite the caveats of biological relevance for bZIPs in *in vitro* binding assays, it is still tempting to speculate on the implications of the SWIZ binding targets identified from DAP-seq. Perhaps the most interesting avenue suggested from this data involves the crosstalk of auxin, gibberellin, and ethylene signaling. A number of these sites are associated with genes annotated as auxin response factors (ARFs) and small auxin upregulated RNA (SAUR) genes. Gibberellin metabolism and signalling genes in this

data set include GRAS family transcription factors and an ortholog of AtGA2OX2.

Ethylene responsive binding proteins are implicated in touch response, and an annotated APETALA2/Ethylene responsive binding protein is present in the DAP-seq results. Cross talk between these hormone signalling pathways is implicated in secondary wall development. In maize stems ethylene signalling controls auxin and GA, resulting in altered cell wall synthesis (Zhang *et al.*, 2020),

Aspects of force perception and signalling such as wall associated kinases, receptor like kinases, mitogen activated protein kinases, calcium dependent protein kinases, calmodulin, and calmodulin-like genes. Calcium fluxes have been described in response to touch (Lee *et al.*, 2005; Monshausen *et al.*, 2009), and both calcium dependent protein kinases and mitogen activated protein kinases are known to phosphorylate bZIPs (Djamei *et al.*, 2007; Ishida *et al.*, 2008; Pitzschke *et al.*, 2009; Ito *et al.*, 2014). Wall integrity sensors such as wall associated kinases and receptor like kinases have been suggested to play a role in force perception as well (Monshausen & Haswell, 2013; Leblanc-Fournier *et al.*, 2014; Kohorn, 2016). These putative SWIZ regulatory targets suggest a scenario where SWIZ translocation and transcriptional activation may prime the cell for future sensing events by upregulating possible sensing and signalling components.

2.5 Conclusions

SWIZ is a bZIP family transcription factor orthologous to proteins in other species that have been implicated in cell wall development and remodelling. SWIZ appears to control elongation and cell wall thickening in response to mechanical stimuli, which regulates SWIZ translocation into the nucleus by acting on the cellular bioactive GA pool. Touch decreases cellular bioactive GA levels, which causes SWIZ to translocate from the

cytoplasm into the nucleus. This translocation can be reduced by supplementing with exogenous bioactive GA, or induced by chemically inhibiting GA synthesis.

CHAPTER 3

KNOTTED OF BRACHYPODIUM 7 (KNOB7) IS A CLASS II KNOX GENE AND NEGATIVE REGULATOR OF INTERFASCICULAR FIBER SECONDARY CELL WALLS

3.1 Introduction

The *three-amino-acid-loop-extension (TALE)* homeodomain family of transcription factors includes several well characterized regulators of growth and development in eudicots and grasses. The *KNOTTED1 HOMEODOMAIN (KNOX)* and *BEL* class *TALEs* have been shown to regulate secondary wall synthesis. The founding member of the *KNOX* gene family is *ZmKNOTTED1 (KN1)*, which was first identified in maize as the causative gene in a gain of function mutant whose phenotype was of bumpy, or knotted looking leaves (Vollbrecht *et al.*, 1991). *KNOX* genes include Class I and Class II types. Class I *KNOX* genes including *KN1*, *SHOOT MERISTEMLESS*, and *GNARLY*, regulate aspects of organ development and meristem maintenance (Hake *et al.*, 2004; Hay & Tsiantis, 2010). Class II *KNOX* genes are not as well characterized, with most work focusing on the function of *KNOTTED OF ARABIDOPSIS THALIANA 7* (Zhong *et al.*, 2008a; Li *et al.*, 2012; Liu *et al.*, 2014; He *et al.*, 2018). *AtKNAT7* was first identified as *IRREGULAR XYLEM 11 (IRX11)* in a screen for transcripts co-expressed with secondary cell wall associated genes (Ehlting *et al.*, 2005; Persson *et al.*, 2005; Brown *et al.*, 2005b). The irregular xylem (*irx*) phenotype, as the name implies, consists of collapsed xylem vessel cells. This phenotype can vary in severity, and has been associated primarily with cellulose defects, but also with altered hemicellulose and lignin biosynthesis (Turner & Somerville, 1997; Brown *et al.*, 2005b). *AtKNAT7* has been shown repeatedly to be a

target of the so called master regulators of cell wall biosynthesis; *SND1*, *NST1*, *NST2*, *VND6*, and *VND7* all positively regulate *AtKNAT7* expression (Zhong *et al.*, 2006b, 2007a, 2008a). MYB46, another target of *SND1*, has also been shown to be a positive regulator of *KNAT7* expression (Zhong *et al.*, 2007a; Zhong & Ye, 2007). All of these master regulators are known to be capable of activating the entire suite of cell wall biosynthetic enzymes, either directly or through other downstream regulators, such as *AtKNAT7*. *AtKNAT7* and orthologs in other species, such as poplar (*PtKNAT7*) and cotton (*GhKNL1*), are generally described in the literature as repressors of cell wall synthesis in fiber cells (Li *et al.*, 2012; Ma *et al.*, 2019). *AtKNAT7* contains a canonical LxLxL EAR motif, known for its role in repressing gene expression. EAR containing proteins recruit histone modifying complexes to their DNA binding sites, resulting in condensation of the chromatin and subsequent transcriptional repression (Kagale & Rozwadowski, 2011). While there is substantial evidence for *AtKNAT7* repressor function, there is also data indicating a role in positive wall regulation. *Atknat7* mutants have thicker interfascicular fiber walls, as expected for knocking out a repressor, but this mutant also shows collapsed xylem with thinner walls. *Atknat7* mutants have greater lignin content, but reduced xylan, suggesting that *AtKNAT7* may differentially regulate aspects of hemicelluloses compared to lignins. *AtKNAT7* protein can bind to the promoter of *AtIRX9*, a gene responsible for xylan backbone synthesis as well as control the expression of several enzymes in the lignin biosynthesis pathways (He *et al.*, 2018).

AtKNAT7 is known to interact with several other protein partners, including another class II KNOX protein, *AtKNAT3*. The double mutant, *knat7/knat3* has more severe cell wall phenotypes than *Atknat7* alone, while the *Atknat3* knockout has no reported

phenotype. AtKNAT7 is also involved in seed coat development through interaction with AtMYB75 (Bhargava *et al.*, 2010, 2013). In other systems such as alfalfa and peach, other class II KNOX genes not orthologous to AtKNAT7 play roles in leaf and seed coat development (Testone *et al.*, 2009; Chai *et al.*, 2016).

Another TALE transcription factor, BEL1-LIKE HOMEODOMAIN6 (BLH6), can repress secondary wall formation in interfascicular fiber cells. Similar to *Atnat7*, *Atblh6* mutants have collapsed xylems and thicker fiber cell walls. Indeed, AtBLH6 and AtKNAT7 protein physically associate, and as a complex repress fiber wall thickening. Genetic analysis has shown that this complex regulates fiber wall development by directly binding the *AtREV* promoter (Liu *et al.* 2014). The *blh6/rev* and *knat7/rev* double mutants exhibit the collapsed xylem phenotype similar to the single *blh6* or *knat7* mutants, but the *rev* double mutants do not have thicker interfascicular fiber walls. This suggests that xylem wall regulation relies on distinct mechanism from interfascicular fibers, and that the direction of transcriptional action by known wall regulators may vary between these tissues.

In grasses, rice *OsKNOR1* (also known as *OsKNAT7*) is the closest ortholog of *AtKNAT7* and has also been shown to negatively regulate cell wall synthesis in interfascicular fiber cells (Zhao *et al.*, 2019; Wang *et al.*, 2019). As in *Atnat7*, *Osknor1* loss-of-function mutants have thicker interfascicular fiber walls, but no reported xylem phenotype. These plants also had an increase in grain size that was attributed to variation in cell size (Wang *et al.*, 2019). Gene similar to BLH6 have not been described as regulators of wall thickening in grasses. However, OsKNOR1 analysis revealed functions unique from AtKNAT7. It was shown to physically interact with OsNAC31 (also known as OsVND7/

OsSWN3) and Os GROWTH REGULATING FACTOR 4 (OsGRF4). Transient gene expression analysis in protoplasts showed that OsKNOR1-OsNAC31 jointly regulated *OsMYB61/103* expression, with OsKNOR1 mitigating the positive regulation by OsNAC31. Similarly, OsGRF4 is known to activate expression of cell expansions genes, and OsKNOR1 interaction reduces this expression (Wang *et al.*, 2019).

3.2 Methods

3.2.1. Plasmid construction

Overexpression constructs were built using the Invitrogen Gateway cloning system. PCR amplified coding sequences were cloned into the pENR-D-TOPO or appropriate pDONR vector for multi site recombination, and further subcloned into a modified pOI001 destination vector (Vogel *et al* 2006). CRISPR-Cas9 guide RNA sequences were designed using the CRISPR-PLANT web resource (<http://www.genome.arizona.edu/crispr/CRISPRsearch.html>). The *knob7-1* allele was targeted by the 5'-CCTGCAGCTGAAGCAAATCAAGA-'3 guide RNA. Guide RNA oligos were annealed by heating to 95C for 2 min followed by slowly cooling to 25C at 2 degrees per minute. Annealed guide RNAs were cloned into the pENTR_OsU3B_sgRN vector by BsaI digestion and ligation. Sequence confirmed clones were recombined using the Invitrogen Gateway cloning system into the pOs-cas9_RC_of_L destination vector.

Sequence confirmed clones for all destination vectors were electroporated into *Agrobacterium tumefaciens* strain AGL-1.

3.2.2 Identification of mutants

Sodium azide mutant population was generated by the Sibout lab at INRAE Versailles-

Grignon (Dalmais et al 2013). Briefly, wildtype Bd21-3 seeds were treated with sodium azide to induce point mutations. Genomic DNA from M2 plants from each family was pooled and sequenced to identify mutation sites. To confirm specific mutations in subsequent generations, PCR primers were designed to flank the mapped mutation locus, and sequencing of the PCR product determined the presence of the mutation. The *knob7-3* allele was identified in line NaN451.

3.2.2. Plant transformation

Transformation was performed according to Vogel & Hill 2008. Immature seeds were collected from ~6 week old plants, deglumed, and surface sterilized with a solution of 1.3% NaClO and 0.01% Triton-X100 for four min. Sterilized seeds were rinsed three times in sterile water. Embryos were dissected from the seeds and placed on callus initiation media (CIM) for four weeks, then subcultured to fresh CIM for two more weeks, the subcultured a final time onto fresh CIM for one week. Seven week old calli were co-cultivated in a suspension of *A. tumefaciens* for ~5 min, then thoroughly dried on sterile filter paper for 3-5 days at 22C in the dark. Calli were moved onto CIM media containing 50 mg/L hygromycin B and 150 mg/L timentin, where they were grown for 3-5 weeks with selective subculture of healthy callus at week 4. After selection, healthy calli were moved to Linsmaier and Skoog media supplemented with 50 mg/L hygromycin B, 150 mg/L timentin, and kinetin to promote shoot growth. Calli that produced green tissue within 3-5 weeks were moved to Murashige and Skoog media supplemented with 50 mg/L hygromycin B and 150 mg/L timentin to allow root growth. After 1-3 weeks, calli that established roots were transplanted to soil and grown as described below.

3.2.3. Plant growth

Brachypodium distachyon line Bd21-3 was used for all experiments. Seeds were stratified on wet paper towel wrapped in foil to exclude light for 10 days at 4C before being planted in Promix BX potting mix in SC10 Ray Leach Cone-tainers (Stuewe & Sons Inc, <https://www.stuewe.com/products/rayleach.php>). Plants were grown in a Percival PGC-15 growth chamber with day/night conditions of 20h light at 22C and 4h dark at 18C respectively.

3.2.4. Transverse stem sections, histology

The main stem of senesced plants was taken and the internode of interest removed and embedded in 8% agarose. Samples were sectioned using a Leica VT1000 Vibratome, making 55um thick sections. Multiple sections of each internode were collected and stored in water at 4C. Histochemical staining was carried out using toluidine blue, phloroglucinol-HCl, and Maule reagent as described in Mitra & Loque (2014). Images were obtained at 4, 10, and 20x using a Nikon Eclipse E200MV R light microscope and PixeLINK 3 MP camera.

3.2.5 Measuring cell wall thickness

Transverse sections imaged at 20x were used for cell wall thickness measurements. Interfascicular fiber cells separated by one cell layer from the mestome cells on the phloem side of major vascular bundles were targeted for measurement. Using ImageJ, lines were drawn across two walls of adjoining cells. The resulting line length was divided by two to give one cell wall width. ~15 measurements were made for each plant.

3.2.6. Cell wall material insoluble in alcohol (MIA)

The main stem of mature, senesced plants was collected and cut into small pieces (~2 cm)

into a 2 ml tube. Two metal beads were added and the stem was ground to a fine powder using a Retsch 440 bead beater. Ground material was transferred to a glass screw cap tube. Cell wall material was washed with 5ml of water in an 80°C water bath for 10 min with agitation. The cell wall material was pelleted by centrifugation at 3700 rpm for 10 min and the supernatant aspirated by vacuum. This was repeated for a second water wash. The cell wall material was then washed three times with 100% ethanol at 80°C for 15 min per wash, with collection by centrifugation and aspiration of the supernatant between washes as described above. The cell wall material was then washed twice with acetone for 15 min per wash at room temperature, then left to dry under a fume hood overnight. Modified from INRAE protocols.

3.2.7. ABSL quantification

Beginning with dry cell wall MIA samples, 4.5-5.5 mg of each sample was weighed into a 2 mL glass vial using a precision balance. 1ml of acetyl bromide solution(25% acetyl bromide, 75% acetic acid) was carefully added to each vial under a fume hood. The vials were capped and inverted several times to mix. Samples were incubated in a drying oven at 55°C for 2 h 30 min, with mixing by gentle inversion every 30 min to ensure full sample solubilization. The samples were cooled to room temperature before proceeding. 0.1 ml of sample was diluted into 1.2 ml of acidified 2MNaOH, then mixed with 0.3 ml of 0.5 M hydroxylamine chlorhydrate and 1.4 ml of acetic acid. Using a glass pipette, air was bubbled through the sample to ensure full homogenization of the reaction mixture. Absorbance at 280 nm was measured on a SpectraMaX M6 plate reader, and the lignin content was calculated using the following equation: %lignin= $100 \times (A_{280} \times \text{Vol reaction} \times \text{Vol dilution}) / (20 \times \text{Vol sample solution} \times \text{Mass sample (mg)})$. Modified from

INRAE protocols.

3.2.8. Mild alkaline hydrolysis

Beginning with solvent free cell wall samples, 10mg per sample was weighed out into tubes. 100 ul of *o*-coumaric acid (1mg/ml) was added to each sample as an internal control. 1ml of 1N NaOH was added to each sample and mixed well by inversion. The samples should turn a bright, fluorescent yellow. The tubes were wrapped in foil to protect them from light and placed on a rotating agitator overnight. The next day, samples were removed from the agitator and acidified with 250 ul of 6M HCl. Samples were centrifuged at 2000g for 5 min to remove any remaining cell wall debris, and the supernatant transferred to a clean tube. Hydroxycinnamate extraction was done on silica columns bound with C21 hydrocarbons. Columns were washed with methanol, then primed with 2 ml of acidic water (H₂O + 0.1% formic acid). 0.5 ml of sample was run through the column. Excess salts were flushed out with 2 ml of acidic water, then the column was eluted into glass vials with 1ml of methanol. Eluted samples were chilled at -20°C for 15 min to precipitate any insoluble components. Samples were analyzed by HPLC-MS with a diode array detector using a MacheryNagel - EC 50/2 (mm) nucleoshell - RP (rev phase) C18, 2.7 mm granularity column. Modified from INARE protocols.

3.2.9 Thioacidolysis

Thioacidolysis reagent was carefully prepared in a chemical fume hood as previously described (Méchin *et al.*, 2014), resulting in a 9:1 dioxane:ethanethiol mixture with 0.1M tetrafluoroboric acid dimethylether. For each sample, 10 mg of cell wall material insoluble in alcohol was weighed into screw cap tubes. 7 ml of thioacidolysis reagent was

added, along with 2.5 mg/ml of heneicosane C21 as an internal standard. The tubes were incubated in a 100°C oil bath for 4 h and then cooled in ice water. 0.2M NaHCO₃ was added to each tube, followed by 0.1 ml of 6M HCl. 7 ml of dichloromethane was added and tubes were gently mixed. The lower organic fraction was taken and dried over anhydrous sodium sulfate, then concentrated by rotoevaporation to approximately 0.5 ml. 5 ul of the concentrated sample was taken for trimethylsilylation with 100ul N,O-bis(trimethylsilyl)trifluoroacetamide and 10ul pyridine for 1h. Samples were analyzed by GC-MS. Modified from INARE protocols.

3.2.10. Neutral sugar analysis

Beginning with cell wall material insoluble in alcohol, 10 mg of each sample was hydrolyzed in 2.5M trifluoroacetic acid for 2h at 100°C, as described in (Harholt *et al.*, 2006). To determine the cellulose content, the residual pellet obtained after the monosaccharide analysis was rinsed twice with ten volumes of ethanol and once with 10 volumes of acetone and hydrolysed with H₂SO₄ as described (Updegraff, 1969). The released monosaccharides of hemicellulose were diluted 500 times and the released glucose of cellulose was diluted 1000 times. Then the monosaccharides were quantified using an HPAEC-PAD chromatography as described in (Harholt *et al.*, 2006). Modified from INARE protocols.

3.2.11. Yeast one-hybrid assay for protein DNA interaction

In a yeast one-hybrid assay, the interaction between a transcription factor (TF) of interest and a DNA sequence of interest are assayed by measuring the activation of a reporter gene in a heterologous yeast system.

The DNA sequence of interest is usually the promoter region of a gene representing approximately 1kb of sequence upstream from the gene's start codon. This sequence is cloned and tested in three overlapping fragments for approximately 400bp each. The promoter sequence fragment is cloned into the pLUC vector, just upstream from the luciferase reporter gene. The finished vector is linearized by restriction digest, and then stably transformed into YM4271 yeast to generate reporter lines. Homologous recombination of the linearized vector targets the insertion to a specific locus in the yeast genome, controlling for transcriptional effects based on insertion point. A number of these lines are grown on selective media and then tested for luciferase activity. Lines that are not "self active" are selected for use in testing protein-DNA interaction.

The coding sequence for the TF of interest is cloned into the pDEST22 expression vector in frame with the Gal4 activation domain (Gal4AD), which induces transcriptional activity when bound to DNA. This vector is then transformed into the yeast reporter lines. If the Gal4AD:TF fusion protein binds to the promoter fragment being tested, the Gal4AD will activate transcription of the luciferase gene. Luciferase activity is measured by adding coelenterazine, a substrate that the luciferase enzyme cleaves. This cleavage releases light, which is quantified on a plate reader. By normalizing the luminescent reading by the density of cells being tested, we generate a value for relative luciferase activity that indicates the degree of protein-DNA interaction. Protein-DNA interactions are tested in triplicate.

3.2.12. Genomic DNA Extraction

Tissue samples were collected in 1.5 ml tubes with two metal beads and flash frozen in liquid nitrogen. They were ground to a fine powder in frozen blocks in Retsch 440 bead

beater. 600 ul of DNA extraction buffer (100 mM NaCl, 50 mM Tris, 25 mM EDTA pH8, 1% SDS, a 10mM 2-mercaptoethanol) was added to each sample while still frozen, then vortexed vigorously to mix. Samples were incubated at 65°C for 10 min. 250ul of potassium acetate was added, the samples were mixed by inversion and then incubated on ice for 20 min. Tubes were centrifuged at 12,000 rpm for 10 min and the supernatant was carefully removed and placed in a new tube containing 600 ul of isopropanol. The samples were incubated on ice for 20 min to precipitate the nucleic acids, then centrifuged at 10,000 rpm. The supernatant was removed and the pellet was washed once with 300ul of 70% ethanol followed by a centrifugation at 15,000 rpm for 1 min. The supernatant was removed and the pellet was dried under a fume hood for 1h before resuspending in 30 ul of DNase free water.

3.2.13. RNA extraction and RT-qPCR

RNA was extracted from the main stem of plants one day after flowering using the Qiagen RNeasy Plant Mini Kit with on-column DNA digestion with RNase-free DNase I (Qiagen). First strand cDNA synthesis was performed using 500ng of total RNA with the Invitrogen SuperScript™ III First-Strand Synthesis SuperMix for qRT-PCR. cDNA samples were diluted by a factor of 10 with RNase-free water. Quantitative PCR was done in 10ul reactions with 1ul of diluted cDNA using the Qiagen QuantiFast SYBR Green PCR Kit. Reactions were run in triplicate on an Eppendorf RealPlex2 Mastercycler.

3.3 Results

3.3.1 *KNOB7* is a candidate wall regulator and a Class II KNOX gene

To identify genes involved in cell wall regulation, microarray analysis of transcript abundance was measured in *B. distachyon* leaf, root, and stem tissue. The *Bradi1g76970* transcript was highly abundant in root and stem compared to leaf. Additionally, *Bradi1g76970* expression was highly correlated with other genes known to function in cell wall biosynthesis, including secondary cellulose synthases and members of the lignin biosynthesis pathway, as well as other known and candidate cell wall regulators such as *SWAM1* and *SWAM4*. Phylogenetic analysis of *Bradi1g76970*, henceforth referred to as *KNOTTED OF BRACHYPODIUM DISTACHYON 7 (KNOB7)* showed it to be an ortholog of *AtKNAT7*, a Class II KNOX gene.

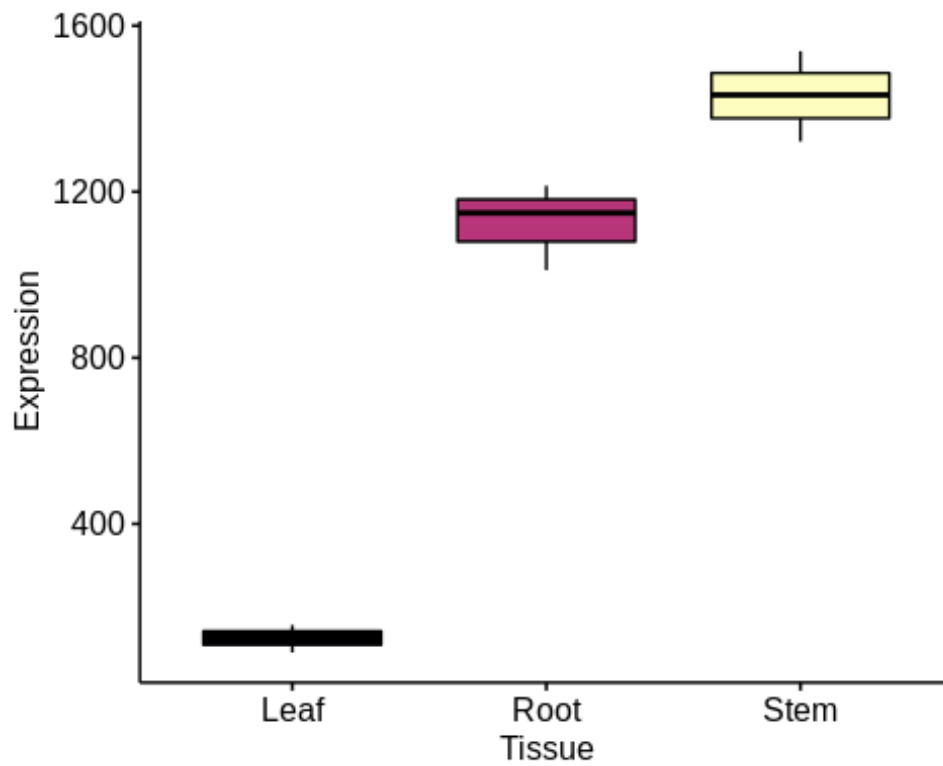


Figure 3.1 *Bradi1g76970* is highly expressed in maturing stem and root. *Bradi1g76970* transcript measured by microarray from *Brachypodium distachyon* leaf, root, and stem tissue. Mean +/- standard deviation of three biological replicates.

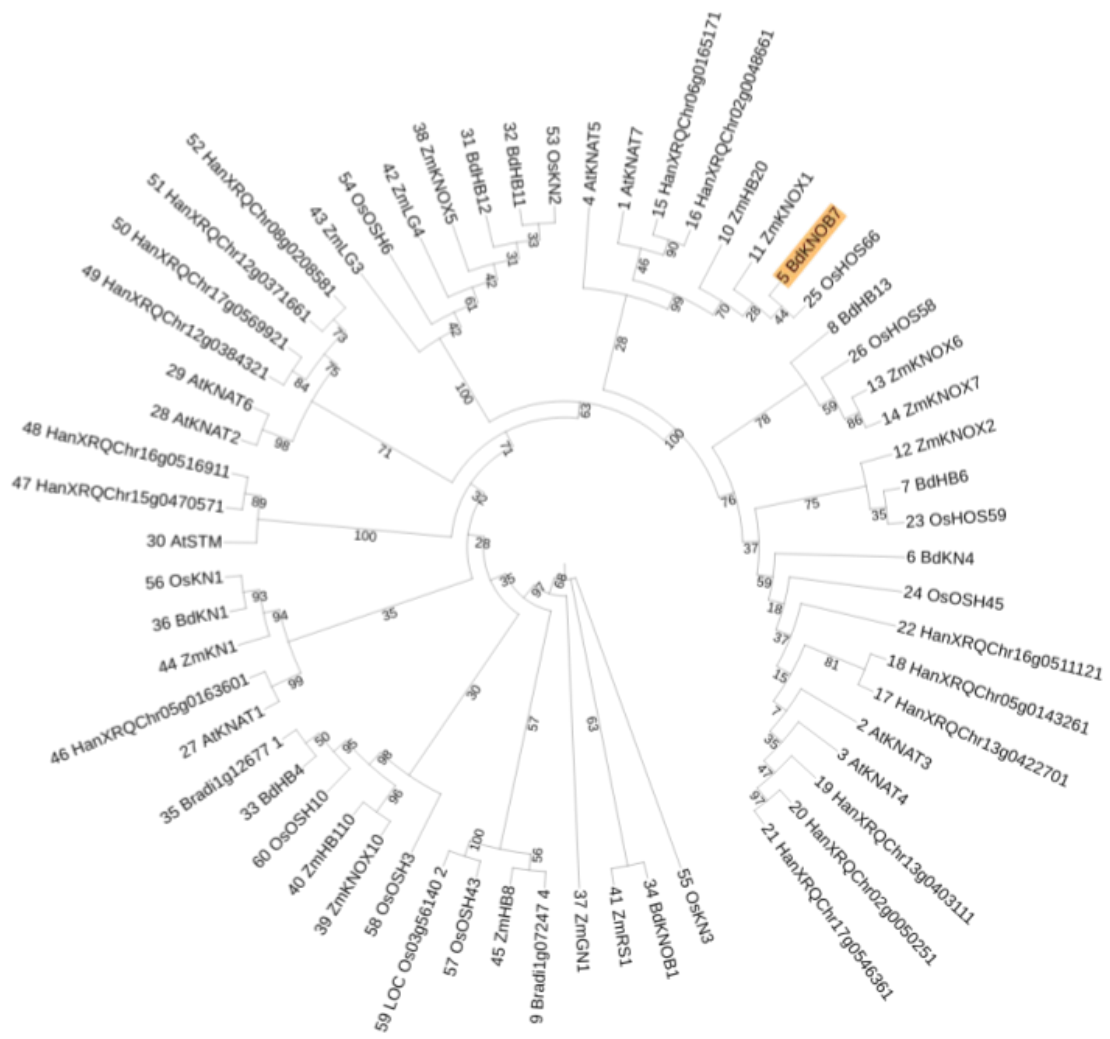


Figure 3.2 KNOX protein phylogeny. Class I and II KNOX genes from *B. distachyon*, *Z. mays*, *O. sativa*, *A. thaliana*, and *H. neglectus*. KNOB7 (orange) falls in the Class II clade as an ortholog of *AtKMAT7*. Phylogeny is based on amino acid sequence, bootstrap values listed on branches.

DNA binding data from a yeast one-hybrid assay further supported *KNOB7* as a candidate cell wall regulator. From a panel of cell wall gene regulatory regions, *KNOB7* protein was found to interact with elements of the *COMT6* and *SWAM1* promoters. *COMT6*, as described in Chapter 1, is a biosynthetic enzyme involved in monolignol biosynthesis. *SWAM1*, also described in Chapter 1, is an R2R3 MYB transcription factor that activates secondary cell wall biosynthesis in *B. distachyon* interfascicular fiber cells (Handakumbura *et al.*, 2018). Interestingly, when the *KNOB7* promoter was screened against our transcription factor library, *SWAM1* protein interacted with *KNOB7* regulatory sequences. This suggests that *SWAM1* and *KNOB7* may regulate each other through protein-DNA interactions.

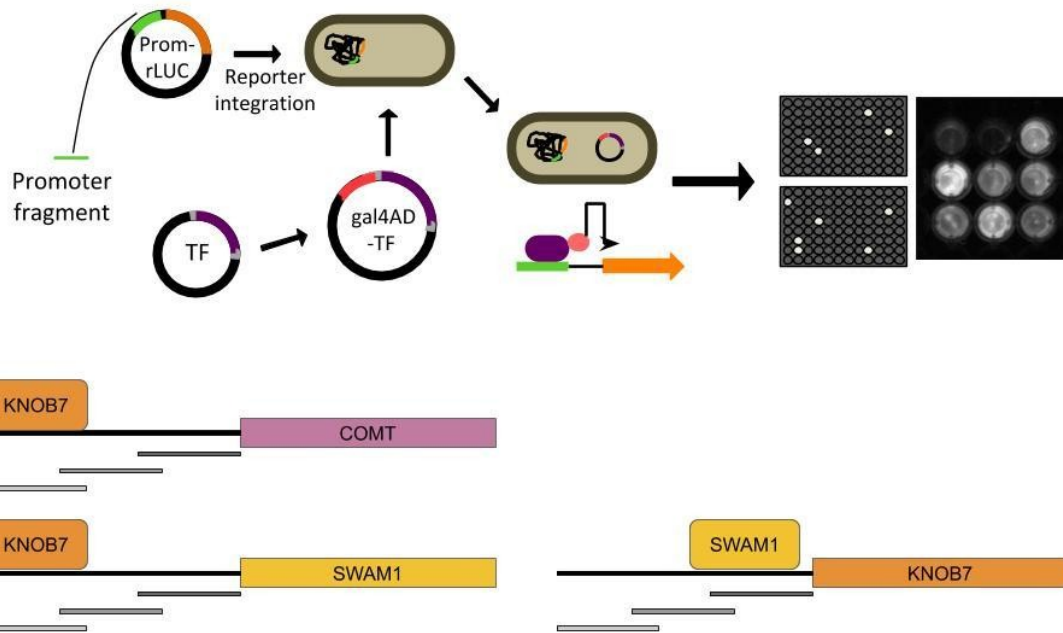


Figure 3.3 *KNOB7* protein interacts with cell wall gene regulatory regions. Yeast one-hybrid assay of protein-DNA interaction using a luciferase reporter. *KNOB7* coding sequence fused with the Gal4 activation domain was transformed into yeast lines containing promoter:reporter constructs of cell wall promoter fragments driving luciferase expression. A) Schematic of three yeast one-hybrid assay. Reporter lines were tested for self activity prior to screening, with two non-self active lines of each construct chosen for assay. Activation of the reporter was measured in triplicate, with quantitative determination luciferase activity. B) Schematic showing *KNOB7* positive interactions with promoter regions from *COMT6* and *SWAM1*. *SWAM1* protein was also found to interact with the *KNOB7* promoter.

3.3.2 *KNOB7* genetic reagents

To investigate the role of *KNOB7* in plant growth and secondary cell wall development, transgenic lines with enhanced or perturbed *KNOB7* function were generated (Figure 3.4). Overexpression lines employed the maize ubiquitin promoter to drive expression of the *KNOB7* coding sequence fused with engineered green fluorescent protein (*GFP*), hereafter referred to as *KNOB7:GFP-OE*. Three independent events were selected for analysis. Two mutant lines were isolated, *knob7-1* and *knob7-3*. In *knob7-1*, CRISPR-Cas9 was used to create a mutation in the DNA binding homeobox domain. This editing resulted in a single base pair insertion, causing a frameshift in the homeobox domain. *knob7-3* was identified from a sodium azide (NaN) mutagenized population (Dalmis *et al.*, 2013). Whole genome sequencing of mutants identified families with multiple mutations. PCR amplification of the mutation site in multiple individuals of those families followed by sequencing identified plants homozygous for the *knob7-3* allele, which results in a change from a glycine to a serine.

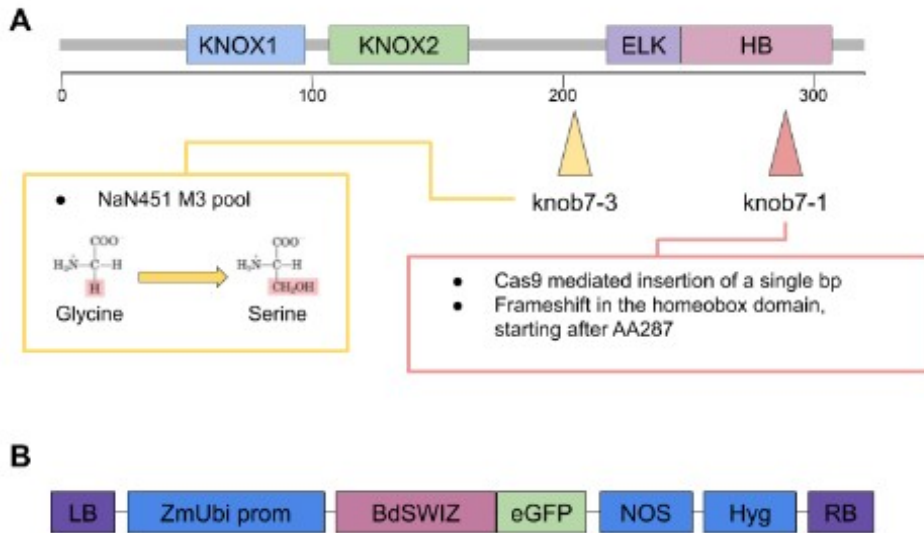


Figure 3.4 Diagram of *KNOB7* genetic reagents. A) Schematic of the *KNOB7* protein showing domain annotation and position of mutations . Numbers represent amino acid position. *knob7-1* contains a frameshift in the DNA binding homeobox domain (HB) caused by targeted mutagenesis with CRISPR/Cas9. *knob7-3* is a sodium azide (NaN) induced point mutation causing a change from a wildtype glycine to a serine near the ELK domain. B) *KNOB7* overexpression transgene. The maize ubiquitin promoter was used to drive expression of the *KNOB7* coding sequence fused in frame with eGFP. LB, left border; ZmUbi prom, maize ubiquitin promoter; Hyg, hygromycin phosphotransferase gene; NOS, nopaline synthase terminator; RB, right border.

In both *knob7-1* and *knob7-3* mutant lines, expression of *KNOB7* transcript was not affected by the mutations. In *KNOB7:GFP OE* lines, the *KNOB7* transcript was overexpressed compared to the wildtype (Fig 3.5.)

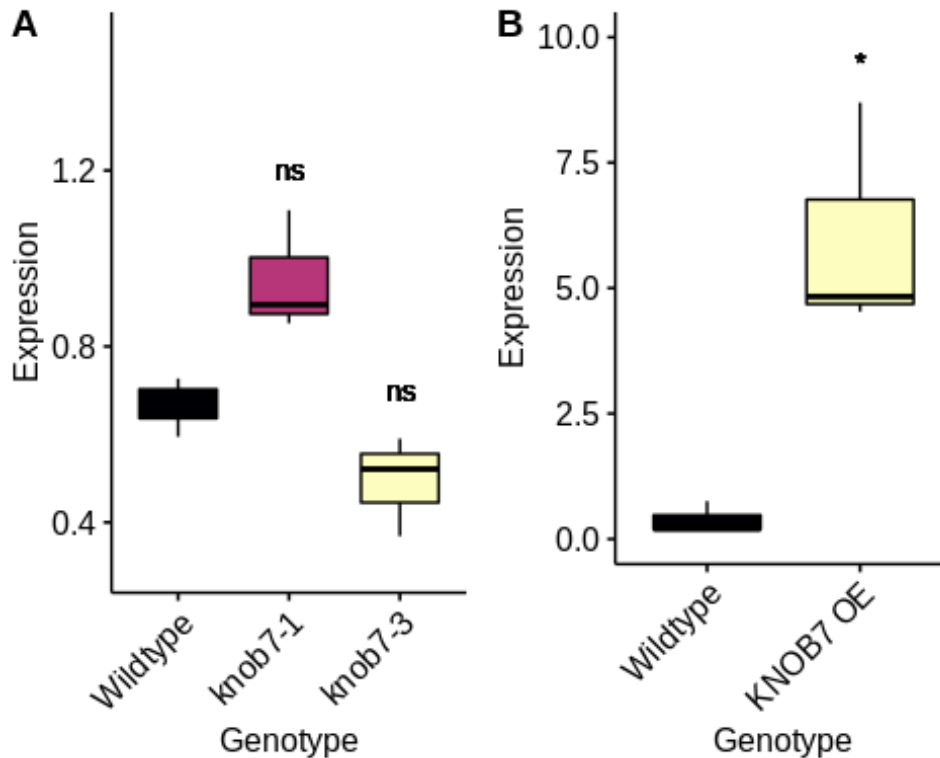


Figure 3.5 Expression of *KNOB7* in mutant and overexpression lines. Relative level of *KNOB7* gene expression measured by RT-qPCR in *KNOB7* mutant (A) and *KNOB7 OE* (B) lines. Whole stem tissue was collected 1 day after inflorescence emergence.

3.3.3 KNOB7 localizes to the nucleus

KNOB7 localization was first examined by transient expression in *Physcomitrella patens* (Figure 3.6A). Transformation with *KNOB7:GFP-OE* resulted in a localized GFP signal that resembles a nuclear localized GFP control (*Ubi::NLS:GFP*). Constitutive GFP lacking a nuclear localization signal (*Ubi::GFP*) was present throughout the cell, and overlapped with the constitutive mCherry control (*Ubi::mCherry*). KNOB7 localization was further confirmed in planta when analyzing transgenic plants regenerated from tissue culture. *KNOB7:GFP-OE* plants showed nuclear localized GFP signal in leaf tissue, compared with wildtype non-transgenic controls (Figure 3.6B).

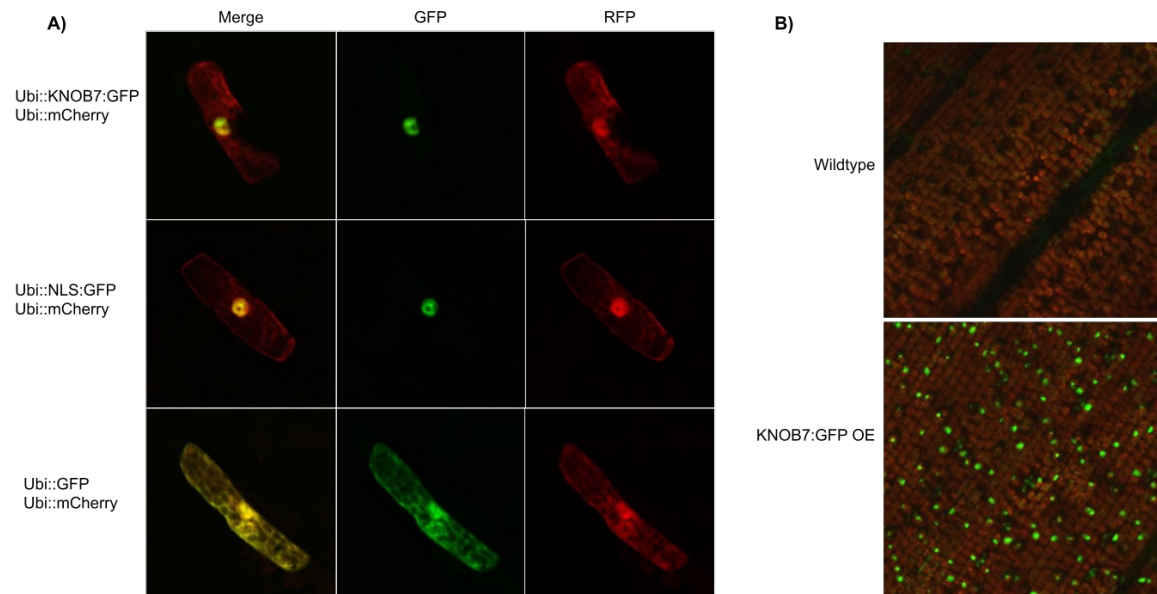


Figure 3.6 KNOB7 localizes to the nucleus. A) Transient expression of *KNOB7:GFP* in *P. patens* shows nuclear localization. *Ubi::mCherry* and *Ubi::GFP* are used as constitutively localized controls. Nuclear localized GFP (*Ubi::NLS:GFP*) showed the same localization pattern as *KNOB7:GFP*. B) *KNOB7:GFP-OE* transgenics show nuclear localization in leaf epidermal cells. GFP nuclear signal is seen in *KNOB7:GFP-OE* leaf and not in wildtype. Red signal is chlorophyll autofluorescence.

3.3.4 *KNOB7* is a negative regulator of interfascicular fiber wall thickening and lignification

Cell wall deposition and stem biology was measured in the *KNOB7* reagent panel.

Transverse sections of the senesced second stem internode and stained with phloroglucinol-HCl and Toluidine blue (Figure 3.7). Phloroglucinol-HCl acts as a general stain for lignin, causing a reddish-pink pigmentation when reacting with lignified cinnamyl aldehydes. Toluidine blue is a polychromatic stain that interacts with both lignin and polysaccharides. Lignin stains a blueish-green hue, while polysaccharide components such as cellulose and hemicelluloses stain a darker blue-purple. Compared to wildtype, *knob7-1* and *knob7-3* appeared somewhat similar when stained with phloroglucinol, but both showed greater blue-green coloration when dyed with toluidine blue, indicating a higher lignin content in the interfascicular fiber walls. *KNOB7:GFP-OE* plants showed almost no red coloration when stained with phloroglucinol, and toluidine blue staining resulted in a dark blue/purple coloration. Both of these observations indicate a relative lack of lignin in the interfascicular fiber walls. Lignin content was further measured by the acetyl bromide soluble lignin method (ABSL). Results quantitatively reflected what was observed by histology; that there was greater lignin content in *knob7-1* and *knob7-3* stems, with significantly less lignin in *KNOB7:GFP OE* (Figure 3.8).

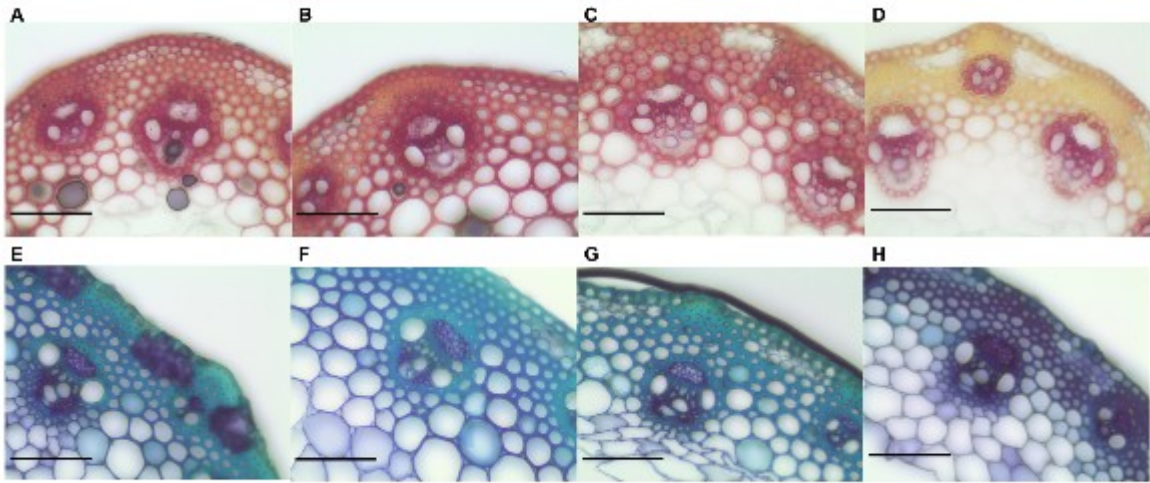


Figure 3.7 *KNOB7* negatively regulates lignification in interfascicular fibers. (A-D) Second internode sections of senesced stems stained with phloroglucinol-HCL, with red coloration as a proxy for lignin. (E-H) Second internode sections of senesced stems stained with Toluidine blue, with blue-purple indicating polysaccharides and teal-green indicating lignin. Compared to wildtype Bd21-3 (A,E), *knob7-1* (B,F) and *knob7-3* (C,G) mutants have more lignin staining, particularly evident in the toluidine blue stained sections. *KNOB7:GFP OE* plants (D,F) have drastically less lignin, evident in both phloroglucinol and toluidine blue staining. Scale bar = 100um.

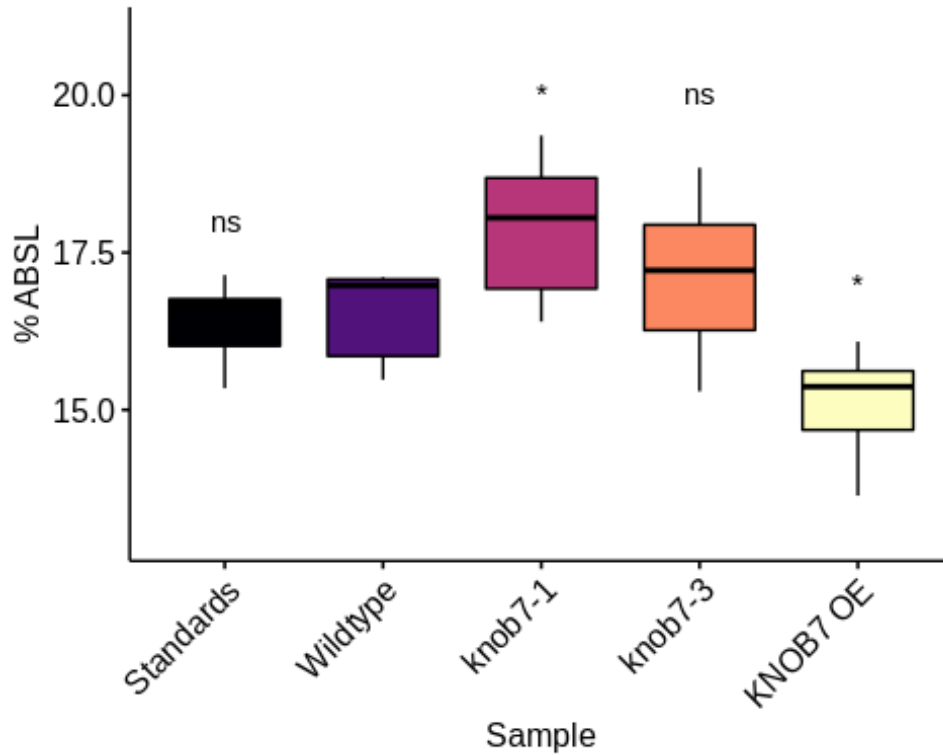


Figure 3.8 *KNOB7* is a negative regulator of lignin. Acetyl bromide soluble lignin measured in extractive free cell wall material prepared from the main stem after senescence. ns: $p > 0.05$, *: $p \leq 0.05$. $n = 8-12$ plants per genotype.

Interfascicular fiber wall thickness was also quantified in the *KNOB7* reagent panel.

knob7-1 plants had thicker walls compared to wildtype, while *knob7-3* and

KNOB7:GFP-OE walls were not significantly different (Figure 3.9).

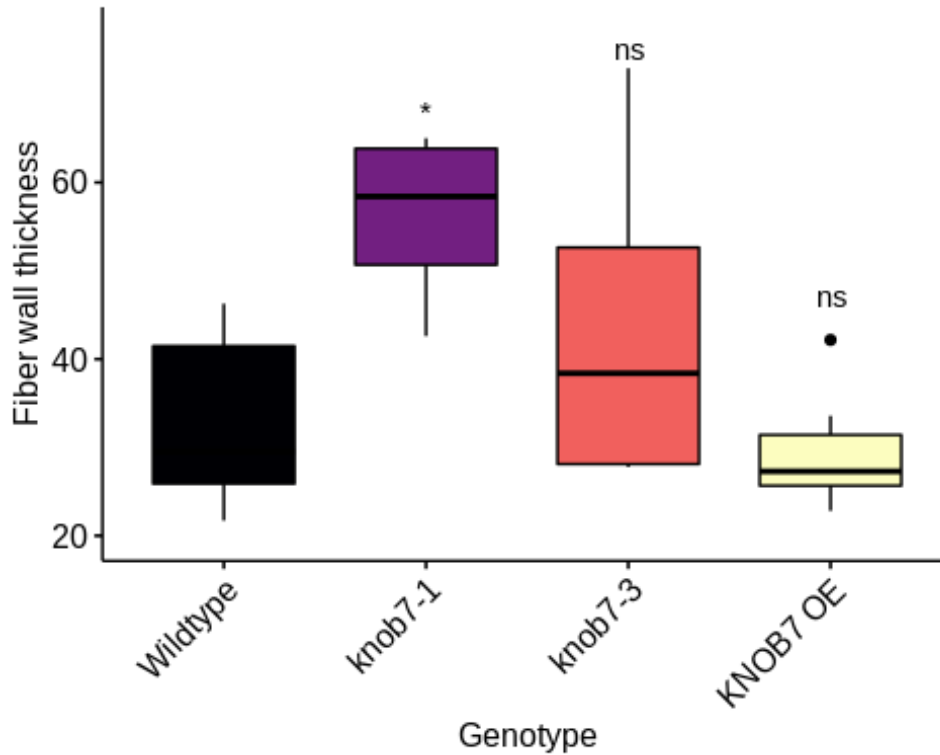


Figure 3.9 *KNOB7* is a negative regulator of interfascicular fiber wall thickness. Cell wall thickness was quantified for interfascicular fiber cells in transverse sections of the second elongated internode. ns: $p > 0.05$, *: $p \leq 0.05$. $n = 5-8$ plants per genotype.

3.3.5 *KNOB7* alters lignin composition and levels of wall bound hydroxycinnamic acids

Other aspects of *KNOB7* reagent secondary cell wall content was assessed. For *knob7-1* and *knob7-3*, measurements were made of hydroxycinnamic acid content by mild alkaline hydrolysis followed by HPLC-MS. Ferulic acid (FA) and *p*-coumaric acid (*p*CA) content was measured, and both mutants showed significantly higher levels of FA compared to their respective wildtype controls. *knob7-3* also showed significantly higher *p*CA levels, while *knob7-1* showed a non-significant increase (Figure 3.10).

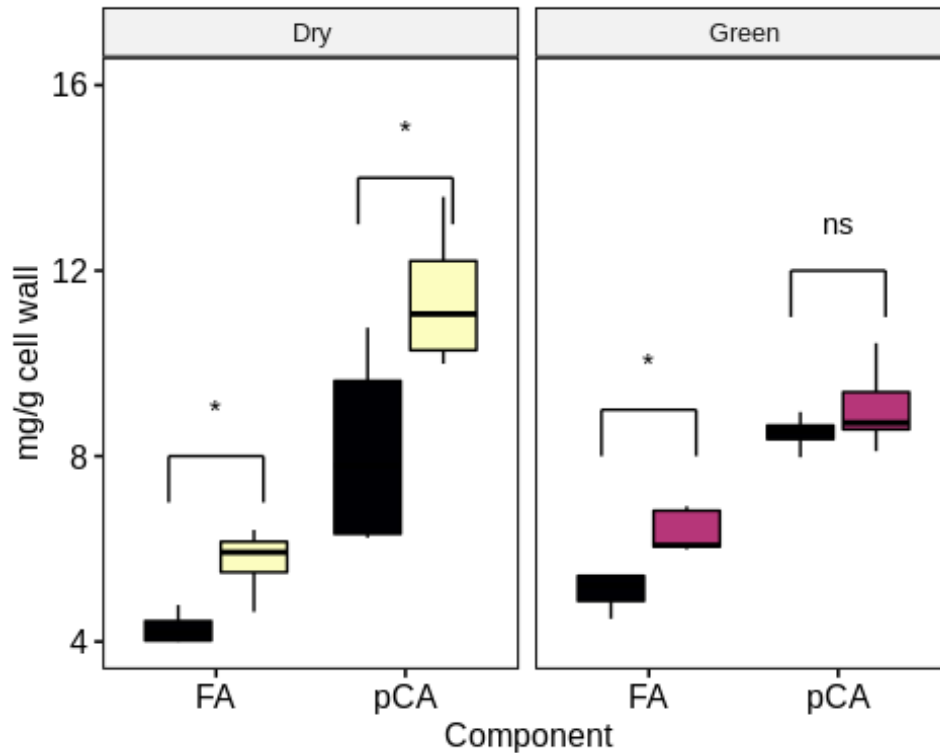


Figure 3.10 Wall-bound hydroxycinnamic acids are increased in *knob7-1* and *knob7-3* mutant lines. Mild alkaline hydrolysis on extractive free cell wall material prepared from the main stem of *knob7-1* plants one day after flowering (green tissue) or *knob7-3* plants after senescence (dry) released ferulic acid (FA) *p*-coumaric acid (*pCA*) from secondary cell wall polymers and quantified by HPLC-MS. Mean comparison by pairwise t-test after ANOVA testing. ns: $p > 0.05$, *: $p \leq 0.05$. $n = 4-7$ plants per genotype.

Lignin composition was measured in wildtype and *knob7-3* plants by thioacidolysis and GC-MS. This method allows quantification of the three main monolignol subunits, S, G, and H. Compared to wildtype, *knob7-3* plants had more S lignin and less G lignin (Figure 3.11A). This was further reflected in the entire *KNOB7* genetic reagent panel stained with Maule reagent. This stain identifies S lignin units with a cherry red coloration (Figure 3.11B). Compared to wildtype, *knob7-1* and *knob7-3* stems show brighter red color in the interfascicular fibers, while *KNOB7:GFP OE* still stains red, but a duller hue than the mutants or wildtype.

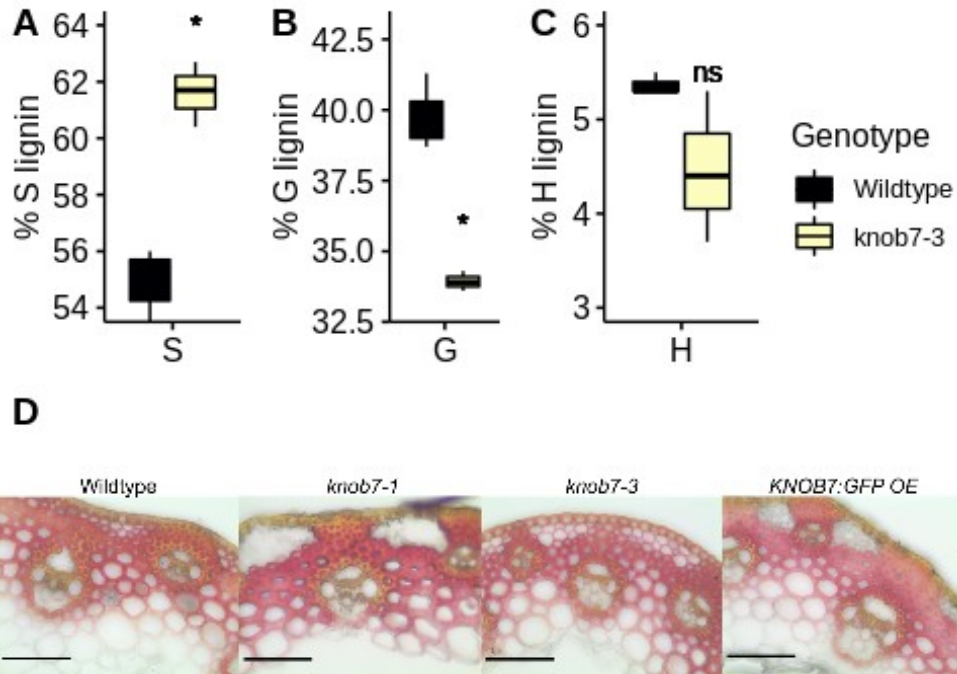


Figure 3.11 *KNOB7* mutant alleles have increased S lignin content. Thioacidolysis of extractive free cell wall material prepared from the main stem of *knob7-3* plants after senescence released lignin monomer components (A-C), which were quantified by GC-MS. D) Transverse sections of the second elongated internode of the main stem after senescence were stained with Maule reagent to identify S lignin. Cherry-red coloration represents greater quantities of S lignin. ns: $p > 0.05$, *: $p \leq 0.05$. $n = 3$ plants per genotype.

3.3.6 *KNOB7* alters cell wall polysaccharide content

In *knob7-1* plants, neutral sugar analysis was conducted to look at the secondary cell wall polysaccharide content. Compared to wildtype, *knob7-1* plants had significantly more xylose (Figure 3.12). *knob7-1* also showed a significant decrease in arabinose and rhamnose levels, with no change in glucose, non-cellulosic glucose, or galactose.

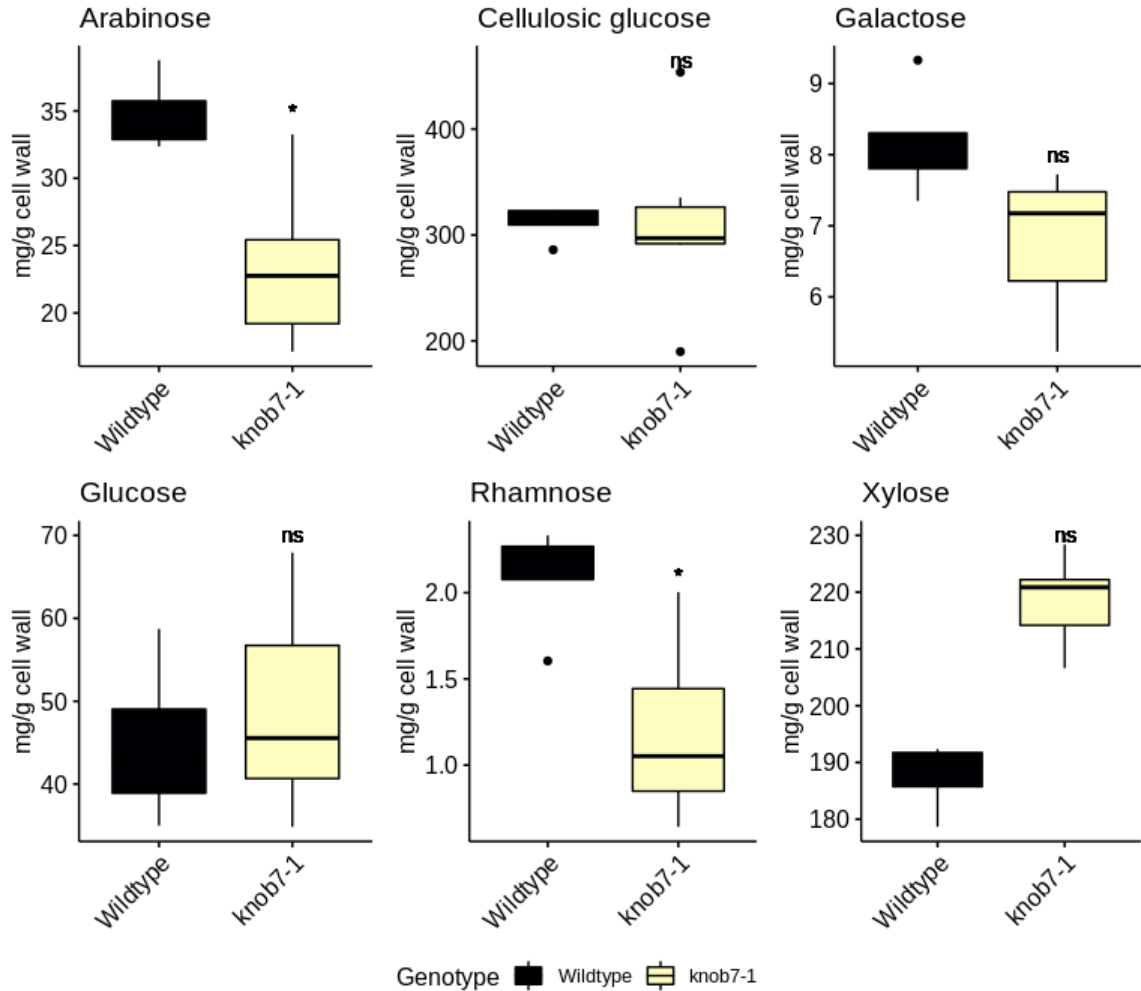


Figure 3.12 Neutral sugar analysis of *knob7-1*. Hydrolysis of lyophilized, extractive free cell wall material prepared from the main stem of *knob7-1* plants one day after flowering. Trifluoroacetic acid hydrolysis released cellulosic glucose, while sulfuric acid hydrolysis was employed to release arabinose, galactose, glucose, rhamnose, and xylose. Compounds were identified and quantified by HPLC. ns: $p > 0.05$, *: $p \leq 0.05$. $n = 4-6$ plants per genotype.

3.4 Discussion

KNOB7 was identified as a candidate wall regulator based on homology with the well characterized ortholog in *A. thaliana*, *AtKNAT7*. As with *AtKNAT7*, *KNOB7* is highly enriched for secondary cell walls. The *KNOB7* protein interacted with the promoter of genes that encode the lignin pathway enzyme *COMT6* in a yeast one-hybrid assay.

AtKNAT7 is a known regulator of secondary cell wall synthesis, including regulation of lignin synthesis (Zhong *et al.*, 2008a; Li *et al.*, 2012; Liu *et al.*, 2014; He *et al.*, 2018).

This evidence prompted us to further characterize *KNOB7* function as a regulator of wall thickening.

KNOB7 overexpression and two mutant alleles did not display any overt growth or stature phenotypes, but stem cross section histology revealed distinct changes in cell wall composition and morphology. Histo-chemical staining of *KNOB7-OE* plants showed a drastic decrease in interfascicular fiber lignin content, while *knob7-1* and *knob7-3* showed an increase. These observations were further substantiated by measuring lignin content in mature stems. *KNOB7-OE* showed significantly less lignin content, while *knob7-1* showed significantly more, supporting the histochemical staining. *knob7-3* did not show a significant difference, possibly due to large variance among the replicates. These data support the role of *KNOB7* as a negative regulator of lignin deposition in interfascicular fiber cells. Similarly, *AtKNAT7* and *PoptrKNAT7* mutants exhibited an increase in lignin accumulation (Li *et al.*, 2012; Wang *et al.*, 2020). A lignin phenotype was not observed in mutants of *KNOB7* the rice ortholog *OsKNOR1* (Wang *et al.*, 2019). Yeast data also substantiates *KNOB7*'s role in regulating lignin synthesis. *KNOB7* bound

the *COMT6* promoter, a key enzyme in the final steps of lignin synthesis. Repression of *COMT6* would be consistent with the observed changes in lignin quantity in the *KNOB7* reagents, with less accumulation in the *KNOB7-OE* and more in *knob7-1*. *COMT6* regulation is also consistent with the observed increase in S lignin in *knob7-1* and *knob7-3* by Maule staining and thioacidolysis. *COMT6* mediates the conversion of coniferaldehyde to sinapaldehyde, and de-repression of this activity in *knob7-1* and *knob7-3* could result in more S lignin derived from sinapaldehyde.

Cell wall thickness is another hallmark trait impacted by *AtKNAT7* and orthologs in other species (Zhong *et al.*, 2008a; Li *et al.*, 2012; Wang *et al.*, 2020). Interestingly, *AtKNAT7* appears to have an opposite effect on interfascicular fibers and xylem. Xylem cells have thin walls and some will collapse, while the interfascicular fibers are significantly thicker. We did not observe a collapsed xylem phenotype in either *knob7-1* or *knob7-3* mutant lines. However, while collapsed or irregular xylem is a common feature of wall mutants in *A. thaliana* and a trait used to identify cell wall mutants, it has only been reported once in a grass to my knowledge, in the *B. distachyon spaghetti 1 (spa1)* mutant. (Turner & Somerville, 1997; Ehltng *et al.*, 2005; Persson *et al.*, 2005; Brown *et al.*, 2005b; Timpano *et al.*, 2015). The causative gene behind the *spa1* phenotype has yet to be determined (Timpano *et al.*, 2015). *OsKNOR1* mutants do not have irregular xylem (Wang *et al.*, 2019). There may be differences in grass vasculature such as a surrounding layer of mestome and bundle sheath cells or differences in xylem physical properties (Coomey *et al.*, 2020). Fiber wall thickness is impacted in *knob7-1* plants, with thicker walls than wild type. This is consistent with the observation in both *AtKNAT7* and *OsKNOR1* mutants (Zhong *et al.*, 2008a; Li *et al.*, 2012; Wang *et al.*, 2020).

Overexpression of *AtKNAT7* or *OsKNOR1* resulted in thinner fiber cell walls. In my study, *KNOB7-OE* fiber walls are not significantly thinner.

Other aspects of cell wall chemistry were also assayed in *KNOB7* mutants. The hydroxycinnamates *pCA* and *FA* are derivatives of the lignin biosynthetic pathway and in grass secondary cell walls they can be linked to either heteroxylans and lignins (Bartley *et al.*, 2013; Petrik *et al.*, 2014; Smith *et al.*, 2017). Both *knob7-1* and *knob7-3* had a significant increase in cell wall bound *FA*, and *knob7-3* also had a significant increase in *pCA*. These measurements were not made in *OsKNOR1* or *AtKNAT7*. There was also a shift in lignin chemistry observed in *KNOB7* reagents. The proportions of each main monolignol, S, G, and H, was measured in *knob7-3*, to reveal an increase in S lignin with a commensurate decrease in G lignin. Maule staining detects S lignin, and both *knob7-1* and *knob7-3* showed increased Maule staining intensity while *KNOB7:GFP-OE* showed less. This is the opposite phenotype that was described in *AtKNAT7* mutants, where an increase in G lignin was observed (Wang *et al.*, 2020). Together with the increase in *FA* and *pCA*, the shift towards S lignin in *KNOB7* mutants suggests a somewhat different mechanism for lignin regulation in grasses. Several aspects of grass lignin biosynthesis are distinct from eudicots and the difference in *KNOB7* mutant phenotypes may reflect such differences (Lan *et al.*, 2015; Barros *et al.*, 2016, 2019; Coomey *et al.*, 2020).

Polysaccharide content was also measured by trifluoroacetic acid and sulfuric acid hydrolysis to release neutral sugars. *knob7-1* showed a significant increase in xylose content, and a significant decrease in arabinose and rhamnose. As with S and G lignin content, these measures of xylose and arabinose show the opposite trend reported for *AtKNAT7* mutants. In *A. thaliana*, *AtKNAT7* activates xylan biosynthesis, and mutants

had less xylose and more arabinose (He *et al.*, 2018). Again, this may be a result of the fundamental difference in grass secondary cell walls compared to eudicots such as a xylose backbone decorated with side chains of xylose, arabinose, and glucuronic acid in grasses and xyloglucan in eudicots (Coomey *et al.*, 2020). The decrease in arabinose and increase in *pCA* is noteworthy, as the addition of *pCA* to heteroxylans is through arabinose linkage, which may suggest that the increased *pCA* in *knob7-3* may be associated with lignin (Petrik *et al.*, 2014).

Reciprocal binding between *KNOB7* and *SWAM1* in yeast one-hybrid assays raises the interesting question of negative feedback regulation. *SWAM1* is a characterized activator of interfascicular fiber secondary cell walls (Handakumbura *et al.*, 2018), and my data suggests that *KNOB7* is a repressor in this tissue. In *SWAM1-OE* plants *KNOB7* is upregulated, and similarly down regulated in the *SWAM1* dominant repressor lines (Hazen lab unpublished data), further suggesting *KNOB7* is a direct target of *SWAM1* regulation. I would expect to find an increase in *SWAM1* expression in *KNOB7* mutants, and a decrease in *KNOB7-OE*, although these measurements have not yet been made. It would be interesting to investigate the *SWAM1-KNOB7* relationship over time to better understand how these two transcription factors with similar expression patterns, reciprocal binding, but opposite transcriptional polarities may act in a feedback loop to fine tune fiber wall synthesis.

CHAPTER 4

CONCLUSIONS

The focus of my research was to better understand the factors that regulate growth in grasses. While we have uncovered many aspects of growth dynamics in eudicot systems, grasses represent an understudied region of the plant kingdom that is of great ecological, agricultural, and economic importance. I chose to study the genetic regulation of secondary cell wall synthesis. Grasses have distinct secondary cell wall properties from eudicots, and are critical to proper growth and development, and as such drew my interest to better understand this aspect of growth. To this end, I chose two candidate cell wall regulators, *SWIZ* and *KNOB7*, to characterize for their roles in the regulation of secondary cell wall synthesis.

SWIZ is a Group I bZIP that is highly expressed in root and stem tissue. Gain of function and loss of function lines both had reduced height and thick fiber cell walls. Like other characterid Group I bZIPs, *SWIZ* translocates within the cell in response to mechanical stimuli and cellular bioactive GA levels. This mode of action prompted me to look at the connection between *SWIZ* function and touch responsive growth. *B. distachyon* shows classic thigmomorphogenic traits such as reduced height and increased branching in response to mechanical stimulus. *SWIZ* appears to play a role in regulating cell wall thickening in response to touch, specifically the touch induced inactivation of cellular GA. Under touched conditions, *SWIZ-OE* lines had thicker cell walls in the touched portion of their stems. The direct genetic targets of *SWIZ* regulation that are responsible for these phenotypic outputs have yet to be identified, but components of lignin and

cellulose biosynthesis identified in yeast as binding targets are likely candidates. I found SWIZ to bind a motif similar to close orthologs in *A. thaliana*, and *in vitro* protein-DNA binding has identified a number of regulatory candidates with suggestive roles in other aspects thigmomorphogenesis.

KNOB7 is the ortholog of *AtKNAT7*, a known regulator of cell wall thickening and lignification in *A. thaliana*. The role of similar genes in cell wall synthesis have been shown in other species such as rice and poplar, and *KNOB7* phenotypes are largely consistent with these reports. I generated gain of function lines overexpressing *KNOB7* and loss of function lines with a frameshift in the DNA binding domain and a non-synonymous point mutation. I showed distinct and reciprocal changes in interfascicular fiber cell wall thickness and lignification in these lines, as well as changes in lignin and polysaccharide chemistry that are all consistent with the role of *KNOB7* as a negative regulator of secondary cell wall synthesis in interfascicular fiber cells.

In summary, I characterized *SWIZ*, a novel component of thigmomorphogenic signalling that impacts stem elongation and fiber wall thickening, as well as *KNOB7*, an ortholog of an established negative regulator of cell wall synthesis and lignification. These findings contribute to our growing understanding of secondary cell wall synthesis and growth dynamics in grasses.

APPENDIX 1.

SUPPLEMENTAL DATA

Table A1. GO terms from BdSWIZ DAP-seq, all peaks. BP: biological process, CC: cellular compartment, MF: molecular function

term_name	p_value	source
cellular process	0.0000000	GO:BP
cellular metabolic process	0.0000000	GO:BP
primary metabolic process	0.0000000	GO:BP
metabolic process	0.0000000	GO:BP
organic substance metabolic process	0.0000000	GO:BP
macromolecule metabolic process	0.0000000	GO:BP
developmental process	0.0000000	GO:BP
anatomical structure development	0.0000000	GO:BP
nitrogen compound metabolic process	0.0000000	GO:BP
cellular macromolecule metabolic process	0.0000000	GO:BP
system development	0.0000000	GO:BP
multicellular organism development	0.0000000	GO:BP
multicellular organismal process	0.0000000	GO:BP
organic cyclic compound metabolic process	0.0000000	GO:BP
nucleobase-containing compound metabolic process	0.0000000	GO:BP
nucleic acid metabolic process	0.0000001	GO:BP
heterocycle metabolic process	0.0000001	GO:BP
cellular nitrogen compound metabolic process	0.0000002	GO:BP
gene expression	0.0000002	GO:BP

reproductive structure development	0.0000004	GO:BP
cellular biosynthetic process	0.0000005	GO:BP
reproductive system development	0.0000005	GO:BP
cellular aromatic compound metabolic process	0.0000006	GO:BP
organic substance biosynthetic process	0.0000010	GO:BP
biosynthetic process	0.0000012	GO:BP
RNA metabolic process	0.0000015	GO:BP
post-embryonic development	0.0000015	GO:BP
shoot system development	0.0000026	GO:BP
cellular nitrogen compound biosynthetic process	0.0000031	GO:BP
plant organ development	0.0000036	GO:BP
developmental process involved in reproduction	0.0000060	GO:BP
biological regulation	0.0000067	GO:BP
organic cyclic compound biosynthetic process	0.0000068	GO:BP
heterocycle biosynthetic process	0.0000073	GO:BP
cellular macromolecule biosynthetic process	0.0000107	GO:BP
nucleobase-containing compound biosynthetic process	0.0000213	GO:BP
macromolecule biosynthetic process	0.0000247	GO:BP
aromatic compound biosynthetic process	0.0000463	GO:BP
regulation of biological process	0.0000564	GO:BP
regulation of gene expression	0.0000936	GO:BP
reproductive process	0.0001303	GO:BP
reproduction	0.0001868	GO:BP
regulation of cellular biosynthetic process	0.0005636	GO:BP

regulation of metabolic process	0.0005645	GO:BP
response to chemical	0.0006048	GO:BP
regulation of biosynthetic process	0.0006053	GO:BP
flower development	0.0008218	GO:BP
response to hormone	0.0008666	GO:BP
reproductive shoot system development	0.0009754	GO:BP
regulation of macromolecule metabolic process	0.0012356	GO:BP
phyllome development	0.0013152	GO:BP
regulation of macromolecule biosynthetic process	0.0013204	GO:BP
response to endogenous stimulus	0.0014990	GO:BP
transcription, DNA-templated	0.0019793	GO:BP
nucleic acid-templated transcription	0.0020197	GO:BP
regulation of cellular process	0.0020463	GO:BP
RNA biosynthetic process	0.0021665	GO:BP
regulation of cellular macromolecule biosynthetic process	0.0026062	GO:BP
gene silencing by RNA	0.0027765	GO:BP
organelle organization	0.0030782	GO:BP
regulation of biological quality	0.0033614	GO:BP
cellular component organization or biogenesis	0.0033679	GO:BP
plant organ senescence	0.0041155	GO:BP
response to organic substance	0.0051848	GO:BP
leaf senescence	0.0052706	GO:BP
aging	0.0084409	GO:BP
regulation of cellular metabolic process	0.0090811	GO:BP

response to abiotic stimulus	0.0101369	GO:BP
leaf development	0.0110133	GO:BP
negative regulation of biological process	0.0127206	GO:BP
macromolecule modification	0.0127621	GO:BP
regulation of RNA biosynthetic process	0.0130470	GO:BP
regulation of nucleic acid-templated transcription	0.0130470	GO:BP
regulation of multicellular organismal development	0.0130605	GO:BP
cellular component organization	0.0182790	GO:BP
response to stimulus	0.0195774	GO:BP
regulation of nucleobase-containing compound metabolic process	0.0217206	GO:BP
regulation of transcription, DNA-templated	0.0232153	GO:BP
response to acid chemical	0.0250820	GO:BP
regulation of RNA metabolic process	0.0255394	GO:BP
regulation of primary metabolic process	0.0269112	GO:BP
regulation of nitrogen compound metabolic process	0.0290404	GO:BP
root system development	0.0301771	GO:BP
response to oxygen-containing compound	0.0343170	GO:BP
negative regulation of gene expression	0.0383999	GO:BP
chromosome organization	0.0397219	GO:BP
transport	0.0443506	GO:BP
regulation of developmental process	0.0461319	GO:BP
cellular response to auxin stimulus	0.0462899	GO:BP
intracellular membrane-bounded organelle	0.0000000	GO:CC
intracellular	0.0000000	GO:CC

membrane-bounded organelle	0.0000000	GO:CC
intracellular organelle	0.0000000	GO:CC
organelle	0.0000000	GO:CC
cellular anatomical entity	0.0000000	GO:CC
cytoplasm	0.0000001	GO:CC
nucleus	0.0000439	GO:CC
chloroplast	0.0092619	GO:CC
plastid	0.0100642	GO:CC
phragmoplast	0.0456189	GO:CC
binding	0.0000016	GO:MF
heterocyclic compound binding	0.0002803	GO:MF
organic cyclic compound binding	0.0003742	GO:MF
nucleic acid binding	0.0015161	GO:MF
quinone binding	0.0024166	GO:MF
NADH dehydrogenase (quinone) activity	0.0183459	GO:MF
NADH dehydrogenase (ubiquinone) activity	0.0183459	GO:MF
DNA binding	0.0232223	GO:MF
purine ribonucleoside triphosphate binding	0.0326870	GO:MF
regulatory region nucleic acid binding	0.0446473	GO:MF
transcription regulatory region DNA binding	0.0446473	GO:MF
Flower Development (Initiation)	0.0499796	WP

Table A2. GO terms from BdSWIZ DAP-seq, filtered for those containing the conserved bZIPS binding motif. BP: biological process, CC: cellular compartment, MF: molecular function

term_name	p_value	source
-----------	---------	--------

macromolecule metabolic process	0.0000035	GO:BP
cellular process	0.0000045	GO:BP
nitrogen compound metabolic process	0.0000122	GO:BP
primary metabolic process	0.0000156	GO:BP
developmental process	0.0000163	GO:BP
organic substance metabolic process	0.0000360	GO:BP
anatomical structure development	0.0000890	GO:BP
cellular macromolecule metabolic process	0.0001476	GO:BP
cellular metabolic process	0.0002232	GO:BP
metabolic process	0.0005963	GO:BP
macromolecule modification	0.0006115	GO:BP
system development	0.0010455	GO:BP
nucleic acid metabolic process	0.0014878	GO:BP
regulation of biological process	0.0015938	GO:BP
biological regulation	0.0016184	GO:BP
multicellular organism development	0.0017097	GO:BP
organelle organization	0.0026917	GO:BP
cellular protein modification process	0.0028097	GO:BP
protein modification process	0.0028097	GO:BP
regulation of cellular process	0.0041738	GO:BP
multicellular organismal process	0.0065802	GO:BP
regulation of metabolic process	0.0079294	GO:BP

peptidyl-amino acid modification	0.0094872	GO:BP
organic cyclic compound metabolic process	0.0139963	GO:BP
RNA metabolic process	0.0158412	GO:BP
chromosome organization	0.0183656	GO:BP
regulation of cellular metabolic process	0.0200114	GO:BP
gene expression	0.0263629	GO:BP
heterocycle metabolic process	0.0285357	GO:BP
protein phosphorylation	0.0341980	GO:BP
intracellular	0.0000001	GO:CC
cellular anatomical entity	0.0000184	GO:CC
intracellular organelle	0.0000208	GO:CC
intracellular membrane-bounded organelle	0.0000215	GO:CC
membrane-bounded organelle	0.0000341	GO:CC
organelle	0.0000435	GO:CC
nucleus	0.0250913	GO:CC
cytoplasm	0.0262437	GO:CC
H4 histone acetyltransferase complex	0.0443973	GO:CC
tubulin complex	0.0499389	GO:CC
heterocyclic compound binding	0.0000009	GO:MF
organic cyclic compound binding	0.0000013	GO:MF
purine ribonucleoside triphosphate binding	0.0000030	GO:MF
binding	0.0000143	GO:MF
purine ribonucleotide binding	0.0000168	GO:MF
purine nucleotide binding	0.0000192	GO:MF
drug binding	0.0000197	GO:MF
ribonucleotide binding	0.0000290	GO:MF
ATP binding	0.0000314	GO:MF

carbohydrate derivative binding	0.0000627	GO:MF
adenyl ribonucleotide binding	0.0001601	GO:MF
small molecule binding	0.0001660	GO:MF
adenyl nucleotide binding	0.0001788	GO:MF
nucleotide binding	0.0002200	GO:MF
nucleoside phosphate binding	0.0002200	GO:MF
anion binding	0.0004213	GO:MF
ion binding	0.0034454	GO:MF
phosphotransferase activity, alcohol group as acceptor	0.0144359	GO:MF
kinase activity	0.0220999	GO:MF
protein serine/threonine kinase activity	0.0231489	GO:MF
protein kinase activity	0.0246808	GO:MF

Table A3. SWIZ protein-DNA interactions from yeast one hybrid assay

TARGET	TARGET SEQUENCE	TF	TF Locus ID	At homolog
	ACATAATTCGCGGGA TCAATTTCCACCTCCG GGCAATCGAGCGAGA TGTGAATATCTGATCC CACGACAACTTCCAC ACACAGGCTGAGATG ATATTTTTTTTTCATC CTCTGCACTAAAAAA GAAAAGCTTAAGCTA GCCACAGAAGATCCA GCCGCACAATGATAG AAAACGCGCCCCACC TGATCACGGCTGCCG			
CAD-1-1	CTGGCAGTCAGTT	SWIZ	Bradi1g17700	bZip52
CAD-2	AGATCATGTCCTAGT CCTTCTACCAAACAA	SWIZ	Bradi1g17700	bZip52

	ATACATCACCTGCTCC CATTCGACGATGATC ATCTTGACTTGACGTA GCAATTAGCATATAC CAACGAGCGGGGCCG ATGAAAGAGCTTAAC ACACCTTCGGTTACGT GCTCGCATTTCATATT TCCACTTGTTAACATA TCCTCCCTTAGCTTGG CCTCTCTTGTACACAA GAGGAGAGGGCCAAA TTAATTCTCGAATATA AATTGCGCATCCAAA CTGTTTGAAAATCAA ATCTGCTACTAATAA GAAGGACATGAATAC AACAAACATAATTCGC GGGATCAATTTCCAC CTCCGGGCAATCGAG CGAGATGTGAATATC TGATCCCACGACAAC TTCCACACACAGGCT GAGATGATATTTTTTT TTCATCCTCTGCACTA AAAAAGAAAAGCT			
CESA4-1	GCCTGGAGAAGTGGC CGAGCAGTGTTTTGC AGAGAttggtgattactttgcaa aaggcctcagctaagtgtttgagg caatctctgatctgttatgttggtttgc actctgatagcttatggtaaaagata cagaaatgttgaggtttgtatgcca ccaagtttctcacttgatagctt atgacaagacatcgttgggtgcata ataatctatggatatcacagcataaa atattgccgttttgttaaaacatttc catcagcattcccagctggcaciaa cggaagctggcatacgcacgtata atcttcccttcttctcattagatca cgtccctgcttggatgcttaggtac	SWIZ	Bradi1g17700	bZip52

	aagttgattttgtgc			
COMT-1	ATCCTCATGTCGTGTG CATGGGATGGTAACT CCGACAGGATGTTGC ACCACCAACCCTTCG CGACAACAAGTATAT CTTTTTTATCCTAACG TGACGTATATATTTGA TCTGAGTATACGCAA AATAAAAAACTATCA GGAAAACAACCCAC TTATCAACAACA ACTACTATGATGTAA ACACACACATATTTTT CCCCGGTACCACATTT CTCCCTCACCTTTTCT CCCAAAGTCGAAGAA GAAGGGGAAAAAAA CTCAGTTGGTGTGGT GTGGTGGTTGGTGAA TGCAGAAAAGCCATA TAACCCCTCCCACATC CTCCCTCCCAAATCAC ACCCTCATCTCCTCTC AGTCGCTCACTACA CCAAGAAGGCAAGAA CACACCTACCAAGCA GAAAGAAGAAGCAGC CAGCAACCCCCAGCA GCAATTCGATCC	SWIZ	Bradi1g17700	bZip52
COMT-3	ATCCTCAAGTTGAGG ACATGGCATAGCTGA TCCAAACGAATCCGT AAAGACCTTAACCTA AAAGTGAAATGATAA CATGTTGTCAGCAGG TCAAATTTAAACCA GGCTCATGTCAAAT CTTGAGAGAAATTTT AGTTTAGGAGTTGAG CCAGGGATCAAATTC	KNOB7	Bradi1g76970	KNAT7

	AGAGACCAAAAGTAT CCTTTTTCTTCTTATTT TCCGTTTTGTCTGATC CTGACGACGGGTGTA TAGGCTATGATGACA AGGAATCCGGACTTG AAAAATGAAAACCTTG TCGACCGCTATCACT GACCAAGCGTGACAC ACATTGCTGGCCACTT GATCACACTTGCTCA CGCTTCAACTCCA AAACCCTGCATCTGC ATGCGTTCCACCCAC CCTCCATCACCATCAC GAGACCGATCAA GAATTTTCCTACTCTC GTCATTGCTATCTCCA			
SWAM1	AACGATTTTAGGGGC AGTGATCCGGTTATTC CCGTTTCGAGAAAAAC AGCGTTCTATTTACAC GGGCGAGTGGGACCT CAGCCACCCGCATCG AACGTTTCGACCCTA GCTAGCTAGCTCGCC TAGCGTGGTGTAGCG TCAGGTTGTACGGTT CACCACCGCGCGGGC GACGGGATTAATTGC GCGCTCGGCCCATTT GCAAATCGATATGGA CGGAACGCGGCAGTC AAGCAAAAGCCTGTC GATAGCATATGACAC ACAGGGTTAGTGCGA TCAATGTAATCCAAG CACAGCTAATACGAG ACTATTATATAGCAG CACAACGTGGCCGCT CTGTTGAAATGTTCTG	KNOB7	Bradi1g76970	KNAT7

	CATTGATGTGTTGTGT TTGCGCCAGTA			
--	---------------------------------	--	--	--

Table A4. Primers used in these studies.

Primer	Sequence	Purpose
Hpt_F	agaatctcgtgctttcagcttcga	Hygromycin resistance gene marker for genotyping
Hpt_R	tcaagaccaatgaggagcatatac	Hygromycin resistance gene marker for genotyping
Zm_Ubi_F	agctacgggggattccttt	Genotyping OE lines
HB9cas9_2geno_F	ccgagctagttagcacttagc	Genotyping the knob7-1 locus
HB9cas9_2geno_R	gccattggtcagactagtgg	Genotyping the knob7-1 locus
KNOB7:GFP_F	gcagcaacactccaagtggcc	Confirming KNOB7:GFP fusion construct. Binds the top strand of KNOB7
KNOB7:GFP_R	ccttgaagaagatggtgcgctcc	Confirming KNOB7:GFP fusion construct. Binds the bottom strand of GFP
NaN451F	GTATGATCGTCAGGTGCGACG	Genotyping the knob7-3 allele
NaN451R2	CCTTGACTTGAAGCCCTGCAA	Genotyping the knob7-3 allele
qPCR_CESA8_F	caaagcacaagtccgctgtg	Gene expression of BdCESA8 (Bradi2g49912)
qPCR_CESA8_R	tggctcgtatgcatctgtcaaac	Gene expression of BdCESA8 (Bradi2g49912)
qPCR_CESA4_F	gcgttcgcatacacaacacc	Gene expression of BdCESA4 (Bradi3g28350)
qPCR_CESA4_R	actcgtaggtttcagtggtg	Gene expression of BdCESA4 (Bradi3g28350)
qPCR_COMT6_F	tggagagctggtactacctaag	Gene expression of BdCOMT6 (Bradi3g16530)
qPCR_COMT6_R	cgacatcccgtatgccttgtg	Gene expression of BdCOMT6 (Bradi3g16530)
qPCR_CAD1_F	aggatagaatgggcagcatcgc	Gene expression of BdCAD1 (Bradi3g06480)
qPCR_CAD1_R	atcttcagggcctgtcttctgag	Gene expression of BdCAD1 (Bradi3g06480)
qPCR_CESA7_F	gcgattcgcctacatcaacacc	Gene expression of BdCESA7 (Bradi4g30540)
qPCR_CESA7_R	ggctggcaaatgtgctaacgg	Gene expression of BdCESA7 (Bradi4g30540)
qPCR_UBC18_F	tcacccgcaatgactgtaagttc	Gene expression of BdUBC18, housekeeping Bd5g25870
qPCR_UBC_R	ttgtcttcggacgttgctttg	Gene expression of BdUBC18, housekeeping Bd5g25870
BdActin-F	TGGATTGGAGGATCCATCTTG GCA	Gene expression of BRADI1g10630 (homolog of ACT11), housekeeping
BdActin-R	AGCATTTCCTGTGCACAATGG ACG	Gene expression of BRADI1g10630 (homolog of ACT11), housekeeping
KNOB7_qPCR_F	tccttcaggacctaactggtg	Gene expression of BdKNOB7 (Bradi1g76970)
KNOB7_qPCR_R	ttctcctctgacatggttgcg	Gene expression of BdKNOB7 (Bradi1g76970)
qPCR_HYG_F	atttcggtccaacaatgc	Gene expression of HPT hygromycin resistance

		gene
qPCR_HYG_R	gcgacctcgattggCaat	Gene expression of HPT hygromycin resistance gene
bZZIP6miR-s2	agtgactgggaagagattcagtttga	Constructing swiz-miRNA
bZZIP6miR-a2	tgtagcgtgaacctgctgctacagcc	Constructing swiz-miRNA
bZZIP6miR-*s2	cttagcgagaagctgctgctaggctg	Constructing swiz-miRNA
bZZIP6miR-*a2	aatgactgggaagaggcaaaagtgaa	Constructing swiz-miRNA

BIBLIOGRAPHY

- Agarwal T, Grotewold E, Doseff AI, Gray J. 2016.** MYB31/MYB42 syntelogs exhibit divergent regulation of phenylpropanoid genes in maize, sorghum and rice. *Scientific Reports* **6**: 28502.
- Altartouri B, Bidhendi AJ, Tani T, Suzuki J, Conrad C, Chebli Y, Liu N, Karunakaran C, Scarcelli G, Geitmann A. 2019.** Pectin Chemistry and Cellulose Crystallinity Govern Pavement Cell Morphogenesis in a Multi-Step Mechanism. *Plant physiology* **181**: 127–141.
- Altschul SF, Gish W, Miller W, Myers EW, Lipman DJ. 1990.** Basic local alignment search tool. *Journal of molecular biology* **215**: 403–410.
- Anders N, Wilkinson MD, Lovegrove A, Freeman J, Tryfona T, Pellny TK, Weimar T, Mortimer JC, Stott K, Baker JM, et al. 2012.** Glycosyl transferases in family 61 mediate arabinofuranosyl transfer onto xylan in grasses. *Proceedings of the National Academy of Sciences of the United States of America* **109**: 989–993.
- Arioli T, Peng L, Betzner AS, Burn J, Wittke W, Herth W, Camilleri C, Hofte H, Plazinski J, Birch R, et al. 1998.** Molecular analysis of cellulose biosynthesis in Arabidopsis. *Science* **279**: 717–720.
- Atmodjo MA, Hao Z, Mohnen D. 2013.** Evolving views of pectin biosynthesis. *Annual Review of Plant Biology* **64**: 747–779.
- Barriere Y, Ralph J, Mechin V, Guillaumie S, Grabber JH. 2004.** Genetic and molecular basis of grass cell wall biosynthesis and degradability. II. Lessons from *brown-midrib* mutants. *Comptes Rendus Biologies* **327**: 847.
- Barros J, Escamilla-Trevino L, Song L, Rao X, Serrani-Yarce JC, Palacios MD, Engle N, Choudhury FK, Tschaplinski TJ, Venables BJ, et al. 2019.** 4-Coumarate 3-hydroxylase in the lignin biosynthesis pathway is a cytosolic ascorbate peroxidase. *Nature Communications* **10**: 1994.
- Barros J, Serrani-Yarce JC, Chen F, Baxter D, Venables BJ, Dixon RA. 2016.** Role of bifunctional ammonia-lyase in grass cell wall biosynthesis. *Nature Plants* **2**: 16050.
- Bartley LE, Peck ML, Kim S-R, Ebert B, Manisseri C, Chiniquy DM, Sykes R, Gao L, Rautengarten C, Vega-Sánchez ME, et al. 2013.** Overexpression of a BAHD acyltransferase, *OsAt10*, alters rice cell wall hydroxycinnamic acid content and saccharification. *Plant Physiology* **161**: 1615–1633.
- Basu D, Haswell ES. 2017.** Plant mechanosensitive ion channels: an ocean of possibilities. *Current opinion in plant biology* **40**: 43–48.
- Basu D, Shoots JM, Harkess A, Veley KM, Haswell ES. 2019.** Interactions between the N- and C- termini of mechanosensitive ion channel AtMSL10 support a three-step mechanism for activating its signaling function. *bioRxiv*: 726521.
- Bauer WD, Talmadge KW, Keegstra K, Albersheim P. 1973.** The structure of plant cell walls:

II. The hemicellulose of the walls of suspension-cultured sycamore cells. *Plant Physiology* **51**: 174–187.

Berthet S, Demont-Caulet N, Pollet B, Bidzinski P, Cézard L, Le Bris P, Borrega N, Hervé J, Blondet E, Balzergue S, et al. 2011. Disruption of *LACCASE4* and *17* results in tissue-specific alterations to lignification of *Arabidopsis thaliana* stems. *The Plant Cell* **23**: 1124–1137.

Betekhtin A, Milewska-Hendel A, Lusinska J, Chajec L, Kurczynska E, Hasterok R. 2018. Organ and tissue-specific localisation of selected cell wall epitopes in the zygotic embryo of *Brachypodium distachyon*. *International Journal of Molecular Sciences* **19**.

Bhargava A, Ahad A, Wang S, Mansfield SD, Haughn GW, Douglas CJ, Ellis BE. 2013. The interacting MYB75 and KNAT7 transcription factors modulate secondary cell wall deposition both in stems and seed coat in *Arabidopsis*. *Planta* **237**: 1199–1211.

Bhargava A, Mansfield SD, Hall HC, Douglas CJ, Ellis BE. 2010. MYB75 functions in regulation of secondary cell wall formation in the *Arabidopsis* inflorescence stem. *Plant physiology* **154**: 1428–1438.

Bhatia R, Dalton S, Roberts LA, Moron-Garcia OM, Iacono R, Kosik O, Gallagher JA, Bosch M. 2019. Modified expression of *ZmMYB167* in *Brachypodium distachyon* and *Zea mays* leads to increased cell wall lignin and phenolic content. *Scientific Reports* **9**: 8800.

Bidhendi AJ, Altartouri B, Gosselin FP, Geitmann A. 2019. Mechanical Stress Initiates and Sustains the Morphogenesis of Wavy Leaf Epidermal Cells. *Cell reports* **28**: 1237–1250.e6.

Bidhendi AJ, Geitmann A. 2018. Finite Element Modeling of Shape Changes in Plant Cells. *Plant physiology* **176**: 41–56.

Bogamuwa SP, Jang J-C. 2014. Tandem CCCH zinc finger proteins in plant growth, development and stress response. *Plant & Cell Physiology* **55**: 1367–1375.

Bokor B, Ondoš S, Vaculík M, Bokorová S, Weidinger M, Lichtscheidl I, Turňa J, Lux A. 2017. Expression of genes for Si uptake, accumulation, and correlation of Si with other elements in ionome of maize kernel. *Frontiers in Plant Science* **8**: 1063.

Bouvier d'Yvoire M, Bouchabke-Coussa O, Voorend W, Antelme S, Cézard L, Legée F, Lebris P, Legay S, Whitehead C, McQueen-Mason SJ, et al. 2013. Disrupting the *cinnamyl alcohol dehydrogenase 1 gene (BdCAD1)* leads to altered lignification and improved saccharification in *Brachypodium distachyon*. *The Plant Journal* **73**: 496–508.

Braam J. 2004. In touch: plant responses to mechanical stimuli: Tansley review. *The New phytologist* **165**: 373–389.

Braam J, Davis RW. 1990. Rain-, wind-, and touch-induced expression of calmodulin and calmodulin-related genes in *Arabidopsis*. *Cell* **60**: 357–364.

Brabham C, Singh A, Stork J, Rong Y, Kumar I, Kikuchi K, Yingling YG, Brutnell TP, Rose JKC, Debolt S. 2019. Biochemical and physiological flexibility accompanies reduced cellulose biosynthesis in *Brachypodium cesa1 S830N*. *Annals of Botany Plants* **11**: lz041.

Bragg JN, Wu J, Gordon SP, Guttman ME, Thilmony R, Lazo GR, Gu YQ, Vogel JP. 2012. Generation and characterization of the Western Regional Research Center *Brachypodium* T-DNA

insertional mutant collection. *PLoS One* 7: e41916.

Bromley JR, Busse-Wicher M, Tryfona T, Mortimer JC, Zhang Z, Brown DM, Dupree P. 2013. GUX1 and GUX2 glucuronyltransferases decorate distinct domains of glucuronoxylan with different substitution patterns. *The Plant Journal* 74: 423–434.

Brown DM, Zeef LAH, Ellis J, Goodacre R, Turner SR. 2005a. Identification of novel genes in *Arabidopsis* involved in secondary cell wall formation using expression profiling and reverse genetics. *The Plant Cell* 17: 2281–2295.

Brown DM, Zeef LAH, Ellis J, Goodacre R, Turner SR. 2005b. Identification of novel genes in *Arabidopsis* involved in secondary cell wall formation using expression profiling and reverse genetics. *The Plant cell* 17: 2281–2295.

Brown DM, Zhang ZN, Stephens E, Dupree P, Turner SR. 2009. Characterization of IRX10 and IRX10-like reveals an essential role in glucuronoxylan biosynthesis in *Arabidopsis*. *The Plant Journal* 57: 732.

Buanafina MM de O, Fescemyer HW, Sharma M, Shearer EA. 2016. Functional testing of a PF02458 homologue of putative rice arabinoxylan feruloyl transferase genes in *Brachypodium distachyon*. *Planta* 243: 659–674.

Buliga GS, Brant DA, Fincher GB. 1986. The sequence statistics and solution conformation of a barley (1 → 3, 1 → 4)-beta-D-glucan. *Carbohydrate Research* 157: 139–156.

Bulone V, Schwerdt JG, Fincher GB. 2019. Co-evolution of enzymes involved in plant cell wall metabolism in the grasses. *Frontiers in Plant Science* 10: 1009.

Burton RA, Collins HM, Kibble NAJ, Smith JA, Shirley NJ, Jobling SA, Henderson M, Singh RR, Pettolino F, Wilson SM, et al. 2011. Over-expression of specific *HvCslF* cellulose synthase-like genes in transgenic barley increases the levels of cell wall (1,3;1,4)-β-d-glucans and alters their fine structure. *Plant Biotechnology Journal* 9: 117–135.

Burton RA, Fincher GB. 2012. Current challenges in cell wall biology in the cereals and grasses. *Frontiers in Plant Science* 3: 130.

Burton RA, Fincher GB. 2014. Evolution and development of cell walls in cereal grains. *Frontiers in Plant Science* 5: 456.

Burton RA, Gidley MJ, Fincher GB. 2010a. Heterogeneity in the chemistry, structure and function of plant cell walls. *Nature Chemical Biology* 6: 724–732.

Burton RA, Ma G, Baumann U, Harvey AJ, Shirley NJ, Taylor J, Pettolino F, Bacic A, Beatty M, Simmons CR, et al. 2010b. A customized gene expression microarray reveals that the brittle stem phenotype *fs2* of barley is attributable to a retroelement in the *HvCesA4* cellulose synthase gene. *Plant Physiology* 153: 1716–1728.

Busse-Wicher M, Gomes TCF, Tryfona T, Nikolovski N, Stott K, Grantham NJ, Bolam DN, Skaf MS, Dupree P. 2014. The pattern of xylan acetylation suggests xylan may interact with cellulose microfibrils as a twofold helical screw in the secondary plant cell wall of *Arabidopsis thaliana*. *The Plant Journal* 79: 492–506.

Carpita NC, McCann MC. 2010. The maize mixed-linkage (1->3),(1->4)-beta-D-glucan

polysaccharide is synthesized at the golgi membrane. *Plant Physiology* **153**: 1362–1371.

Cass CL, Peraldi A, Dowd PF, Mottiar Y, Santoro N, Karlen SD, Bukhman YV, Foster CE, Thrower N, Bruno LC, et al. 2015. Effects of *PHENYLALANINE AMMONIA LYASE (PAL)* knockdown on cell wall composition, biomass digestibility, and biotic and abiotic stress responses in *Brachypodium*. *Journal of Experimental Botany* **66**: 4317–4335.

Cesarino I, Araújo P, Sampaio Mayer JL, Vicentini R, Berthet S, Demedts B, Vanholme B, Boerjan W, Mazzafera P. 2013. Expression of *SofLAC*, a new laccase in sugarcane, restores lignin content but not S:G ratio of *Arabidopsis lac17* mutant. *Journal of Experimental Botany* **64**: 1769–1781.

Chai M, Zhou C, Molina I, Fu C, Nakashima J, Li G, Zhang W, Park J, Tang Y, Jiang Q, et al. 2016. A class II KNOX gene, *KNOX4*, controls seed physical dormancy. *Proceedings of the National Academy of Sciences of the United States of America* **113**: 6997–7002.

Chambliss AB, Khatau SB, Erdenberger N, Robinson DK, Hodzic D, Longmore GD, Wirtz D. 2013. The LINC-anchored actin cap connects the extracellular milieu to the nucleus for ultrafast mechanotransduction. *Scientific reports* **3**: 1087.

Chehab EW, Eich E, Braam J. 2009. Thigmomorphogenesis: a complex plant response to mechano-stimulation. *Journal of experimental botany* **60**: 43–56.

Chiniquy D, Sharma V, Schultink A, Baidoo EE, Rautengarten C, Cheng K, Carroll A, Ulvskov P, Harholt J, Keasling JD, et al. 2012. XAX1 from glycosyltransferase family 61 mediates xylosyltransfer to rice xylan. *Proceedings of the National Academy of Sciences of the United States of America* **109**: 17117–17122.

Christensen U, Alonso-Simon A, Scheller HV, Willats WG, Harholt J. 2010. Characterization of the primary cell walls of seedlings of *Brachypodium distachyon* - a potential model plant for temperate grasses. *Phytochemistry* **71**: 62–69.

Clarke HT, Gillespie HB, Weisshaus SZ. 1933. The action of formaldehyde on amines and amino acids. *Journal of the American Chemical Society* **55**: 4571–4587.

Coomey J, Hazen SP. 2015. *Brachypodium* as a model for the cell wall and biomass crops. In: Vogel JP, ed. *Plant Genetics and Genomics: Crops and Models*. Genetics and Genomics of *Brachypodium*. New York: Springer-Verlag.

Coomey JH, Sibout R, Hazen SP. 2020. Tansley reviews: Grass secondary cell walls, *Brachypodium distachyon* as a model for discovery. *The New phytologist*.

Coutand C, Martin L, Leblanc-Fournier N, Decourteix M, Julien J-L, Moulia B. 2009. Strain mechanosensing quantitatively controls diameter growth and *PtaZFP2* gene expression in poplar. *Plant physiology* **151**: 223–232.

Dai S, Petrucci S, Ordiz MI, Zhang Z, Chen S, Beachy RN. 2003. Functional analysis of *RF2a*, a rice transcription factor. *The Journal of biological chemistry* **278**: 36396–36402.

Dai S, Wei X, Alfonso AA, Pei L, Duque UG, Zhang Z, Babb GM, Beachy RN. 2008. Transgenic rice plants that overexpress transcription factors *RF2a* and *RF2b* are tolerant to rice tungro virus replication and disease. *Proceedings of the National Academy of Sciences of the*

United States of America **105**: 21012–21016.

Dai S, Zhang Z, Chen S, Beachy RN. 2004. RF2b, a rice bZIP transcription activator, interacts with RF2a and is involved in symptom development of rice tungro disease. *Proceedings of the National Academy of Sciences of the United States of America* **101**: 687–692.

Dalmais M, Antelme S, Ho-Yue-Kuang S, Wang Y, Darracq O, d'Yvoire MB, Cézard L, Légée F, Blondet E, Oria N, et al. 2013. A TILLING platform for functional genomics in *Brachypodium distachyon*. *PloS One* **8**: e65503.

D'Auria JC. 2006. Acyltransferases in plants: a good time to be BAHD. *Current Opinion in Plant Biology* **9**: 331–340.

Deppmann CD, Acharya A, Rishi V, Wobbles B, Smeekens S, Taparowsky EJ, Vinson C. 2004. Dimerization specificity of all 67 B-ZIP motifs in *Arabidopsis thaliana*: a comparison to *Homo sapiens* B-ZIP motifs. *Nucleic acids research* **32**: 3435–3445.

Deshmukh RK, Ma JF, Bélanger RR. 2017. Editorial: Role of silicon in plants. *Frontiers in Plant Science* **8**: 1858.

Dimitroff G, Little A, Lahnstein J, Schwerdt JG, Srivastava V, Bulone V, Burton RA, Fincher GB. 2016. (1,3;1,4)- β -glucan biosynthesis by the CSLF6 enzyme: position and flexibility of catalytic residues influence product fine structure. *Biochemistry* **55**: 2054–2061.

Djamei A, Pitzschke A, Nakagami H, Rajh I, Hirt H. 2007. Trojan horse strategy in *Agrobacterium* transformation: abusing MAPK defense signaling. *Science* **318**: 453–456.

Do C-T, Pollet B, Thévenin J, Sibout R, Denoue D, Barrière Y, Lapierre C, Jouanin L. 2007. Both caffeoyl Coenzyme A 3-*O*-methyltransferase 1 and caffeic acid *O*-methyltransferase 1 are involved in redundant functions for lignin, flavonoids and sinapoyl malate biosynthesis in *Arabidopsis*. *Planta* **226**: 1117–1129.

Dröge-Laser W, Snoek BL, Snel B, Weiste C. 2018. The *Arabidopsis* bZIP transcription factor family—an update. *Current opinion in plant biology* **45**: 36–49.

Ehlert A, Weltmeier F, Wang X, Mayer CS, Smeekens S, Vicente-Carbajosa J, Dröge-Laser W. 2006. Two-hybrid protein-protein interaction analysis in *Arabidopsis* protoplasts: establishment of a heterodimerization map of group C and group S bZIP transcription factors. *The Plant journal: for cell and molecular biology* **46**: 890–900.

Ehltung J, Mattheus N, Aeschliman DS, Li E, Hamberger B, Cullis IF, Zhuang J, Kaneda M, Mansfield SD, Samuels L, et al. 2005. Global transcript profiling of primary stems from *Arabidopsis thaliana* identifies candidate genes for missing links in lignin biosynthesis and transcriptional regulators of fiber differentiation. *The Plant journal: for cell and molecular biology* **42**: 618–640.

Eloy NB, Voorend W, Lan W, Saleme M de LS, Cesarino I, Vanholme R, Smith RA, Goeminne G, Pallidis A, Morreel K, et al. 2017. Silencing *CHALCONE SYNTHASE* in maize impedes the incorporation of tricetin into lignin and increases lignin content. *Plant Physiology* **173**: 998–1016.

Esau K. 1977. *Anatomy of seed plants*. New York: John Wiley & Sons.

- Eudes A, Dutta T, Deng K, Jacquet N, Sinha A, Benites VT, Baidoo EEK, Richel A, Sattler SE, Northen TR, et al. 2017.** SbCOMT (Bmr12) is involved in the biosynthesis of triclin-lignin in sorghum. *PLoS one* **12**: e0178160.
- Fal K, Asnacios A, Chabouté M-E, Hamant O. 2017.** Nuclear envelope: a new frontier in plant mechanosensing? *Biophysical reviews* **9**: 389–403.
- Fan M, Herburger K, Jensen JK, Zemelis-Durfee S, Brandizzi F, Fry SC, Wilkerson CG. 2018.** A trihelix family transcription factor is associated with key genes in mixed-linkage glucan accumulation. *Plant Physiology* **178**: 1207–1221.
- Fincher GB. 2009.** Exploring the evolution of (1,3;1,4)-beta-D-glucans in plant cell walls: comparative genomics can help! *Current Opinion in Plant Biology* **12**: 140–147.
- Floyd SK, Bowman JL. 2006.** Distinct developmental mechanisms reflect the independent origins of leaves in vascular plants. *Current Biology* **16**: 1911–1917.
- Fornalé S, Rencoret J, García-Calvo L, Encina A, Rigau J, Gutiérrez A, Del Río JC, Caparros-Ruiz D. 2017.** Changes in cell wall polymers and degradability in maize mutants lacking 3'- and 5'-O-methyltransferases involved in lignin biosynthesis. *Plant & Cell Physiology* **58**: 240–255.
- Fornalé S, Shi X, Chai C, Encina A, Irar S, Capellades M, Fuguet E, Torres J-L, Rovira P, Puigdomènech P, et al. 2010.** ZmMYB31 directly represses maize lignin genes and redirects the phenylpropanoid metabolic flux. *The Plant Journal* **64**: 633–644.
- Fornalé S, Sonbol F-M, Maes T, Capellades M, Puigdomènech P, Rigau J, Caparrós-Ruiz D. 2006.** Down-regulation of the maize and *Arabidopsis thaliana* caffeic acid O-methyltransferase genes by two new maize R2R3-MYB transcription factors. *Plant Molecular Biology* **62**: 809–823.
- Francin-Allami M, Alvarado C, Daniel S, Geairon A, Saulnier L, Guillon F. 2019.** Spatial and temporal distribution of cell wall polysaccharides during grain development of *Brachypodium distachyon*. *Plant Science* **280**: 367–382.
- Fry SC. 1989.** The structure and functions of xyloglucan. *Journal of Experimental Botany* **40**: 1–11.
- Fukazawa J, Nakata M, Ito T, Matsushita A, Yamaguchi S, Takahashi Y. 2011.** bZIP transcription factor RSG controls the feedback regulation of NtGA20ox1 via intracellular localization and epigenetic mechanism. *Plant signaling & behavior* **6**: 26–28.
- Fukazawa J, Nakata M, Ito T, Yamaguchi S, Takahashi Y. 2010.** The transcription factor RSG regulates negative feedback of NtGA20ox1 encoding GA 20-oxidase. *The Plant journal: for cell and molecular biology* **62**: 1035–1045.
- Fukazawa J, Sakai T, Ishida S, Yamaguchi I, Kamiya Y, Takahashi Y. 2000.** Repression of shoot growth, a bZIP transcriptional activator, regulates cell elongation by controlling the level of gibberellins. *The Plant cell* **12**: 901–915.
- Gibalová A, Steinbachová L, Hafidh S, Bláhová V, Gadiou Z, Michailidis C, Müller K, Pleskot R, Dupl'áková N, Honys D. 2017.** Characterization of pollen-expressed bZIP protein

- interactions and the role of ATbZIP18 in the male gametophyte. *Plant reproduction* **30**: 1–17.
- Gibeaut DM, Pauly M, Bacic A, Fincher GB. 2005.** Changes in cell wall polysaccharides in developing barley (*Hordeum vulgare*) coleoptiles. *Planta* **221**: 729–738.
- Gladala-Kostarz A, Doonan JH, Bosch M. 2020.** Mechanical stimulation in *Brachypodium distachyon*: implications for fitness, productivity and cell wall properties. *Plant, cell & environment*.
- Głazowska S, Baldwin L, Mravec J, Bukh C, Hansen TH, Jensen MM, Fangel JU, Willats WGT, Glasius M, Felby C, et al. 2018a.** The impact of silicon on cell wall composition and enzymatic saccharification of *Brachypodium distachyon*. *Biotechnology for Biofuels* **11**: 171.
- Głazowska S, Murozuka E, Persson DP, Castro PH, Schjoerring JK. 2018b.** Silicon affects seed development and leaf macrohair formation in *Brachypodium distachyon*. *Physiologia Plantarum* **163**: 231–246.
- Goodstein DM, Shu S, Howson R, Neupane R, Hayes RD, Fazo J, Mitros T, Dirks W, Hellsten U, Putnam N, et al. 2011.** Phytozome: a comparative platform for green plant genomics. *Nucleic acids research* **40**: D1178–D1186.
- Gordon SP, Contreras-Moreira B, Woods DP, Des Marais DL, Burgess D, Shu S, Stritt C, Roulin AC, Schackwitz W, Tyler L, et al. 2017.** Extensive gene content variation in the *Brachypodium distachyon* pan-genome correlates with population structure. *Nature Communications* **8**: 2184.
- Granier F, Lemaire A, Wang Y, LeBris P, Antelme S, Vogel J, Laudencia-Chingcuanco D, Sibout R. 2015.** Chemical and radiation mutagenesis: induction and detection by whole genome sequencing. In: *Genetics and Genomics of Brachypodium*. Genetics and Genomics of *Brachypodium*.
- Graumann K, Vanrobays E, Tutois S, Probst AV, Evans DE, Tatout C. 2014.** Characterization of two distinct subfamilies of SUN-domain proteins in *Arabidopsis* and their interactions with the novel KASH-domain protein AtTIK. *Journal of experimental botany* **65**: 6499–6512.
- Grigoryan G, Keating AE. 2006.** Structure-based prediction of bZIP partnering specificity. *Journal of molecular biology* **355**: 1125–1142.
- Guillon F, Bouchet B, Jamme F, Robert P, Quemener B, Barron C, Larre C, Dumas P, Saulnier L. 2011a.** *Brachypodium distachyon* grain: characterization of endosperm cell walls. *Journal of Experimental Botany* **62**: 1001–1015.
- Guillon F, Bouchet B, Jamme F, Robert P, Quéméner B, Barron C, Larré C, Dumas P, Saulnier L. 2011b.** *Brachypodium distachyon* grain: characterization of endosperm cell walls. *Journal of Experimental Botany* **62**: 1001–1015.
- Ha CM, Escamilla-Trevino L, Yarce JCS, Kim H, Ralph J, Chen F, Dixon RA. 2016.** An essential role of caffeoyl shikimate esterase in monolignol biosynthesis in *Medicago truncatula*. *The Plant Journal* **86**: 363–375.
- Hake S, Smith HMS, Holtan H, Magnani E, Mele G, Ramirez J. 2004.** The role of knox genes

in plant development. *Annual review of cell and developmental biology* **20**: 125–151.

Hamant O, Heisler MG, Jönsson H, Krupinski P, Uyttewaal M, Bokov P, Corson F, Sahlin P, Boudaoud A, Meyerowitz EM, et al. 2008. Developmental patterning by mechanical signals in Arabidopsis. *Science* **322**: 1650–1655.

Hamilton ES, Jensen GS, Maksaev G, Katims A, Sherp AM, Haswell ES. 2015a. Mechanosensitive channel MSL8 regulates osmotic forces during pollen hydration and germination. *Science* **350**: 438–441.

Hamilton ES, Schlegel AM, Haswell ES. 2015b. United in Diversity: Mechanosensitive Ion Channels in Plants. *Annual review of plant*.

Handakumbura PP, Brow K, Whitney IP, Zhao K, Sanguinet KA, Lee SJ, Olins J, Romero-Gamboa SP, Harrington MJ, Bascom CJ, et al. 2018. SECONDARY WALL ASSOCIATED MYB1 is a positive regulator of secondary cell wall thickening in *Brachypodium distachyon* and is not found in the Brassicaceae. *The Plant journal: for cell and molecular biology* **0**.

Handakumbura P, Matos D, Osmont K, Harrington M, Heo K, Kafle K, Kim S, Baskin T, Hazen S. 2013. Perturbation of *Brachypodium distachyon* CELLULOSE SYNTHASE A4 or 7 results in abnormal cell walls. *BMC Plant Biology* **13**: 131.

Harholt J, Jensen JK, Sørensen SO, Orfila C, Pauly M, Scheller HV. 2006. ARABINAN DEFICIENT 1 is a putative arabinosyltransferase involved in biosynthesis of pectic arabinan in Arabidopsis. *Plant physiology* **140**: 49–58.

Haswell ES, Peyronnet R, Barbier-Brygoo H, Meyerowitz EM, Frachisse J-M. 2008. Two MscS homologs provide mechanosensitive channel activities in the Arabidopsis root. *Current biology: CB* **18**: 730–734.

Hatfield RD, Marita JM, Frost K, Grabber J, Ralph J, Lu F, Kim H. 2009. Grass lignin acylation: *p*-coumaroyl transferase activity and cell wall characteristics of C3 and C4 grasses. *Planta* **229**: 1253–1267.

Hatfield RD, Rancour DM, Marita JM. 2016. Grass cell walls: A story of cross-linking. *Frontiers in Plant Science* **7**: 2056.

Hattori T, Inanaga S, Araki H, An P. 2005. Application of silicon enhanced drought tolerance in *Sorghum bicolor*. *Physiologia*.

Hay A, Tsiantis M. 2010. KNOX genes: versatile regulators of plant development and diversity. *Development* **137**: 3153–3165.

Heinz S, Benner C, Spann N, Bertolino E, Lin YC, Laslo P, Cheng JX, Murre C, Singh H, Glass CK. 2010. Simple combinations of lineage-determining transcription factors prime cis-regulatory elements required for macrophage and B cell identities. *Molecular cell* **38**: 576–589.

Herbaut M, Zoghalmi A, Habrant A, Falourd X, Foucat L, Chabbert B, Paës G. 2018. Multimodal analysis of pretreated biomass species highlights generic markers of lignocellulose recalcitrance. *Biotechnology for Biofuels* **11**: 52.

He J-B, Zhao X-H, Du P-Z, Zeng W, Beahan CT, Wang Y-Q, Li H-L, Bacic A, Wu A-M. 2018. KNAT7 positively regulates xylan biosynthesis by directly activating IRX9 expression in

Arabidopsis. *Journal of integrative plant biology*.

Higuchi T, Ito Y, Kawamura I. 1967. *p*-hydroxyphenylpropane component of grass lignin and role of tyrosine-ammonia lyase in its formation. *Phytochemistry* **6**: 875–881.

Hirano K, Kondo M, Aya K, Miyao A, Sato Y, Antonio BA, Namiki N, Nagamura Y, Matsuoka M. 2013. Identification of transcription factors involved in rice secondary cell wall formation. *Plant & Cell Physiology* **54**: 1791–1802.

Høj PB, Fincher GB. 1995. Molecular evolution of plant beta-glucan endohydrolases. *The Plant Journal* **7**: 367–379.

Huang D, Wang S, Zhang B, Shang-Guan K, Shi Y, Zhang D, Liu X, Wu K, Xu Z, Fu X, et al. 2015. A gibberellin-mediated DELLA-NAC signaling cascade regulates cellulose synthesis in rice. *The Plant Cell* **27**: 1681–1696.

Huang P, Yoshida H, Yano K, Kinoshita S, Kawai K, Koketsu E, Hattori M, Takehara S, Huang J, Hirano K, et al. 2018. OsIDD2, a zinc finger and INDETERMINATE DOMAIN protein, regulates secondary cell wall formation. *Journal of Integrative Plant Biology* **60**: 130–143.

Iida H. 2014. Mugifumi, a beneficial farm work of adding mechanical stress by treading to wheat and barley seedlings. *Frontiers in plant science* **5**: 453.

Ishida S, Fukazawa J, Yuasa T, Takahashi Y. 2004. Involvement of 14-3-3 signaling protein binding in the functional regulation of the transcriptional activator REPRESSION OF SHOOT GROWTH by gibberellins. *The Plant cell* **16**: 2641–2651.

Ishida S, Yuasa T, Nakata M, Takahashi Y. 2008. A tobacco calcium-dependent protein kinase, CDPK1, regulates the transcription factor REPRESSION OF SHOOT GROWTH in response to gibberellins. *The Plant cell* **20**: 3273–3288.

Ito T, Ishida S, Oe S, Fukazawa J, Takahashi Y. 2017. Autophosphorylation Affects Substrate-Binding Affinity of Tobacco Ca²⁺-Dependent Protein Kinase1. *Plant physiology* **174**: 2457–2468.

Ito T, Nakata M, Fukazawa J, Ishida S, Takahashi Y. 2014. Scaffold Function of Ca²⁺-Dependent Protein Kinase: Tobacco Ca²⁺-DEPENDENT PROTEIN KINASE1 Transfers 14-3-3 to the Substrate REPRESSION OF SHOOT GROWTH after Phosphorylation. *Plant physiology* **165**: 1737–1750.

Jaffe MJ. 1973. Thigmomorphogenesis: The response of plant growth and development to mechanical stimulation : With special reference to *Bryonia dioica*. *Planta* **114**: 143–157.

Jaffe MJ, Biro R, Bridle K. 1980. Thigmomorphogenesis: Calibration of the parameters of the sensory function in beans. *Physiologia plantarum* **49**: 410–416.

Jaffe MJ, Leopold AC, Staples RC. 2002. Thigmo responses in plants and fungi. *American journal of botany* **89**: 375–382.

Jakoby M, Weisshaar B, Dröge-Laser W, Vicente-Carbajosa J, Tiedemann J, Kroj T, Parcy F, bZIP Research Group. 2002. bZIP transcription factors in Arabidopsis. *Trends in plant science* **7**: 106–111.

- Jensen JK, Wilkerson CG. 2017.** *Brachypodium* as an experimental system for the study of stem parenchyma biology in grasses. *PLoS One* **12**: e0173095.
- Jobling SA. 2015.** Membrane pore architecture of the CslF6 protein controls (1-3,1-4)- β -glucan structure. *Science Advances* **1**: e1500069.
- Kagale S, Rozwadowski K. 2011.** EAR motif-mediated transcriptional repression in plants: An underlying mechanism for epigenetic regulation of gene expression. *Epigenetics: official journal of the DNA Methylation Society* **6**: 141–146.
- Kapp N, Barnes WJ, Richard TL, Anderson CT. 2015.** Imaging with the fluorogenic dye Basic Fuchsin reveals subcellular patterning and ecotype variation of lignification in *Brachypodium distachyon*. *Journal of Experimental Botany* **66**: 4295–4304.
- Karlen SD, Zhang C, Peck ML, Smith RA, Padmakshan D, Helmich KE, Free HCA, Lee S, Smith BG, Lu F, et al. 2016.** Monolignol ferulate conjugates are naturally incorporated into plant lignins. *Science Advances* **2**: e1600393.
- Kido N, Yokoyama R, Yamamoto T, Furukawa J, Iwai H, Satoh S, Nishitani K. 2015.** The matrix polysaccharide (1;3,1;4)- β -D-glucan is involved in silicon-dependent strengthening of rice cell wall. *Plant & Cell Physiology* **56**: 1679.
- Kim W-C, Ko J-H, Han K-H. 2012.** Identification of a *cis*-acting regulatory motif recognized by MYB46, a master transcriptional regulator of secondary wall biosynthesis. *Plant Molecular Biology* **78**: 489–501.
- Kim S-J, Zemelis-Durfee S, Jensen JK, Wilkerson CG, Keegstra K, Brandizzi F. 2018.** In the grass species *Brachypodium distachyon*, the production of mixed-linkage (1,3; 1,4)- β -glucan (MLG) occurs in the Golgi apparatus. *The Plant Journal* **93**: 1062–1075.
- Kim S-J, Zemelis S, Keegstra K, Brandizzi F. 2015.** The cytoplasmic localization of the catalytic site of CSLF6 supports a channeling model for the biosynthesis of mixed-linkage glucan. *The Plant Journal* **81**: 537–547.
- Kohorn BD. 2016.** Cell wall-associated kinases and pectin perception. *Journal of experimental botany* **67**: 489–494.
- Ko J-H, Kim W-C, Han K-H. 2009.** Ectopic expression of MYB46 identifies transcriptional regulatory genes involved in secondary wall biosynthesis in *Arabidopsis*. *The Plant Journal* **60**: 649–665.
- Kotake T, Aohara T, Hirano K, Sato A, Kaneko Y, Tsumuraya Y, Takatsuji H, Kawasaki S. 2011.** Rice *Brittle culm 6* encodes a dominant-negative form of CesA protein that perturbs cellulose synthesis in secondary cell walls. *Journal of Experimental Botany* **62**: 2053–2062.
- Kubo M, Udagawa M, Nishikubo N, Horiguchi G, Yamaguchi M, Ito J, Mimura T, Fukuda H, Demura T. 2005.** Transcription switches for protoxylem and metaxylem vessel formation. *Genes & Development* **19**: 1855–1860.
- Lam PY, Tobimatsu Y, Matsumoto N, Suzuki S, Lan W, Takeda Y, Yamamura M, Sakamoto M, Ralph J, Lo C, et al. 2019.** OsCALdOMT1 is a bifunctional O-methyltransferase involved in the biosynthesis of tricin-lignins in rice cell walls. *Scientific Reports* **9**: 11597.

- Lam PY, Tobimatsu Y, Takeda Y, Suzuki S, Yamamura M, Umezawa T, Lo C. 2017.** Disrupting flavone synthase II alters lignin and improves biomass digestibility. *Plant Physiology* **174**: 972–985.
- Lange MJP, Lange T. 2015.** Touch-induced changes in Arabidopsis morphology dependent on gibberellin breakdown. *Nature plants* **1**: 14025.
- Langer RHM. 1979.** *How grasses grow*. Edward Arnold.
- Lan W, Lu F, Regner M, Zhu Y, Rencoret J, Ralph SA, Zakai UI, Morreel K, Boerjan W, Ralph J. 2015.** Tricin, a flavonoid monomer in monocot lignification. *Plant Physiology* **167**: 1284–1295.
- Lan W, Rencoret J, Lu F, Karlen SD, Smith BG, Harris PJ, Del Río JC, Ralph J. 2016.** Tricin-lignins: occurrence and quantitation of tricin in relation to phylogeny. *The Plant Journal* **88**: 1046–1057.
- Lan W, Yue F, Rencoret J, Del Río JC, Boerjan W, Lu F, Ralph J. 2018.** Elucidating tricin-lignin structures: assigning correlations in HSQC spectra of monocot lignins. *Polymers* **10**.
- Lapierre C, Voxeur A, Boutet S, Ralph J. 2019.** Arabinose conjugates diagnostic of ferulate-ferulate and ferulate-monomethyl ether cross-coupling are released by mild acidolysis of grass cell walls. *Journal of Agricultural and Food Chemistry* **67**: 12962–12971.
- Lazaridou A, Biliaderis CG. 2007.** Molecular aspects of cereal β -glucan functionality: Physical properties, technological applications and physiological effects. *Journal of Cereal Science* **46**: 101–118.
- Leblanc-Fournier N, Martin L, Lenne C, Decourteix M. 2014.** To respond or not to respond, the recurring question in plant mechanosensitivity. *Frontiers in plant science* **5**: 401.
- Le Bris P, Wang Y, Barbereau C, Antelme S, Cézard L, Legée F, D’Orlando A, Dalmais M, Bendahmane A, Schuetz M, et al. 2019.** Inactivation of *LACCASE8* and *LACCASE5* genes in *Brachypodium distachyon* leads to severe decrease in lignin content and high increase in saccharification yield without impacting plant integrity. *Biotechnology for Biofuels* **12**: 181.
- Lee K-H, Du Q, Zhuo C, Qi L, Wang H. 2019a.** LBD29-involved auxin signaling represses NAC master regulators and fiber wall biosynthesis. *Plant Physiology* **181**: 595–608.
- Lee CP, Maksaev G, Jensen GS, Murcha MW, Wilson ME, Fricker M, Hell R, Haswell ES, Millar AH, Sweetlove LJ. 2016.** MSL 1 is a mechanosensitive ion channel that dissipates mitochondrial membrane potential and maintains redox homeostasis in mitochondria during abiotic stress. *The Plant journal: for cell and molecular biology* **88**: 809–825.
- Lee CH, O’Neill MA, Tsumuraya Y, Darvill AG, Ye ZH. 2007.** The *irregular xylem9* mutant is deficient in xylan xylosyltransferase activity. *Plant & Cell Physiology* **48**: 1624.
- Lee D, Polisensky DH, Braam J. 2005.** Genome-wide identification of touch- and darkness-regulated Arabidopsis genes: a focus on calmodulin-like and XTH genes. *The New phytologist* **165**: 429–444.
- Lee C, Teng Q, Zhong R, Yuan Y, Ye Z-H. 2014.** Functional roles of rice glycosyltransferase family GT43 in xylan biosynthesis. *Plant Signaling & Behavior* **9**: e27809.

- Lee SJ, Warnick TA, Pattathil S, Alvelo-Maurosa JG, Serapiglia MJ, McCormick H, Brown V, Young NF, Schnell DJ, Smart LB, et al. 2012.** Biological conversion assay using *Clostridium phytofermentans* to estimate plant feedstock quality. *Biotechnology for biofuels* 5: 5.
- Lee JS, Wilson ME, Richardson RA, Haswell ES. 2019b.** Genetic and physical interactions between the organellar mechanosensitive ion channel homologs MSL1, MSL2, and MSL3 reveal a role for inter-organelle communication in plant development. *Plant direct* 3: e00124.
- Li E, Bhargava A, Qiang W, Friedmann MC, Forneris N, Savidge RA, Johnson LA, Mansfield SD, Ellis BE, Douglas CJ. 2012.** The Class II KNOX gene KNAT7 negatively regulates secondary wall formation in Arabidopsis and is functionally conserved in Populus. *The New phytologist* 194: 102–115.
- Little A, Schwerdt JG, Shirley NJ, Khor SF, Neumann K, O'Donovan LA, Lahnstein J, Collins HM, Henderson M, Fincher GB, et al. 2018.** Revised phylogeny of the cellulose synthase gene superfamily: Insights into cell wall evolution. *Plant Physiology* 177: 1124–1141.
- Liu X, Chu Z. 2015.** Genome-wide evolutionary characterization and analysis of bZIP transcription factors and their expression profiles in response to multiple abiotic stresses in *Brachypodium distachyon*. *BMC genomics* 16: 227.
- Liu L, Hsia MM, Dama M, Vogel J, Pauly M. 2016.** A xyloglucan backbone 6-O-acetyltransferase from *Brachypodium distachyon* modulates xyloglucan xylosylation. *Molecular Plant* 9: 615–617.
- Liu Y, You S, Taylor-Teeple M, Li WL, Schuetz M, Brady SM, Douglas CJ. 2014.** BEL1-LIKE HOMEODOMAIN6 and KNOTTED ARABIDOPSIS THALIANA7 interact and regulate secondary cell wall formation via repression of REVOLUTA. *The Plant cell* 26: 4843–4861.
- Liu D, Zehfroosh N, Hancock BL, Hines K, Fang W, Kilfoil M, Learned-Miller E, Sanguinet KA, Goldner LS, Baskin TI. 2017.** Imaging cellulose synthase motility during primary cell wall synthesis in the grass *Brachypodium distachyon*. *Scientific Reports* 7: 15111.
- Lozano-Sotomayor P, Chávez Montes RA, Silvestre-Vañó M, Herrera-Ubaldo H, Greco R, Pablo-Villa J, Galliani BM, Diaz-Ramirez D, Weemen M, Boutilier K, et al. 2016.** Altered expression of the bZIP transcription factor DRINK ME affects growth and reproductive development in Arabidopsis thaliana. *The Plant journal: for cell and molecular biology* 88: 437–451.
- MacKinnon KJ-M, Cole BJ, Yu C, Coomey JH, Hartwick NT, Remigereau M-S, Duffy T, Michael TP, Kay SA, Hazen SP. 2020.** Changes in ambient temperature are the prevailing cue in determining *Brachypodium distachyon* diurnal gene regulation. *bioRxiv*: 762021.
- Marita JM, Hatfield RD, Rancour DM, Frost KE. 2014.** Identification and suppression of the *p*-coumaroyl CoA:hydroxycinnamyl alcohol transferase in *Zea mays* L. *The Plant Journal* 78: 850–864.
- Marriott PE, Sibout R, Lapierre C, Fangel JU, Willats WGT, Hofte H, Gómez LD, McQueen-Mason SJ. 2014.** Range of cell-wall alterations enhance saccharification in *Brachypodium distachyon* mutants. *Proceedings of the National Academy of Sciences, India. Section A. Physical Sciences* 111: 14601–14606.

- Martínez-Abad A, Berglund J, Toriz G, Gatenholm P, Henriksson G, Lindström M, Wohler J, Vilaplana F. 2017.** Regular motifs in xylan modulate molecular flexibility and interactions with cellulose surfaces. *Plant Physiology* **175**: 1579–1592.
- Martin L, Leblanc-Fournier N, Julien J-L, Moulia B, Coutand C. 2010.** Acclimation kinetics of physiological and molecular responses of plants to multiple mechanical loadings. *Journal of experimental botany* **61**: 2403–2412.
- Matos DA, Whitney IP, Harrington MJ, Hazen SP. 2013.** Cell walls and the developmental anatomy of the *Brachypodium distachyon* stem internode. *PloS One* **8**: e80640.
- Ma Q, Wang N, Hao P, Sun H, Wang C, Ma L, Wang H, Zhang X, Wei H, Yu S. 2019.** Genome-wide identification and characterization of TALE superfamily genes in cotton reveals their functions in regulating secondary cell wall biosynthesis. *BMC plant biology* **19**: 432.
- Ma JF, Yamaji N. 2006.** Silicon uptake and accumulation in higher plants. *Trends in Plant Science* **11**: 392–397.
- Ma JF, Yamaji N, Tamai K, Mitani N. 2007.** Genotypic difference in silicon uptake and expression of silicon transporter genes in rice. *Plant Physiology* **145**: 919–924.
- Méchin V, Laluc A, Legée F, Cézard L, Denoue D, Barrière Y, Lapierre C. 2014.** Impact of the brown-midrib *bm5* mutation on maize lignins. *Journal of Agricultural and Food Chemistry* **62**: 5102–5107.
- Mitani-Ueno N, Yamaji N, Ma JF. 2016.** High silicon accumulation in the shoot is required for down-regulating the expression of Si transporter genes in rice. *Plant & Cell Physiology* **57**: 2510–2518.
- Mitchell RAC, Dupree P, Shewry PR. 2007.** A novel bioinformatics approach identifies candidate genes for the synthesis and feruloylation of arabinoxylan. *Plant Physiology* **144**: 43–53.
- Mitsuda N, Iwase A, Yamamoto H, Yoshida M, Seki M, Shinozaki K, Ohme-Takagi M. 2007.** NAC transcription factors, NST1 and NST3, are key regulators of the formation of secondary walls in woody tissues of *Arabidopsis*. *The Plant Cell* **19**: 270–280.
- Miyamoto T, Takada R, Tobimatsu Y, Takeda Y, Suzuki S, Yamamura M, Osakabe K, Osakabe Y, Sakamoto M, Umezawa T. 2019.** OsMYB108 loss-of-function enriches *p*-coumaroylated and triclin lignin units in rice cell walls. *The Plant Journal* **98**: 975–987.
- Mnich E, Bjarnholt N, Eudes A, Harholt J, Holland C, Jørgensen B, Larsen FH, Liu M, Manat R, Meyer AS, et al. 2020.** Phenolic cross-links: building and de-constructing the plant cell wall. *Natural Product Reports*.
- Monshausen GB, Bibikova TN, Weisenseel MH, Gilroy S. 2009.** Ca²⁺ Regulates Reactive Oxygen Species Production and pH during Mechanosensing in *Arabidopsis* Roots. *The Plant cell* **21**: 2341–2356.
- Monshausen GB, Haswell ES. 2013.** A force of nature: molecular mechanisms of mechanoperception in plants. *Journal of experimental botany* **64**: 4663–4680.
- Moulija B, Coutand C, Julien J-L. 2015.** Mechanosensitive control of plant growth: bearing the load, sensing, transducing, and responding. *Frontiers in plant science* **6**: 52.

- Nakano Y, Yamaguchi M, Endo H, Rejab NA, Ohtani M. 2015.** NAC-MYB-based transcriptional regulation of secondary cell wall biosynthesis in land plants. *Frontiers in Plant Science* **6**.
- Nemeth C, Freeman J, Jones HD, Sparks C, Pellny TK, Wilkinson MD, Dunwell J, Andersson AAM, Aman P, Guillon F, et al. 2010.** Down-regulation of the *CSLF6* gene results in decreased (1,3;1,4)- β -D-glucan in endosperm of wheat. *Plant Physiology* **152**: 1209–1218.
- Noda S, Koshiba T, Hattori T, Yamaguchi M, Suzuki S, Umezawa T. 2015.** The expression of a rice secondary wall-specific cellulose synthase gene, *OsCesA7*, is directly regulated by a rice transcription factor, OsMYB58/63. *Planta* **242**: 589–600.
- Ohashi-Ito K, Iwamoto K, Fukuda H. 2018.** LOB DOMAIN-CONTAINING PROTEIN 15 positively regulates expression of *VND7*, a master regulator of tracheary elements. *Plant & Cell Physiology* **59**: 989–996.
- Ohtani M, Nishikubo N, Xu B, Yamaguchi M, Mitsuda N, Goué N, Shi F, Ohme-Takagi M, Demura T. 2011.** A NAC domain protein family contributing to the regulation of wood formation in poplar. *The Plant Journal* **67**: 499–512.
- Okada K, Ito T, Fukazawa J, Takahashi Y. 2017.** Gibberellin Induces an Increase in Cytosolic Ca²⁺ via a DELLA-Independent Signaling Pathway. *Plant physiology* **175**: 1536–1542.
- Olins JR, Lin L, Lee SJ, Trabucco GM, MacKinnon KJM, Hazen SP. 2018.** Secondary wall regulating NACs differentially bind at the promoter at a *CELLULOSE SYNTHASE A4* cis-eQTL. *Frontiers in Plant Science* **9**: 1895.
- O'Malley RC, Huang S-SC, Song L, Lewsey MG, Bartlett A, Nery JR, Galli M, Gallavotti A, Ecker JR. 2016.** Cistrome and Epicistrome Features Shape the Regulatory DNA Landscape. *Cell* **165**: 1280–1292.
- Opanowicz M, Hands P, Betts D, Parker ML, Toole GA, Mills ENC, Doonan JH, Drea S. 2011.** Endosperm development in *Brachypodium distachyon*. *Journal of Experimental Botany* **62**: 735–748.
- Paredes A, Somerville CR, Ehrhardt D. 2006.** Dynamic visualization of cellulose synthase demonstrates functional association with cortical microtubules. *Science* **312**: 1491.
- Pear JR, Kawagoe Y, Schreckengost WE, Delmer DP, Stalker DM. 1996.** Higher plants contain homologs of the bacterial *celA* genes encoding the catalytic subunit of cellulose synthase. *Proceedings of the National Academy of Sciences of the United States of America* **93**: 12637.
- Peña MJ, Zhong R, Zhou G-K, Richardson EA, O'Neill MA, Darvill AG, York WS, Ye Z-H. 2007.** Arabidopsis *irregular xylem8* and *irregular xylem9*: implications for the complexity of glucuronoxylan biosynthesis. *The Plant Cell* **19**: 549–563.
- Perkins M, Smith RA, Samuels L. 2019.** The transport of monomers during lignification in plants: anything goes but how? *Current Opinion in Biotechnology* **56**: 69–74.
- Perry CC, Lu Y. 1992.** Preparation of silicas from silicon complexes: role of cellulose in polymerisation and aggregation control. *Journal of the Chemical Society, Faraday Transactions*

88: 2915–2921.

Persson S, Paredez A, Carroll A, Palsdottir H, Doblin M, Poindexter P, Khitrov N, Auer M, Somerville CR. 2007. Genetic evidence for three unique components in primary cell-wall cellulose synthase complexes in Arabidopsis. *Proceedings of the National Academy of Sciences of the United States of America* **104**: 15566–15571.

Persson S, Wei H, Milne J, Page GP, Somerville CR. 2005. Identification of genes required for cellulose synthesis by regression analysis of public microarray data sets. *Proceedings of the National Academy of Sciences of the United States of America* **102**: 8633–8638.

Petrik DL, Cass CL, Padmakshan D, Foster CE, Vogel JP, Karlen SD, Ralph J, Sedbrook JC. 2016. *BdCESA7*, *BdCESA8*, and *BdPMT* utility promoter constructs for targeted expression to secondary cell-wall-forming cells of grasses. *Frontiers in Plant Science* **7**: 55.

Petrik DL, Karlen SD, Cass CL, Padmakshan D, Lu F, Liu S, Le Bris P, Antelme S, Santoro N, Wilkerson CG, et al. 2014. p-Coumaroyl-CoA:monolignol transferase (PMT) acts specifically in the lignin biosynthetic pathway in *Brachypodium distachyon*. *The Plant Journal* **77**: 713–726.

Peyronnet R, Haswell ES, Barbier-Brygoo H, Frachisse J-M. 2008. AtMSL9 and AtMSL10: Sensors of plasma membrane tension in Arabidopsis roots. *Plant signaling & behavior* **3**: 726–729.

Pillonel C, Mulder MM, Boon JJ, Forster B, Binder A. 1991. Involvement of cinnamyl-alcohol dehydrogenase in the control of lignin formation in *Sorghum bicolor* L. Moench. *Planta* **185**: 538–544.

Piquemal J, Chamayou S, Nadaud I, Beckert M, Barriere Y, Mila I, Lapierre C, Rigau J, Puigdomenech P, Jauneau A, et al. 2002. Down-regulation of caffeic acid *O*-methyltransferase in maize revisited using a transgenic approach. *Plant Physiology* **130**: 1675–1685.

Piston F, Uauy C, Fu L, Langston J, Labavitch J, Dubcovsky J. 2010. Down-regulation of four putative arabinoxylan feruloyl transferase genes from family PF02458 reduces ester-linked ferulate content in rice cell walls. *Planta* **231**: 677–691.

Pitzschke A, Djamei A, Teige M, Hirt H. 2009. VIP1 response elements mediate mitogen-activated protein kinase 3-induced stress gene expression. *Proceedings of the National Academy of Sciences of the United States of America* **106**: 18414–18419.

Polisensky DH, Braam J. 1996. Cold-shock regulation of the Arabidopsis TCH genes and the effects of modulating intracellular calcium levels. *Plant physiology* **111**: 1271–1279.

Polko JK, Kieber JJ. 2019. The regulation of cellulose biosynthesis in plants. *The Plant Cell* **31**: 282–296.

Pradhan Mitra P, Loqué D. 2014. Histochemical staining of Arabidopsis thaliana secondary cell wall elements. *Journal of visualized experiments: JoVE*.

Pyo H, Demura T, Fukuda H. 2007. TERE; a novel cis-element responsible for a coordinated expression of genes related to programmed cell death and secondary wall formation during differentiation of tracheary elements. *The Plant Journal* **51**: 955–965.

- Ralph J, Grabber JH, Hatfield RD. 1995.** Lignin-ferulate cross-links in grasses: active incorporation of ferulate polysaccharide esters into ryegrass lignins. *Carbohydrate Research* **275**: 167–178.
- Ralph J, Hatfield RD, Grabber JH, Jung H-JG, Quideau S, Helm RF. 1998.** Cell wall cross-linking in grasses by ferulates and diferulates. In: ACS Symposium Series. Lignin and lignan biosynthesis. American Chemical Society, 209–236.
- Ralph J, Quideau S, Grabber JH, Hatfield RD. 1994.** Identification and synthesis of new ferulic acid dehydrodimers present in grass cell walls. *Journal of the Chemical Society.*: 3485–3498.
- Rancour D, Marita J, Hatfield RD. 2012.** Cell wall composition throughout development for the model grass *Brachypodium distachyon*. *Frontiers in Plant Science* **3**: 266.
- Rao X, Chen X, Shen H, Ma Q, Li G, Tang Y, Pena M, York W, Frazier TP, Lenaghan S, et al. 2019.** Gene regulatory networks for lignin biosynthesis in switchgrass (*Panicum virgatum*). *Plant Biotechnology Journal* **17**: 580–593.
- Rao X, Dixon RA. 2018.** Current models for transcriptional regulation of secondary cell wall biosynthesis in grasses. *Frontiers in Plant Science* **9**: 399.
- Raudvere U, Kolberg L, Kuzmin I, Arak T, Adler P, Peterson H, Vilo J. 2019.** g:Profiler: a web server for functional enrichment analysis and conversions of gene lists. *Nucleic acids research* **47**: W191–W198.
- Richter GL, Monshausen GB, Krol A, Gilroy S. 2009.** Mechanical stimuli modulate lateral root organogenesis. *Plant physiology* **151**: 1855–1866.
- Ringli C, Keller B. 1998.** Specific interaction of the tomato bZIP transcription factor VSF-1 with a non-palindromic DNA sequence that controls vascular gene expression. *Plant molecular biology* **37**: 977–988.
- del Río JC, Rencoret J, Gutiérrez A, Kim H, Ralph J. 2018.** Structural characterization of lignin from maize (*Zea mays L.*) fibers: Evidence for diferuloylputrescine incorporated into the lignin polymer in maize kernels. *Journal of Agricultural and Food Chemistry* **66**: 4402–4413.
- del Río JC, Rencoret J, Prinsen P, Martínez ÁT, Ralph J, Gutiérrez A. 2012.** Structural characterization of wheat straw lignin as revealed by analytical pyrolysis, 2D-NMR, and reductive cleavage methods. *Journal of agricultural and food chemistry* **60**: 5922–5935.
- Roulin S, Buchala AJ, Fincher GB. 2002.** Induction of (1→3,1→4)-beta-D-glucan hydrolases in leaves of dark-incubated barley seedlings. *Planta* **215**: 51–59.
- Scheller HV, Ulvskov P. 2010.** Hemicelluloses. *Annual Review of Plant Biology* **61**: 263–289.
- Scholthof K-BG, Irigoyen S, Catalan P, Mandadi KK. 2018.** *Brachypodium*: a monocot grass model genus for plant biology. *The Plant Cell* **30**: 1673.
- Schütze K, Harter K, Chaban C. 2008.** Post-translational regulation of plant bZIP factors. *Trends in plant science* **13**: 247–255.
- Scully ED, Gries T, Sarath G, Palmer NA, Baird L, Serapiglia MJ, Dien BS, Boateng AA,**

- Ge Z, Funnell-Harris DL, et al. 2016.** Overexpression of *SbMyb60* impacts phenylpropanoid biosynthesis and alters secondary cell wall composition in *Sorghum bicolor*. *The Plant Journal* **85**: 378–395.
- Shen H, He X, Poovaiah CR, Wuddineh WA, Ma J, Mann DGJ, Wang H, Jackson L, Tang Y, Neal Stewart C, et al. 2012.** Functional characterization of the switchgrass (*Panicum virgatum*) R2R3-MYB transcription factor *PvMYB4* for improvement of lignocellulosic feedstocks. *The New phytologist* **193**: 121–136.
- Sibout R, Le Bris P, Legée F, Cézard L, Renault H, Lapierre C. 2016.** Structural redesigning Arabidopsis lignins into alkali-soluble lignins through the expression of *p*-coumaroyl-CoA:monolignol transferase PMT. *Plant Physiology* **170**: 1358–1366.
- Sibout R, Proost S, Hansen BO, Vaid N, Giorgi FM, Ho-Yue-Kuang S, Legée F, Cézart L, Bouchabké-Coussa O, Soulhat C, et al. 2017.** Expression atlas and comparative coexpression network analyses reveal important genes involved in the formation of lignified cell wall in *Brachypodium distachyon*. *The New Phytologist* **215**: 1009–1025.
- Simmons TJ, Mortimer JC, Bernardinelli OD, Pöppler A-C, Brown SP, deAzevedo ER, Dupree R, Dupree P. 2016.** Folding of xylan onto cellulose fibrils in plant cell walls revealed by solid-state NMR. *Nature Communications* **7**: 13902.
- Sindhu A, Langewisch T, Olek A, Multani DS, McCann MC, Vermerris W, Carpita NC, Johal G. 2007.** Maize *brittle stalk2* encodes a COBRA-like protein expressed in early organ development but required for tissue flexibility at maturity. *Plant Physiology* **145**: 1444–1459.
- Smith RA, Cass CL, Mazaheri M, Sekhon RS, Heckwolf M, Kaeppler H, de Leon N, Mansfield SD, Kaeppler SM, Sedbrook JC, et al. 2017.** Suppression of CINNAMOYL-CoA REDUCTASE increases the level of monolignol ferulates incorporated into maize lignins. *Biotechnology for biofuels* **10**: 109.
- Sonbol F-M, Fornalé S, Capellades M, Encina A, Touriño S, Torres J-L, Rovira P, Ruel K, Puigdomènech P, Rigau J, et al. 2009.** The maize *ZmMYB42* represses the phenylpropanoid pathway and affects the cell wall structure, composition and degradability in *Arabidopsis thaliana*. *Plant Molecular Biology* **70**: 283–296.
- de Souza WR, Martins PK, Freeman J, Pellny TK, Michaelson LV, Sampaio BL, Vinecky F, Ribeiro AP, da Cunha BADB, Kobayashi AK, et al. 2018.** Suppression of a single BAHD gene in *Setaria viridis* causes large, stable decreases in cell wall feruloylation and increases biomass digestibility. *The New Phytologist* **218**: 81–93.
- de Souza WR, Pacheco TF, Duarte KE, Sampaio BL, de Oliveira Molinari PA, Martins PK, Santiago TR, Formighieri EF, Vinecky F, Ribeiro AP, et al. 2019.** Silencing of a BAHD acyltransferase in sugarcane increases biomass digestibility. *Biotechnology for Biofuels* **12**: 111.
- Soyano T, Thitamadee S, Machida Y, Chua N-H. 2008.** *ASYMMETRIC LEAVES2-LIKE19/LATERAL ORGAN BOUNDARIES DOMAIN30* and *ASL20/LBD18* regulate tracheary element differentiation in *Arabidopsis*. *The Plant Cell* **20**: 3359–3373.
- Stewart JJ, Akiyama T, Chapple C, Ralph J, Mansfield SD. 2009.** The effects on lignin structure of overexpression of ferulate 5-hydroxylase in hybrid poplar. *Plant physiology* **150**: 621–635.

- Szczegieliński J, Borkiewicz L, Szurmak B, Lewandowska-Gnatowska E, Statkiewicz M, Klimecka M, Cieśla J, Muszyńska G. 2012.** Maize calcium-dependent protein kinase (ZmCPK11): local and systemic response to wounding, regulation by touch and components of jasmonate signaling. *Physiologia plantarum* **146**: 1–14.
- Takeda Y, Tobimatsu Y, Karlen SD, Koshiba T, Suzuki S, Yamamura M, Murakami S, Mukai M, Hattori T, Osakabe K, et al. 2018.** Downregulation of *p-COUMAROYL ESTER 3-HYDROXYLASE* in rice leads to altered cell wall structures and improves biomass saccharification. *The Plant Journal* **95**: 796–811.
- Tamasloukht B, Wong Quai Lam MS-J, Martinez Y, Tozo K, Barbier O, Jourda C, Jauneau A, Borderies G, Balzergue S, Renou J-P, et al. 2011.** Characterization of a cinnamoyl-CoA reductase 1 (CCR1) mutant in maize: effects on lignification, fibre development, and global gene expression. *Journal of Experimental Botany* **62**: 3837–3848.
- Tanaka K, Murata K, Yamazaki M, Onosato K, Miyao A, Hirochika H. 2003.** Three distinct rice cellulose synthase catalytic subunit genes required for cellulose synthesis in the secondary wall. *Plant Physiology* **133**: 73–83.
- Taylor-Teeples M, Lin L, de Lucas M, Turco G, Toal TW, Gaudinier A, Young NF, Trabucco GM, Veling MT, Lamothe R, et al. 2015.** An Arabidopsis gene regulatory network for secondary cell wall synthesis. *Nature* **517**: 571–575.
- Testone G, Condello E, Verde I, Caboni E, Iannelli MA, Bruno L, Mariotti D, Bitonti MB, Giannino D. 2009.** The peach (*Prunus persica* [L.] Batsch) homeobox gene KNOPE3, which encodes a class 2 knotted-like transcription factor, is regulated during leaf development and triggered by sugars. *Molecular genetics and genomics: MGG* **282**: 47–64.
- Timpano H, Sibout R, Devaux M-F, Alvarado C, Looten R, Falourd X, Pontoire B, Martin M, Legée F, Cézard L, et al. 2015.** Brachypodium Cell Wall Mutant with Enhanced Saccharification Potential Despite Increased Lignin Content. *Bioenergy research* **8**: 53–67.
- Torres-Schumann S, Ringli C, Heierli D, Amrhein N, Keller B. 1996.** In vitro binding of the tomato bZIP transcriptional activator VSF-1 to a regulatory element that controls xylem-specific gene expression. *The Plant journal: for cell and molecular biology* **9**: 283–296.
- Trabucco GM, Matos DA, Lee SJ, Saathoff A, Priest H, Mockler TC, Sarath G, Hazen SP. 2013a.** Functional characterization of cinnamyl alcohol dehydrogenase and caffeic acid O-methyltransferase in *Brachypodium distachyon*. *BMC biotechnology* **13**: 61.
- Trabucco GM, Matos DA, Lee SJ, Saathoff AJ, Priest HD, Mockler TC, Sarath G, Hazen SP. 2013b.** Functional characterization of cinnamyl alcohol dehydrogenase and caffeic acid O-methyltransferase in *Brachypodium distachyon*. *BMC Biotechnology* **13**: 61.
- Trafford K, Haleux P, Henderson M, Parker M, Shirley NJ, Tucker MR, Fincher GB, Burton RA. 2013.** Grain development in *Brachypodium* and other grasses: possible interactions between cell expansion, starch deposition, and cell-wall synthesis. *Journal of Experimental Botany* **64**: 5033–5047.
- Trethewey JAK, Campbell LM, Harris PJ. 2005.** (1 → 3),(1 → 4)-β-d-Glucans in the cell walls of the *Poales (sensu lato)*: an immunogold labeling study using a monoclonal antibody. *American Journal of Botany* **92**: 1660–1674.

- Trethewey JAK, Harris PJ. 2002.** Location of (1 → 3)- and (1 → 3),(1 → 4)-beta-D-glucans in vegetative cell walls of barley (*Hordeum vulgare*) using immunogold labelling. *The New Phytologist* **154**: 347–358.
- Tsugama D, Liu S, Fujino K, Takano T. 2018.** Calcium signalling regulates the functions of the bZIP protein VIP1 in touch responses in *Arabidopsis thaliana*. *Annals of botany* **122**: 1219–1229.
- Tsugama D, Liu S, Takano T. 2012.** A bZIP protein, VIP1, is a regulator of osmosensory signaling in *Arabidopsis*. *Plant physiology* **159**: 144–155.
- Tsugama D, Liu S, Takano T. 2014.** Analysis of functions of VIP1 and its close homologs in osmosensory responses of *Arabidopsis thaliana*. *PloS one* **9**: e103930.
- Tsugama D, Liu S, Takano T. 2016.** The bZIP Protein VIP1 Is Involved in Touch Responses in *Arabidopsis* Roots. *Plant physiology* **171**: 1355–1365.
- Turner SR, Somerville CR. 1997.** Collapsed xylem phenotype of *Arabidopsis* identifies mutants deficient in cellulose deposition in the secondary cell wall. *The Plant cell* **9**: 689–701.
- Tyler L, Fangel JU, Fagerström AD, Steinwand MA, Raab TK, Willats WG, Vogel JP. 2014.** Selection and phenotypic characterization of a core collection of *Brachypodium distachyon* inbred lines. *BMC Plant Biology* **14**: 25.
- Updegraff DM. 1969.** Semimicro determination of cellulose in biological materials. *Analytical biochemistry* **32**: 420–424.
- Urbanowicz BR, Peña MJ, Ratnaparkhe S, Avci U, Backe J, Steet HF, Foston M, Li H, O’Neill MA, Ragauskas AJ, et al. 2012.** 4-O-methylation of glucuronic acid in *Arabidopsis* glucuronoxylan is catalyzed by a domain of unknown function family 579 protein. *Proceedings of the National Academy of Sciences of the United States of America* **109**: 14253–14258.
- Uyttewaal M, Burian A, Alim K, Landrein B, Borowska-Wykręt D, Dedieu A, Peaucelle A, Ludynia M, Traas J, Boudaoud A, et al. 2012.** Mechanical stress acts via katanin to amplify differences in growth rate between adjacent cells in *Arabidopsis*. *Cell* **149**: 439–451.
- Valdivia ER, Herrera MT, Gianzo C, Fidalgo J, Revilla G, Zarra I, Sampedro J. 2013.** Regulation of secondary wall synthesis and cell death by NAC transcription factors in the monocot *Brachypodium distachyon*. *Journal of Experimental Botany* **64**: 1333–1343.
- Vanholme R, De Meester B, Ralph J, Boerjan W. 2019.** Lignin biosynthesis and its integration into metabolism. *Current Opinion in Biotechnology* **56**: 230–239.
- Vanholme R, Storme V, Vanholme B, Sundin L, Christensen JH, Goeminne G, Halpin C, Rohde A, Morreel K, Boerjan W. 2012.** A systems biology view of responses to lignin biosynthesis perturbations in *Arabidopsis*. *The Plant Cell* **24**: 3506–3529.
- Van Leene J, Blomme J, Kulkarni SR, Cannoot B, De Winne N, Eeckhout D, Persiau G, Van De Slijke E, Vercruyssen L, Vanden Bossche R, et al. 2016.** Functional characterization of the *Arabidopsis* transcription factor bZIP29 reveals its role in leaf and root development. *Journal of experimental botany* **67**: 5825–5840.
- Van Oosten MJ, Sharkhuu A, Batelli G, Bressan RA, Maggio A. 2013.** The *Arabidopsis thaliana* mutant air1 implicates SOS3 in the regulation of anthocyanins under salt stress. *Plant*

molecular biology **83**: 405–415.

Vega-Sánchez ME, Loqué D, Lao J, Catena M, Verhertbruggen Y, Herter T, Yang F, Harholt J, Ebert B, Baidoo EEK, et al. 2015. Engineering temporal accumulation of a low recalcitrance polysaccharide leads to increased C6 sugar content in plant cell walls. *Plant Biotechnology Journal* **13**: 903–914.

Vega-Sanchez ME, Verhertbruggen Y, Christensen U, Chen X, Sharma V, Varanasi P, Jobling SA, Talbot M, White RG, Joo M, et al. 2012. Loss of *Cellulose Synthase-like F6* function affects mixed-linkage glucan deposition, cell wall mechanical properties, and defense responses in vegetative tissues of rice. *Plant Physiology* **159**: 56–69.

Vélez-Bermúdez I-C, Salazar-Henao JE, Fornalé S, López-Vidriero I, Franco-Zorrilla J-M, Grotewold E, Gray J, Solano R, Schmidt W, Pagés M, et al. 2015. A MYB/ZML complex regulates wound-induced lignin genes in maize. *The Plant Cell* **27**: 3245–3259.

Vermaas JV, Dixon RA, Chen F, Mansfield SD, Boerjan W, Ralph J, Crowley MF, Beckham GT. 2019. Passive membrane transport of lignin-related compounds. *Proceedings of the National Academy of Sciences of the United States of America* **116**: 23117–23123.

Vogel J, Garvin D, Leong O, Hayden D. 2006. *Agrobacterium*-mediated transformation and inbred line development in the model grass *Brachypodium distachyon*. *Plant cell, tissue and organ culture* **84**: 100179–100191.

Vogel J, Hill T. 2008. High-efficiency *Agrobacterium*-mediated transformation of *Brachypodium distachyon* inbred line Bd21-3. *Plant cell reports* **27**: 471–478.

Vollbrecht E, Veit B, Sinha N, Hake, S. (USDA-ARS Plant Gene Expression Center, 800 Buchanan Street, Albany, CA 94710 (USA)). 1991. The developmental gene Knotted-1 is a member of a maize homeobox gene family. *Nature* **350**.

Wang H, Avci U, Nakashima J, Hahn MG, Chen F, Dixon RA. 2010. Mutation of WRKY transcription factors initiates pith secondary wall formation and increases stem biomass in dicotyledonous plants. *Proceedings of the National Academy of Sciences of the United States of America* **107**: 22338–22343.

Wang Y, Bouchabke-Coussa O, Lebris P, Antelme S, Soulhat C, Gineau E, Dalmais M, Bendahmane A, Morin H, Mouille G, et al. 2015. LACCASE5 Is required for lignification of the *Brachypodium distachyon* culm. *Plant Physiology* **168**: 192.

Wang Y, Chantreau M, Sibout R, Hawkins S. 2013. Plant cell wall lignification and monolignol metabolism. *Frontiers in Plant Science* **4**: 220.

Wang S, Yamaguchi M, Grienberger E, Martone PT, Samuels AL, Mansfield SD. 2020. The Class II KNOX genes KNAT3 and KNAT7 work cooperatively to influence deposition of secondary cell walls that provide mechanical support to Arabidopsis stems. *The Plant journal: for cell and molecular biology* **101**: 293–309.

Wang S, Yang H, Mei J, Liu X, Wen Z, Zhang L, Xu Z, Zhang B, Zhou Y. 2019. A Rice Homeobox Protein KNAT7 Integrates the Pathways Regulating Cell Expansion And Wall Stiffness. *Plant physiology*.

- Warthmann N, Chen H, Ossowski S, Weigel D, Hervre P. 2008.** Highly specific gene silencing by artificial miRNAs in rice. *PLoS one* **3**: e1829.
- Weltmeier F, Ehlert A, Mayer CS, Dietrich K, Wang X, Schütze K, Alonso R, Harter K, Vicente-Carbajosa J, Dröge-Laser W. 2006.** Combinatorial control of Arabidopsis proline dehydrogenase transcription by specific heterodimerisation of bZIP transcription factors. *The EMBO journal* **25**: 3133–3143.
- Whitehead C, Ostos Garrido FJ, Reymond M, Simister R, Distelfeld A, Atienza SG, Piston F, Gomez LD, McQueen Mason SJ. 2018.** A glycosyl transferase family 43 protein involved in xylan biosynthesis is associated with straw digestibility in *Brachypodium distachyon*. *The New Phytologist* **218**: 974–985.
- Wilkerson CG, Mansfield SD, Lu F, Withers S, Park J-Y, Karlen SD, Gonzales-Vigil E, Padmakshan D, Unda F, Rencoret J, et al. 2014.** Monolignol ferulate transferase introduces chemically labile linkages into the lignin backbone. *Science* **344**: 90–93.
- Wilson SM, Burton RA, Doblin MS, Stone BA, Newbigin EJ. 2006.** Temporal and spatial appearance of wall polysaccharides during cellularization of barley (*Hordeum vulgare*) endosperm. *Planta* **224**: 655.
- Wilson SM, Ho YY, Lampugnani ER, Van de Meene AML, Bain MP, Bacic A, Doblin MS. 2015.** Determining the subcellular location of synthesis and assembly of the cell wall polysaccharide (1,3; 1,4)- β -D-glucan in grasses. *The Plant Cell* **27**: 754–771.
- Withers S, Lu F, Kim H, Zhu Y, Ralph J, Wilkerson CG. 2012.** Identification of grass-specific enzyme that acylates monolignols with *p*-coumarate. *The Journal of Biological Chemistry* **287**: 8347–8355.
- Yang L, Zhao X, Yang F, Fan D, Jiang Y, Luo K. 2016.** PtrWRKY19, a novel WRKY transcription factor, contributes to the regulation of pith secondary wall formation in *Populus trichocarpa*. *Scientific Reports* **6**: 18643.
- Ye Y, Liu B, Zhao M, Wu K, Cheng W, Chen X, Liu Q, Liu Z, Fu X, Wu Y. 2015.** CEF1/OsMYB103L is involved in GA-mediated regulation of secondary wall biosynthesis in rice. *Plant Molecular Biology* **89**: 385–401.
- Yin Y, Zhu Q, Dai S, Lamb C, Beachy RN. 1997.** RF2a, a bZIP transcriptional activator of the phloem-specific rice tungro bacilliform virus promoter, functions in vascular development. *The EMBO journal* **16**: 5247–5259.
- Zhang Y, Wang Y, Ye D, Xing J, Duan L, Li Z, Zhang M. 2020.** Ethephon-regulated maize internode elongation associated with modulating auxin and gibberellin signal to alter cell wall biosynthesis and modification. *Plant science: an international journal of experimental plant biology* **290**: 110196.
- Zhang J, Xie M, Tuskan GA, Muchero W, Chen J-G. 2018a.** Recent advances in the transcriptional regulation of secondary cell wall biosynthesis in the woody plants. *Frontiers in Plant Science* **9**: 1535.
- Zhang D, Xu Z, Cao S, Chen K, Li S, Liu X, Gao C, Zhang B, Zhou Y. 2018b.** An uncanonical CCCH-tandem zinc-finger protein represses secondary wall synthesis and controls

mechanical strength in rice. *Molecular Plant* **11**: 163–174.

Zhang B, Zhang L, Li F, Zhang D, Liu X, Wang H, Xu Z, Chu C, Zhou Y. 2017. Control of secondary cell wall patterning involves xylan deacetylation by a GDSL esterase. *Nature Plants* **3**: 17017.

Zhao K, Bartley L. 2014. Comparative genomic analysis of the R2R3 MYB secondary cell wall regulators of *Arabidopsis*, poplar, rice, maize, and switchgrass. *BMC Plant Biology* **14**: 135.

Zhao K, Lin F, Romero-Gamboa SP, Goh H-J, Saha P, An G, Jung K-H, Hazen SP, Bartley LE. 2019. Rice genome-scale network integration reveals transcriptional regulators of grass cell wall synthesis. *Frontiers in plant science*.

Zhong R, Cui D, Dasher RL, Ye Z-H. 2018a. Biochemical characterization of rice xylan O-acetyltransferases. *Planta* **247**: 1489–1498.

Zhong R, Cui D, Phillips DR, Ye Z-H. 2018b. A novel rice xylosyltransferase catalyzes the addition of 2-O-xylosyl side chains onto the xylan backbone. *Plant & Cell Physiology* **59**: 554–565.

Zhong R, Cui D, Ye Z-H. 2017. Regiospecific acetylation of xylan is mediated by a group of DUF231-containing O-acetyltransferases. *Plant & Cell Physiology* **58**: 2126–2138.

Zhong R, Demura T, Ye ZH. 2006a. SND1, a NAC domain transcription factor, is a key regulator of secondary wall synthesis in fibers of *Arabidopsis*. *The Plant Cell* **18**: 3158–3170.

Zhong R, Demura T, Ye Z-H. 2006b. SND1, a NAC domain transcription factor, is a key regulator of secondary wall synthesis in fibers of *Arabidopsis*. *The Plant cell* **18**: 3158–3170.

Zhong R, Lee C, McCarthy RL, Reeves CK, Jones EG, Ye Z-H. 2011. Transcriptional activation of secondary wall biosynthesis by rice and maize NAC and MYB transcription factors. *Plant & Cell Physiology* **52**: 1856–1871.

Zhong R, Lee C, Zhou J, McCarthy RL, Ye Z-H. 2008a. A battery of transcription factors involved in the regulation of secondary cell wall biosynthesis in *Arabidopsis*. *The Plant cell* **20**: 2763–2782.

Zhong R, Lee C, Zhou J, McCarthy RL, Ye Z-H. 2008b. A battery of transcription factors involved in the regulation of secondary cell wall biosynthesis in *Arabidopsis*. *The Plant Cell* **20**: 2763–2782.

Zhong R, Richardson EA, Ye Z-H. 2007a. Two NAC domain transcription factors, SND1 and NST1, function redundantly in regulation of secondary wall synthesis in fibers of *Arabidopsis*. *Planta* **225**: 1603–1611.

Zhong R, Richardson EA, Ye ZH. 2007b. The MYB46 transcription factor is a direct target of SND1 and regulates secondary wall biosynthesis in *Arabidopsis*. *The Plant Cell* **19**: 2776–2792.

Zhong R, Ye Z-H. 2007. Regulation of cell wall biosynthesis. *Current opinion in plant biology* **10**: 564–572.

Zhong R, Ye Z-H. 2012. MYB46 and MYB83 bind to the SMRE sites and directly activate a suite of transcription factors and secondary wall biosynthetic genes. *Plant & Cell Physiology* **53**:

368–380.

Zhong R, Yuan Y, Spiekerman JJ, Guley JT, Egbosiuba JC, Ye Z-H. 2015. Functional characterization of NAC and MYB transcription factors involved in regulation of biomass production in switchgrass (*Panicum virgatum*). *PloS One* **10**: e0134611.